

Protein residue networks from a local search perspective

Susan Khor
slc.khor@gmail.com

Abstract

We propose the use of local search to investigate protein residue networks (PRN). In a local search, clustering is inversely related to average path length. The opposite holds for a global search such as the commonly used breadth first strategy (BFS). The inverse relationship better fits the notion that amino acids get closer to each other as a protein becomes more compact. We use a greedy local search algorithm (EDS) that is Euclidean distance based and allows backtracking. While there are preferable differences between BFS and EDS paths in terms of variation in path length, search cost and link usage, there are also similarities in terms of centrality and hierarchy. EDS identifies a set of short-cut edges for each PRN. Short-cut edges are enriched with short-range links, and the short-cut network (SCN) they form spans most of a PRN's nodes, is adjacent to most of a PRN's edges and is strongly transitive. The short-cuts influence average EDS path length by reducing the difference in length or stretch between path-pairs. A consequence of this role is short-cut sets are more volatile, i.e. they undergo significantly more additions and deletions from step to step in a molecular dynamics (MD) simulation than non-short-cut edge sets. Despite their volatility, about 79% of SCN edge deletions have replacements (a deleted short-cut is replaced when an added short-cut is found in the edge cut-set of the deleted short-cut), and about 88% of added short-cuts are replacement edges. This high edge replacement rate helps with the growth of the largest connected component of a SCN. More work is needed to understand the structure and formation of SCNs, in particular to identify the conditions under which short-cuts get deleted and how their replacements are selected.

1. Introduction

Protein molecules have long been represented as contact maps. The contact map of a protein is the adjacency matrix \mathbf{A} of a graph G representing the protein as a set of nodes V and a set of edges E . We call such a graph a Protein Residue Network (PRN). Each node in a PRN represents an amino acid molecule of a protein or a portion thereof. An edge is placed between a node pair if they satisfy certain conditions, typically if they are within an acceptable Euclidean distance from each other (section 2.1). Pursuant to the introduction of a model of the small-world phenomenon in social networks [1], protein contact maps were classified as small-world networks [2]. This study is performed on globular proteins, although both fibrous and membrane proteins are qualitatively small-world networks also [16, 19].

A small-world network (SWN) combines the order inherent in regular graphs, with the arbitrary connectivity of pure random graphs (where any two vertices have a non-zero probability to link with each other) to supply the short-cuts edges or long-range connections. The second half of this definition has undergone substantial refinement. Briefly, for a SWN to be navigable by a local search algorithm, the short-cut edges need not be long-ranged, but multi-scaled [3, 4, 5]. More formally, a graph with N nodes and average degree K is identified as having SWN structure if: (i) its clustering coefficient C is significantly larger than the clustering coefficient of a comparable Erdos-Renyi (ER) random graph $C_{ER} \sim K / N$; and (ii) its characteristic path-length L approaches that of a comparable ER random graph $L_{ER} \sim \ln(N) / \ln(K)$. For constant K , the latter property implies that L increases logarithmically with N . Most (food webs being an exception) real-world networks can be considered sparse, i.e. their mean vertex degree K remains constant with increase in network size N [6 p.19, 7 p. 134]. The average degree for PRNs is almost constant with N (Fig. 7a). The increase in L can be slower than $\ln(N)$ for small-world networks with power-law degree distribution [9]. PRNs have Gaussian degree distribution which can be explained by the excluded volume argument [8].

The clustering coefficient C reflects the probability that two unique nodes u and v which are directly connected to a third other node w , are themselves connected in the network forming a triangle. Typically, the clustering coefficient for a network with N nodes is $C = \frac{1}{N} \sum_i C_i$ where $C_i = \frac{2e_i}{k_i(k_i - 1)}$ is the clustering coefficient of a node i with degree k_i and e_i is the number of links amongst i 's k_i direct neighbor nodes [1]. Links in an ER graph are independent of each other, so $C_{ER} = p = \frac{2M}{N(N-1)} = \frac{K}{(N-1)}$ where p is the probability of connecting two nodes in the ER graph, M is the number of links and $K = \frac{2M}{N}$. Typically, L is the average length of paths between all unique node-pairs in a network: $L = \frac{2}{N(N-1)} \sum_{i < j} \lambda(i, j)$ where

$\lambda(i, j)$ is the length of a path (number of edges in a path) from node i to node j found through a global search such as breadth-first search (BFS). All networks considered in this paper are simple graphs.

The description of protein molecules as small-world networks is intuitive since the combination of order and randomness in a SWN parallels the coexistence of the highly ordered helical and beta sheet secondary structures with random coils in protein molecules. Further, the short characteristic path-length of a SWN appeals directly to the need for rapid communication between distantly located sites in a protein. Such efficient long-range intra-protein communication enables allostery, signaling, and cooperativity to effect global state transitions in proteins which are crucial for them to be functional [10, 21]. Such long-range information pathways or energy transport channels have also been observed outside the context of protein functionality and is believed to be a fundamental phenomenon of all globular proteins [10, 20]. Indeed, the short characteristic path-length of a SWN is a widely mentioned and frequently applied topological feature of PRNs [2, 11, 12, 13, 14].

With a few exceptions [16, 17, 18], there is less discussion about the role clustering plays in proteins. This may be because clustering in PRNs is seen as an inevitable consequence of protein packing in 3D space. However, the presence of clustering in PRNs needs to be explained *and related to characteristic path-length* of PRNs if we are to fully understand why proteins have SWN structure and to fully exploit this network model of PRNs. We propose that the role of clustering in PRNs can be better understood in the light of a *greedy local search*. In a greedy local search, information available to the algorithm to decide the next step in a path is confined to the neighbourhood within a small radius of the current node, and the algorithm moves to the neighbouring node that is closest to the target node. As such a greedy local search is *directed* and in our case, as in Kleinberg's [3, 4], by proximity to the target. There exists decentralized search algorithms that do not require target location information [e.g. 58]. Where necessary, L_G refers to the characteristic path-length of a PRN found with a global search strategy, and L_W to one obtained with a local search strategy.

The majority of previous research on PRNs has implicitly defined characteristic path-length and other network statistics derived from path length such as node centrality and closeness centrality, in terms of shortest-paths found via a global search strategy such as BFS on un-weighted PRNs or Dijkstra's algorithm on weighted PRNs [14, 18]. An exception is [15] which uses a Markov random walk on PRNs. There are three issues with using global search on PRNs (since our PRNs are un-weighted, we will discuss global search in terms of BFS).

First, "energy flow in globular proteins resembles transport on a percolation cluster with channels through which energy flows easily and dead-end regions where energy flow stalls" [20]. Transport of energy through specific pathways is believed to be a mechanism underlying allosteric interactions in proteins. The energy generated as the result of a ligand binding to a protein site is converted to propagate

this signal, as a sequence of local structural changes in the protein (heat is also dissipated into the environment or solvent), to another site in the protein. Such anisotropic energy flow has been experimentally observed to occur efficiently between two allosterically linked binding sites: FAI in subdomain IB and Sudlow site I in subdomain IIA, in the multi-domain BSA protein [61].

In a BFS on PRNs, there is very little variation in the lengths of paths, i.e. all nodes are easily reached from every other node (section 3.1). Thus BFS models a communication strategy where there is little specificity in inter-nodal communication. But protein sites are not created equal: certain sites are more actively involved in protein activity and are more evolutionarily conserved than others [22]. While there is a fair amount of redundant pathways, specific communication pathways within a protein molecule have been traced, and some of these pathways exist to slow down communication as a way to absorb or localize the after effects of undesirable perturbations to maintain protein stability [12].

Second, a BFS progresses by radiating outward from a source node in all possible directions. Thus, BFS is directionless, and unlike energy flow in proteins which is anisotropic and sub-diffusive [20]. The lack of direction increases the volume of space explored by BFS, i.e. the number of sites or nodes visited during a search. While the average length of shortest paths found with BFS increases only logarithmically with network size (section 3.1), the cost of BFS in terms of the average number of unique nodes visited during the search increases linearly with network size (section 3.2). The linear search cost of BFS is known [6 p.44]. In contrast, a greedy local search is more focused and less diffusive. Hence it is less costly and it turns out that for PRNs, it is possible for a Euclidean distance directed greedy local search with backtrack (our EDS algorithm is described in section 2.4) to produce paths with average length that increases logarithmically with network size (section 3.1), and at a cost that also increases logarithmically with network size (section 3.2). The small-world property of PRNs is preserved with local search, and as such PRNs are *navigable* small-world networks.

Third, the clustering coefficient of folded proteins is significantly larger than C_{ER} , and a high level of clustering forms a barrier to short inter-nodal path-lengths L_G (section 3.1). The direct relationship between C and L_G follows directly from $L_{ER} \sim \ln(N) / \ln(K)$. ER graphs (with typical low link density) have little to no clustering and are therefore locally tree-like. The average degree K then approximates the branching factor of a search tree. By introducing cycles into the search tree, i.e. increasing clustering, some of the branches now loop back to a previous tree level. In other words, clustering reduces the effective branching factor, or effective K . Consequently, L_G becomes larger than L_{ER} .

However, if short inter-nodal distances are important for protein functionality, why should proteins take on a highly clustered conformation that prevents them from having shorter pathways? Molecular dynamics (MD) simulation on the 2EZN protein (section 2.5) confirms the presence of a significant gap in C values between the set of PRNs for configurations at equilibrium, and the set of PRNs for non-

equilibrium configurations (Fig. 1). This contradiction does not arise with a local view of search where suitable clustering is an enabler, not an impediment, to shorter path lengths (section 3.1). The inverse relationship between C and L_w is more attuned to what happens when a protein folds or unfolds. MD simulations of the 2EZN protein reveal that C generally increases (decreases) and L generally decreases (increases) as the protein folds (unfolds) (Fig. 2).

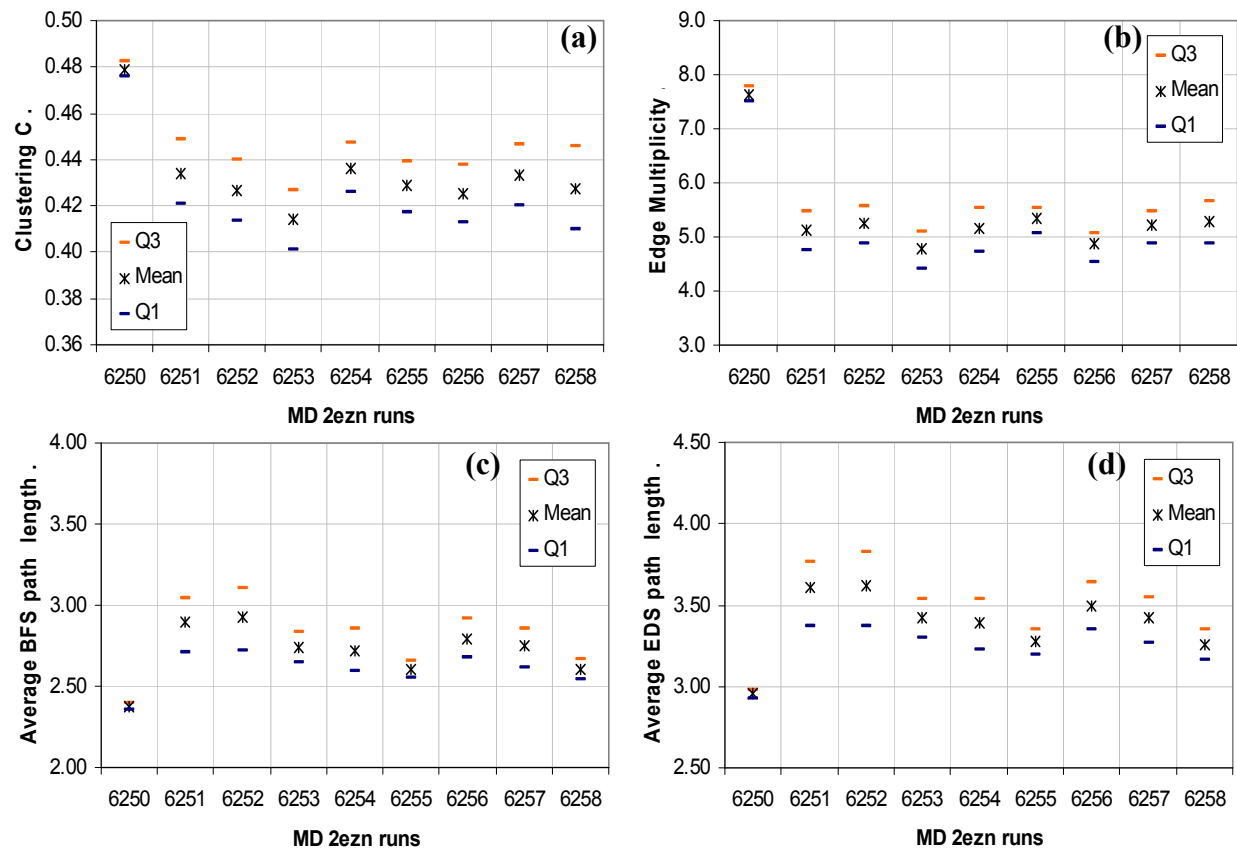


Fig. 1 A topological gap exists between native and non-native configurations. Native configurations are much more clustered and have much shorter paths on average. (a & b) Native state PRNs have significantly higher clustering and stronger transitivity (section 2.3) than non-native state PRNs. (c & d) Regardless of the type of search algorithm (BFS or EDS), paths in native state PRNs are significantly shorter on average than paths in non-native state PRNs. Averages are computed over all snapshots (PRNs) per MD run (section 2.5). Run 6250 is a simulation of the native dynamics of the 2EZN protein, while the remaining runs are simulations of non-equilibrium dynamics of 2EZN. Q1 and Q3 denote values for the first and third quartiles respectively.

2. Materials and Method

Since we are proposing the use of local search to investigate PRNs, this study focuses quite heavily on the differences between global search implemented as BFS (breadth-first search) and local search implemented as EDS (section 2.4). The differences are measured primarily in terms of path length (section 3.1) and search cost (section 3.2), but other differences stemming from path length differences, as well as some unexpected similarities are reported in section 3. To observe the impact of clustering on local search, a null model in the form of the MGEO networks, which are identical to PRNs in many respects including

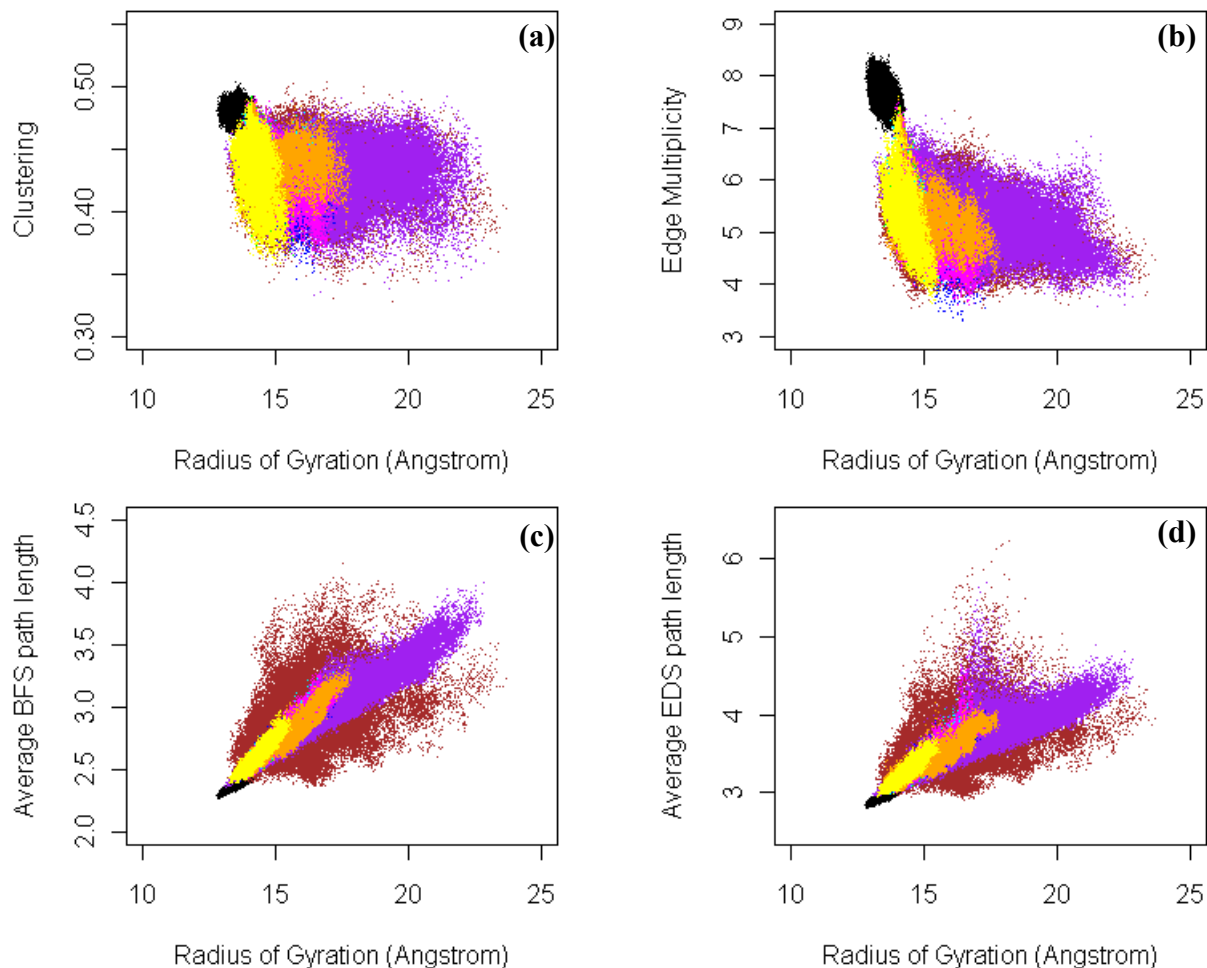


Fig. 2 Because of the inverse relationship between clustering and average path length, a local search perspective of PRNs is more reflective of what happens when a protein folds or unfolds. Higher clustering and stronger transitivity has an inflationary effect on BFS path lengths, but a deflationary effect on EDS path lengths (section 3.1). Since clustering (a) and transitivity (b) increases while average path length decreases (c & d) as a protein becomes more compact (radius of gyration decreases), we propose that a local search perspective of PRNs, e.g. with EDS, makes more sense than a global search perspective, e.g. with BFS. The scatter plots show the network statistic for each snapshot in a run. Black points denote the native state statistics (section 2.5).

the 3D coordinates of nodes, is designed (section 2.2). We will have occasion to refer to PRNs from other research papers that are constructed differently. To avoid confusion, we will refer to these other PRNs as *residue interaction networks* or RINs.

In all figures, the average, standard deviation and median values for a variable are suffixed “_avg”, “_sd”, and “_mid” respectively. A “BFS” prefix denotes that the statistic is measured with a set of paths found through breadth-first search. An “EDS” prefix denotes that the statistic is measured with a set of paths found with the EDS algorithm (section 2.4). Unless stated otherwise, significance tests are made with either R’s `t.test` or `Wilcox.test`, in paired form where applicable, and a p-value < 0.05 is required for significance.

The PRNs and MGEO networks from sections 2.1 and 2.2 are reduced to the same set of 166 proteins after screening out outliers to permit pairwise comparison. Compared to the BFS paths, the EDS paths show much greater variation in length which section 3.1 argues is a more realistic model for proteins. However, the extremely large values skew path-length statistics and spills over to other path-length related statistics such as link usage, node centrality and edge betweenness. Therefore the networks were screened to limit the effect of outliers by excluding networks whose average BFS or EDS path exceeds $\ln(\max(N)) = 7.482119$ where $\max(N)$ is the number of nodes in the largest PRN in a set of 204 PRNs (section 2.1).

2.1 PRN construction

Define a Protein Residue Networks (PRN) as a simple undirected graph $G = (V, E)$ with $|V|^1 = N$ and $|E| = M$. The PRNs are constructed from the PDB coordinates files [24] with side-chain considerations following the method in [17]. Each amino acid (residue) is represented by a node and two nodes u and v are linked *iff* $|u - v| \geq 2$ and their interaction strength I_{uv} is $\geq 50\%$. $I_{uv} = \frac{n_{uv} \times 100}{\sqrt{N_u \times N_v}}$ where n_{uv} is the

number of distinct atom-pairs (i, j) such that i is an atom of residue u , j is an atom of residue v and the Euclidean distance between atoms i and j , $ed(i, j)$ is $\leq 7.5 \text{ \AA}$. All the atoms of a residue, including those of the backbone, are considered when calculating n_{uv} (this departs from [17] where only the side-chain atoms are used to calculate I_{uv}). N_u and N_v are normalization values by residue types. They are obtained from Table 1 in [25] (and expanded in Appendix A of this paper to accommodate alternatives). As in [17], peptide bonds are excluded, i.e. links are prohibited between nodes i and $i+1$ (the nodes of a PRN are labeled in the same order as they appear in the PDB file). The threshold value-pair of 50% and 7.5 Å was chosen after some initial experiments to permit (without unnecessarily increasing link density) most domain-based interactions identified in 3did [26] to be edges in most of the 2000 initial PRNs sampled at random from the list of proteins appearing in the 3did catalog. The 3did links represent intra- or inter-chain residue-residue interactions between contacting domains of a protein [26].

The initial sample produced 204 usable PRNs. Each of these usable PRNs satisfies the following criteria: (i) there are no missing atoms in the PDB coordinate file, (ii) all domain-based interactions cataloged in 3did are represented as links, (iii) the PRN is a single connected component, and (iv) there is a power-law relation between the number of nodes N and link density $2M/[(N-1)(N-2)]$ (Fig. 3a) (we did not purposefully seek this relation out, it so happens that most of the points fall on a straight-line in the log-log plot). The last condition reflects the sparseness of PRNs. The PRNs examined in this paper are

¹ The interpretation of two vertical lines surrounding a variable or an expression as either set cardinality or absolute value is clear from context.

simple graphs. The link density of simple graphs is given by $\frac{2M}{N(N-1)} = \frac{K}{N-1} \sim KN^{-1}$. Since average node

degree $K = \frac{2M}{N}$ is constant (Fig. 7a), the number of edges M is linearly related with the number of nodes

N . The number of short-range edges (SE) is also linearly related with N , which means that the number of long-range edges (LE) also relates linearly with N . The effect of N on both SE and LE cancels out each other to a large extent, and the ratio $|LE|/|SE|$ increases only slightly with N (Fig. 3b). A link connecting nodes u and v is long-range (LE) if u and v are more than 10 residues apart on the protein sequence, i.e. $|u - v| > 10$ [27]. Long-range links represent interactions between residues which are far apart on the protein sequence but close to each other in the tertiary structure. Short-range links represent interactions between residues that are close to each other in the primary and the tertiary structures. The number of 3did edges also increases with N in general (Fig. 4a), but the linear correlation is weaker, 0.6091. The 3did domain-based interactions are mostly long-range links (Fig. 4a).

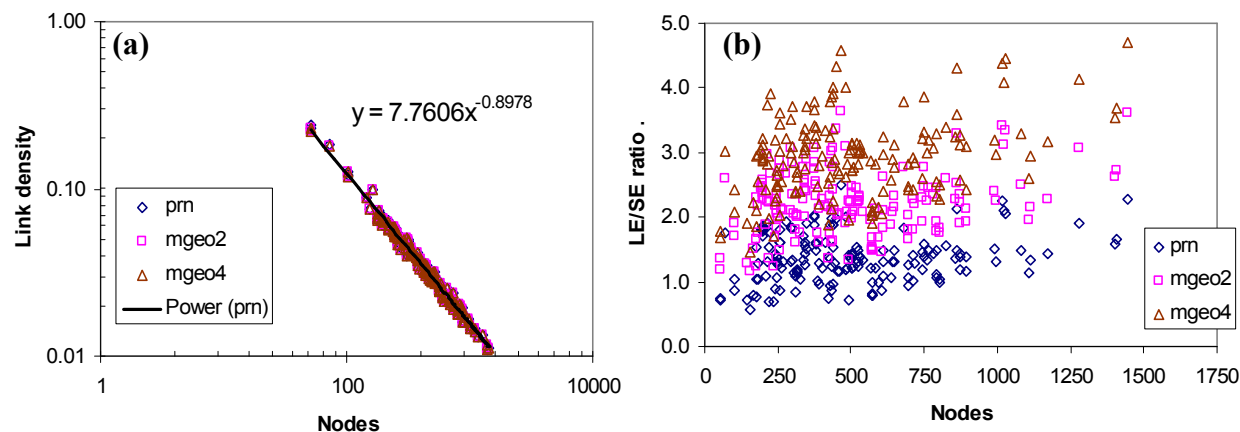


Fig. 3 Network size of the 166 PRNs and their MGE0 networks. (a) Link density of PRNs approximate that of sparse simple graphs. MGE0 networks have identical link density to PRNs. **(b)** LE/SE is the ratio of long-range links to short-range links. A link connecting nodes u and v is long-range if u and v are more than 10 residues apart on the protein sequence [27]. PRNs have a significantly smaller LE/SE ratio than MGE0 networks (section 2.2). In figures where the x-axis is labeled “Nodes”, read as N (number of nodes).

The PRNs constructed with the method described here, even without the did3 links (in 156/166 of the PRNs the longest edge in Euclidean distance is a non-did3 link), have maximum inter-residue Euclidean distances that is twice that normally considered in pure (no side-chain consideration) C_α - C_α or C_β - C_β contact maps (Fig. 4b). This raises the concern that the PRNs are not preserving topological cavities which are proxies for protein binding sites. Ref [23] examined the expansion or isoperimetric constant of residue interaction networks (RINs) and observed that most RINs, especially those of multi-domain proteins with more than 240 nodes, are not homogeneous networks (class I) but belong to the class of networks that exhibits modularity (class II). Following the spectral scaling method in [23], we determined that all but two of our PRNs belong to class II (Fig. 4c) and are therefore cavity preserving.

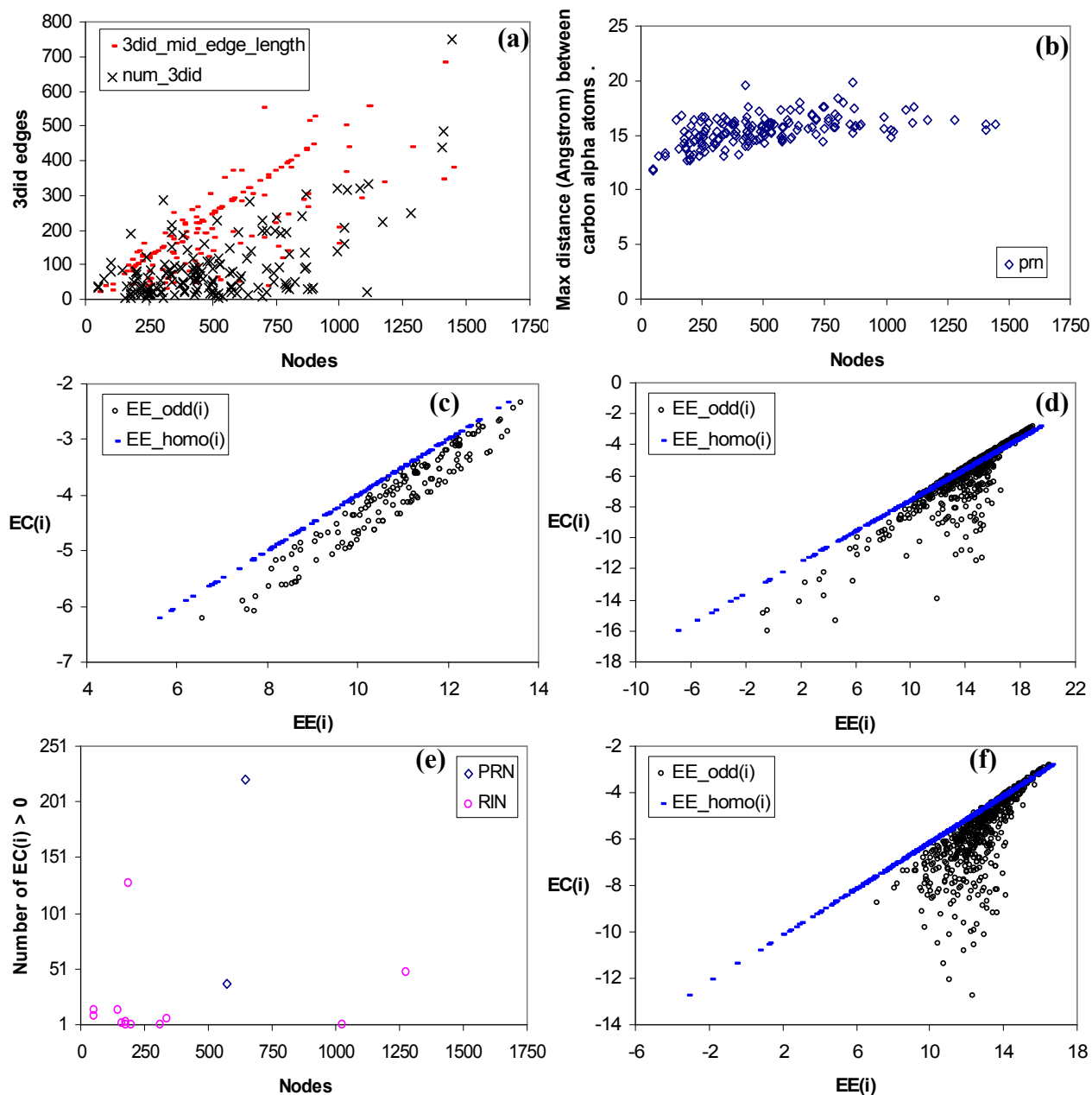


Fig. 4 Although the maximum Euclidean distance between nodes in the 166 PRNs is twice that normally considered in pure (no side-chain consideration) C_{α} - C_{α} or C_{β} - C_{β} contact maps, spectral scaling analysis [23] determined that all but two of the PRNs belong to class II and are therefore cavity preserving. (a) Number of 3did edges and their median sequence distance. (b) The maximum Euclidean distance between nodes in PRNs. (c) Results from the spectral scaling method [23] for the 2FAC PRN which belongs to class II. If the 2FAC PRN is homogeneous, its $EE_{\text{odd}}(i)$ points should fall on the $EE_{\text{homo}}(i)$ line. (d & f) Spectral scaling results for the two PRNs (1YGF and 9LDB) which belong to class IV. In these two plots, there are $EE_{\text{odd}}(i)$ points above the $EE_{\text{homo}}(i)$ line. These two PRNs correspond to the two PRN points in (e). The x- and y- axes in (c, d & f) are log base 2. (e) RIN denotes PRNs that are built as pure C_{α} - C_{α} with 7.5 Å cutoff. The number of RINs belonging to class IV is 12, compared with only two for PRNs. Hence the PRN construction method in this paper allows much larger cutoffs, whilst maintaining the modular structure of proteins.

The other two PRNs belong to class IV (Fig. 4d & 4f). In contrast, when the PRNs were built as pure C_{α} - C_{α} with 7.5 Å cutoff, 12 of the networks belong to class IV (Fig. 4e). This suggests that the PRN

construction method in this paper allows much larger cutoffs, whilst maintaining the modular structure of proteins. Networks in class I are good expanders, i.e. nodes are well connected to all other nodes in the network and therefore the network is less modular and more homogeneous. Networks in class II or class IV exhibit different forms of deviation from class I behavior. In class II, the subgraph centrality of nodes are less than what would be in class I and so the nodes are less well-connected to each other giving rise to modularity and cavities. For completion, class III networks are those with core-periphery structure, which is not found in any of the PRNs tested even when built as pure C_α - C_α with 7.5 Å cutoff.

2.2 MGEO network construction

The MGEO networks are constructed in a similar manner as random geometric networks. Random geometric networks with random coordinates were proposed in [28] as null models for PRNs². However, the MGEO networks use the PDB coordinates of the C_α atoms. To increase the number of single component MGEO networks, the nodes are first connected to form a “backbone” as follows: link u , the most recent node to join the backbone, to a node v which is not already in the backbone and is closest in Euclidean distance to v subject to $|u - v| \geq 2$. The backbone starts with a single node chosen uniformly at random. Due to the way the backbone is constructed, there is no guarantee that the backbone will connect all the nodes in a network. For example, in a network comprising five nodes, if the backbone is built with edge (1, 5) then (5, 3), it is impossible for nodes 2 or 4 to join the backbone. Next, the 3did edges are added. Finally, m edges are added so that a MGEO network will have identical link density as its PRN (Fig. 3a). $m = M - B - D$ where M and D are respectively the number of links and 3did edges of a PRN, and B is the number of links used to construct the backbone. There may be overlap between backbone links and 3did edges. The contact maps of two PRNs and their MGEO4 networks are shown in Fig. 5.

The m edges comprise the shortest (Euclidean distance between the C_α atoms) links such that $|u - v| \geq 2$ and that satisfy the *skip* condition, which defines how many shortest links to ignore between two link inclusion events. The skip condition is introduced to control clustering. Skipping a larger number of shortest links results in a MGEO network with lower C . Thus, the MGEO4 networks, where only every fifth shortest link is included, are significantly less clustered than the MGEO2 networks which include only every third shortest link (Fig. 7b). The 3did edges contribute very little to clustering by themselves, but interact with the other links in a network to form triangles. In fact, 3did edges have significantly larger

² Although [28] reported that random geometric graphs (RGG) have many network statistics that are quantitatively similar to RINs, we note that, apart from the connectivity issue which we address by introducing a “backbone”, the $|LE|/|SE|$ ratio of RGGs depart radically from Fig. 3b and clearly increases linearly with N . The number of short-cuts found by EDS in RGGs is $< N$ and therefore much fewer than the $\sim 2N$ for PRNs and MGEO networks in Fig. 23a. Hence, there are important differences between RGGs and PRNs/RINs. Details in Appendix B.

edge multiplicity (Fig. 8) values than non-3did edges (Fig. 7f). The backbone edges tend to be short (Fig. 6a) and they are not affected by the skip condition.

Every one of the 204 MGEO2 networks formed a single connected component, but only 202 MGEO4 networks were singly connected components. Although more short links are skipped in MGEO4 networks, there is no significant difference in the maximum C α -C α distance spanned by links in the MGEO networks (Fig. 6b). However, the maximum distance of links in MGEO networks is significantly longer than that of PRNs (Fig. 6b) and MGEO networks have significantly larger *LE/SE* ratios (Fig 3b).

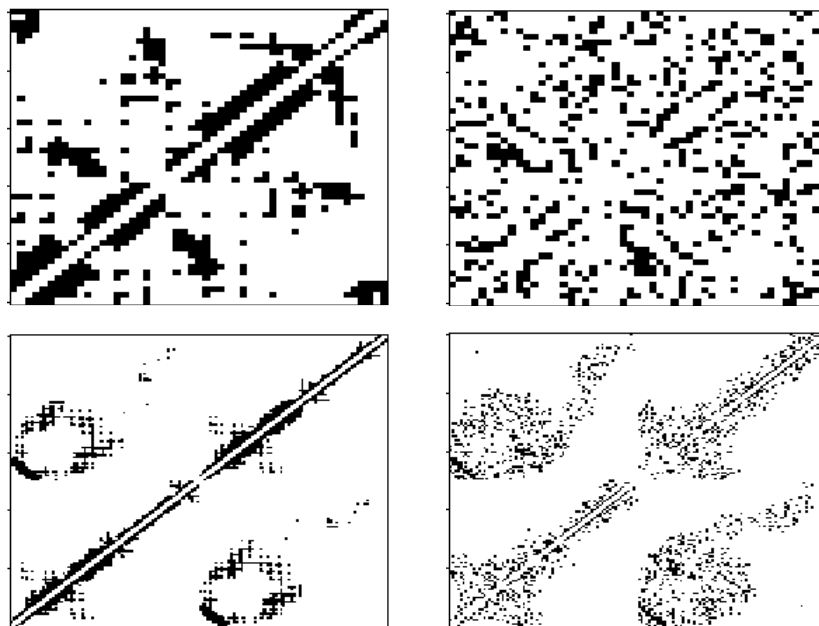


Fig. 5 Contact maps of two PRNs (left) and their respective MGEO4 networks (right). The pair at the top is for protein 1B19 which has 51 nodes and 282 edges. At the bottom, is 2ADL which has 144 nodes and 904 edges. A dark cell denotes an edge. A white cell denotes a non-edge.

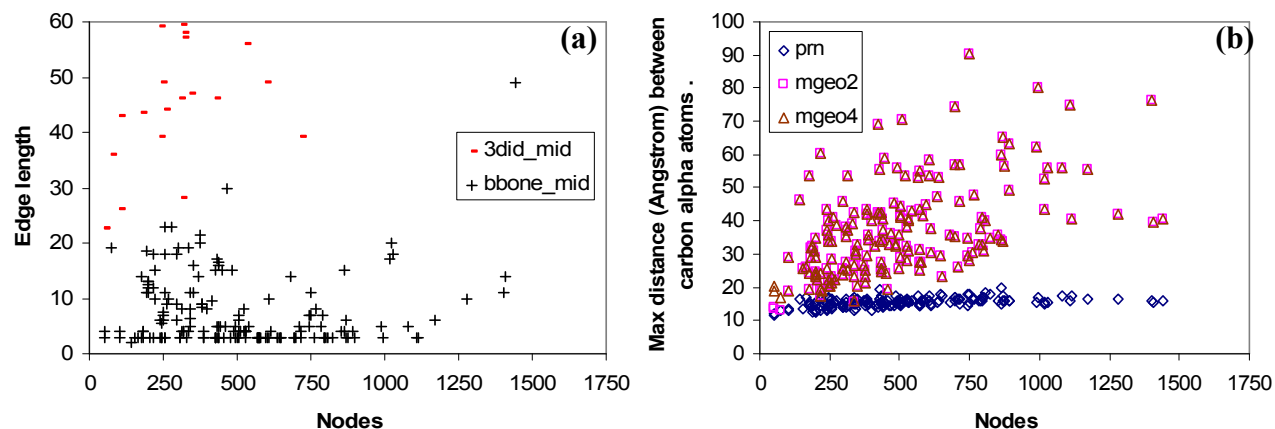


Fig. 6 Edge length (sequence distance) of backbone edges and maximum Euclidean distance of links in MGEO networks. **(a)** The backbone edges introduced into MGEO networks to maintain connectivity are on the shorter side, compared with the 3did links. The median sequence distance of backbone edges in most MGEO networks is less than 20. **(b)** The maximum Euclidean distance between nodes is significantly larger in MGEO networks than in PRNs. Between the MGEO networks, no significant difference in the maximum Euclidean distance between nodes is detected.

2.3 Structural properties of PRNs and MGEO networks

The MGEO2 and MGEO4 networks have identical link density as the PRNs (Fig.3a). Like PRNs, both MGEO2 and MGEO4 networks have Gaussian degree distributions, and we confirm that the MGEO networks have identical average node degree as the PRNs (Fig. 7a). As expected, both MGEO2 and MGEO4 networks have significantly smaller clustering coefficients than PRNs (Fig. 7b). The MGEO4 networks are also significantly less clustered than the MGEO2 networks. These differences in one-vertex clustering extend to dyadic or two-vertex clustering as demonstrated by the significant differences in *edge multiplicity* (Figs. 7c & 7d).

Edge multiplicity (EM) was introduced in [30] and used to quantify the organization of triangles in a network [32]. In its simple form (details about the degree class of the endpoints of edges are ignored here), the multiplicity of an edge e , is the number of distinct triangles that passes through e (Fig.8). $EM \gg 1$ means triangles are packed onto shared edges, or alternatively, edges participate in many triangles. $EM \leq 1$ denotes that the triangles are disjoint. Networks with large EM values have strong transitivity, while those with small EM values have weak transitivity [30]. When the clustering coefficient (which is susceptible to the influence of large node degree variations in scale-free networks) of a network does not reflect the transitivity strength of a network, transitivity strength quantified by EM is a better indicator of the percolation properties of a network than its clustering coefficient [31]. EM is a measure of edge embeddedness, and its use here is equivalent to the number of direct neighbours common to the endpoints of an edge.

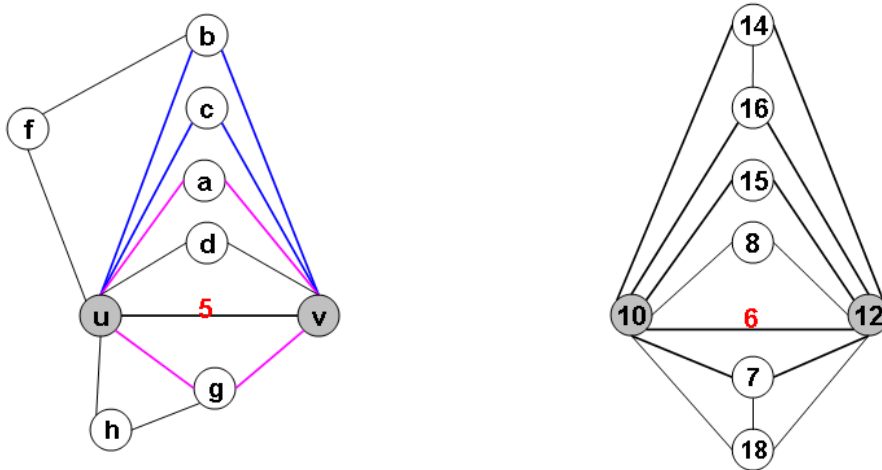


Fig. 8 Edge multiplicity (EM). EM of an edge is the number of triangles the edge completes [30]. In the diagram on the left, EM of edge (u, v) is 5. Nodes u and v also have five direct neighbours in common: $b, c, a, d,$ and g . The blue and pink edges trace out two diamonds (cycles of length four) that are the result of triangles sharing (u, v) . The number of diamonds attached to an edge with EM w is $w(w-1)/2$. Cycles longer than four can form when triangles stick together, e.g. $\langle u, f, b, v, g, h, u \rangle$. The diagram on the right is extracted from the 2FAC PRN. EM of edge $(10, 12)$ is 6.

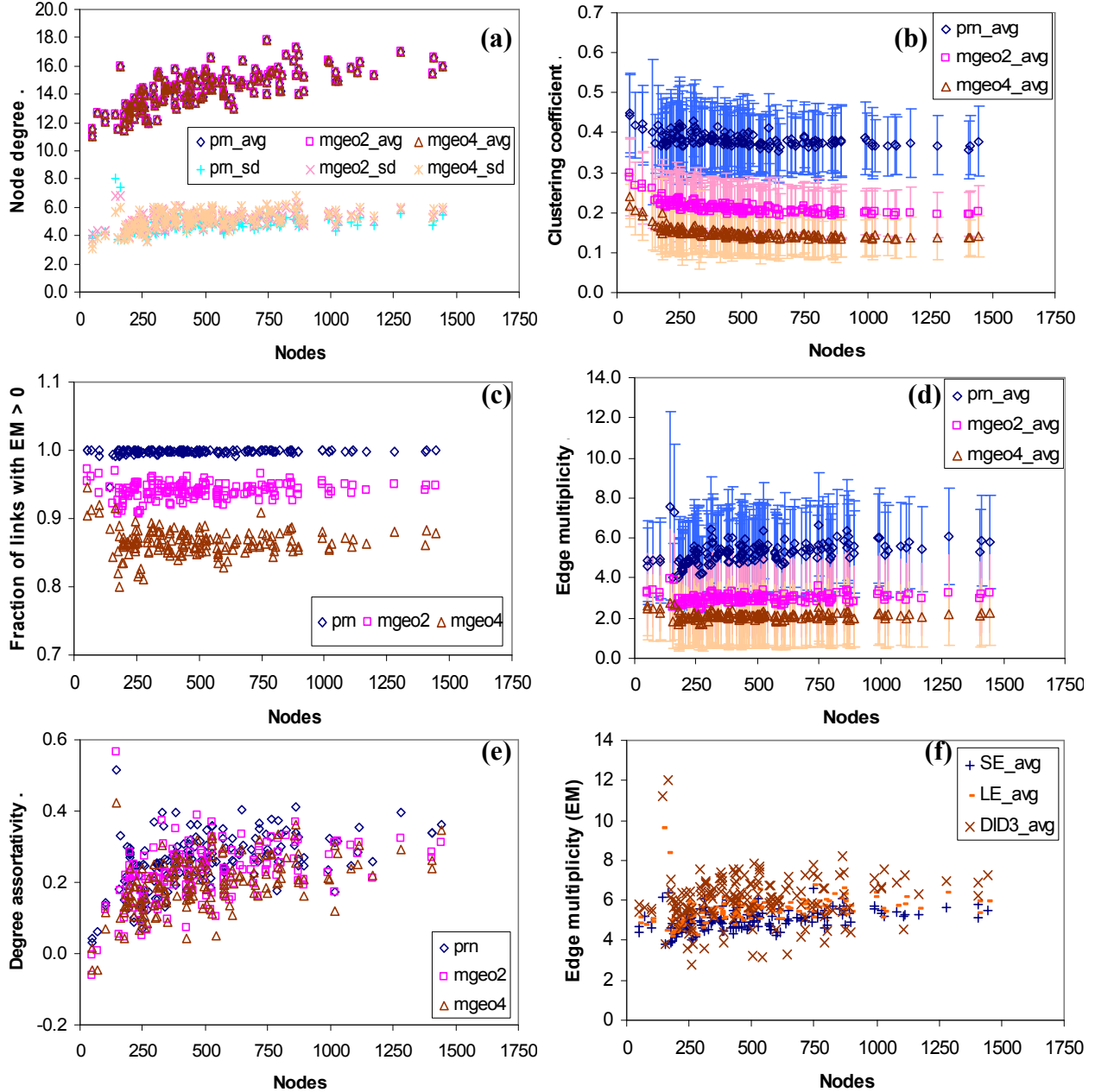


Fig. 7 Structural characteristics of PRNs and MGE0 networks. (a) PRNs and MGE0 networks have Gaussian degree distributions that peak at almost identical average node degrees. (b) The clustering coefficients (C) of PRNs are significantly larger than the C values of MGE0 networks. MGE02 networks have significantly higher clustering than MGE0 4 networks. (c) Almost all PRN edges are part of at least one triangle. Compared with MGE02 edges, a significantly smaller fraction of MGE04 edges have multiplicity > 0 . Edge multiplicity (EM) is the number of distinct triangles that passes through an edge (Fig. 8). (d) PRNs have significantly stronger transitivity than MGE0 networks. The average edge multiplicity of PRN edges is significantly higher than that for MGE0 edges. Stronger transitivity implies more sticky triangles. (e) EM is also the number of direct neighbors common to the endpoints of an edge. Thus it is influenced by degree-degree assortativity, the propensity for nodes with similar degrees to link with each other. Both PRNs and MGE0 networks are mildly positively associative by node degree. (f) Edge multiplicity by edge type. The set of long-range (sequence distance) links, i.e. LE and $DID3$ of a PRN have significantly larger average EM values than the set of short-range links (SE). Nonetheless, we did not find a strong linear correlation between sequence distance and EM . Error bars in (b) and (d) denote one standard deviation around the mean.

Almost all links in PRNs make up a leg of at least one triangle; the fraction is lower in MGEO networks but still above 80% (Fig. 7c). PRNs also have larger EM values than the MGEO networks (Fig. 7d). A large clustering coefficient signals an abundance of triangles and when triangles share edges, they stick together and have the potential to form longer cycles. Large EM values signal an abundance of diamond motifs. The abundance of triangle and diamond motifs induced by the strong transitivity in PRNs makes it feasible as done in [17] to utilize higher order concepts of local organization such as k -cliques and communities (overlapping cliques) to distinguish decoy structures from native ones. Ref. [33] reports a linear relationship between triangle and diamond motifs in their residue interaction networks, and interprets the presence of these local motifs as providing alternative pathways to ensure connectivity as links are made and destroyed when proteins undergo fluctuations at equilibrium. However, their RINs are constructed differently and the diamond motif is also defined differently in [33]. A diamond motif in [33] is a chordless four node cycle. By this definition, nodes b , u , c , and v in Fig. 8 (left) does not form a diamond motif because of the edge between u and v .

The multiplicity of an edge is limited by the degree of its endpoint nodes. Thus, networks whose nodes selectively link by degree, i.e. links are more likely between nodes with similar degrees than between nodes with dissimilar degrees, are more conducive to strong transitivity. Nodes in the PRNs are mildly positively correlated by degree (Fig. 7e). Assortative mixing of nodes by degree has been reported in other residue interaction networks as well [34, 35].

It has been observed that residue interaction networks comprising only long-range links have significantly smaller C values than complete residue interaction networks [27]. In fact, much of the clustering in residue interaction networks have been attributed to short-range links [36]. But even though long-range links (LE) are less transitive than short-range links (SE) when considered separately, when LE and SE are combine in a network, their interaction results in long-range links having significantly larger EM values than short-range links (Fig. 7f). Nonetheless, a strong linear correlation between sequence distance and EM was not observed.

2.4 A Euclidean distance directed local search algorithm (EDS)

In [3, 4], Kleinberg describes a local search algorithm that does greedy routing. In this greedy local search algorithm, information used to decide the next move is confined to the neighbourhood within a small radius of the current node, and the search moves to a neighbouring node that is closest to the target node. As such a greedy local search has *directionality*, i.e. is anisotropic.

Similar to Kleinberg's algorithm, the EDS algorithm does greedy routing based on proximity (Euclidean distance) to a target node. However, EDS differs in two main ways: it keeps a memory of all the nodes visited and enquired so far in the current search, and can therefore back-track and re-route itself

to another more promising path midway through the search. The information used is still local, but this information expands over time as more nodes are visited and their direct neighbours queried for their proximity to the target node. To keep the search local, information gathered during the search for a path is completely forgotten once the path is found. Technically an EDS path is a walk since an EDS path may retrace edges and in the process revisit nodes.

Starting with the source node, EDS performs the steps outlined below for each new node appended to a path until the target node is found. The main steps of the EDS algorithm to find a path from s to d are:

1. Get $N(x)$, the direct neighbors of the most recently visited node x . Initially, x is the source node s .
2. For each n in $N(x)$, compute the Euclidean distance between n and the target node d . (Proximity information for an n to d may already be computed in a previous iteration due to network clustering.)
3. If n is the target node d , stop searching and return path.
4. Otherwise, add the new proximity information to memory, i.e. all distance information gathered so far for this search.
5. Sort nodes in memory by proximity to find the next node to visit, y .
6. Move to y , which is an as yet unvisited node closest to the target. If necessary (when y is not directly reachable from the current node), back-track (retrace the current path but also look at the immediate neighborhood of nodes retraced to find a bridge to y , i.e. a node neighboring y).
7. $x := y$. Go to 1.

The back-track strategy in Step 6 can lead to unnecessary back-tracking. However this apparent inefficiency ensures that the graph an EDS path traces is a tree, and increases the search space for an edge to y . A backtrack stops as soon as an edge to y is found. The search tree begins with a single node, s . In each iteration, the EDS algorithm adds to the existing search tree a single edge with a node not already in the search tree. The only way for EDS to revisit a node is by tracing the edges of the existing search tree. The EDS search is conducted on a finite connected graph and EDS terminates at d .

EDS paths run along the edges of the network. Edges may appear more than once in an EDS path if back-tracking occurs. Edges in an EDS path may be classified as short-cut, back-track, short-cut and backtrack or neither short-cut nor backtrack. An EDS path may have zero or more short-cut and/or backtrack edges. The number of edges in an EDS path is its *length*. Fig. 9 depicts three EDS paths of length four from the 2FAC PRN. The *cost* of an EDS path is the number of unique nodes stored in memory for the search, and is bounded from above by the union of the direct neighbors of all nodes that appear on the path. Table 1 works out the sequence of events to construct the rightmost EDS path in Fig. 9.

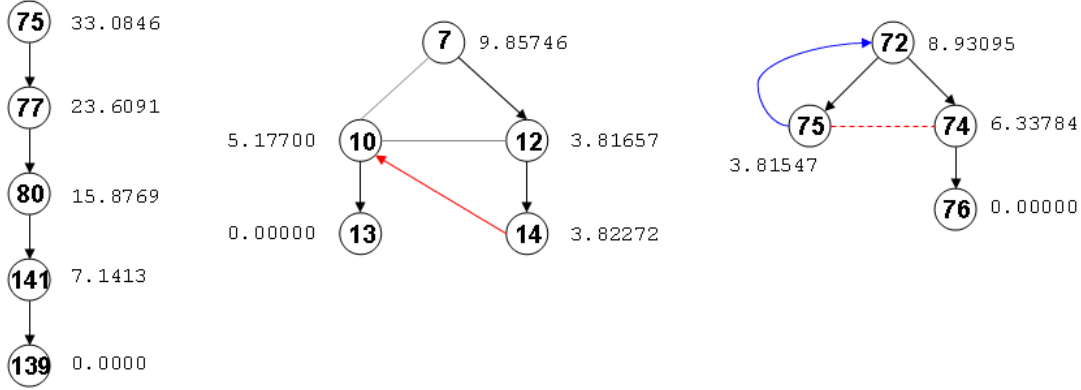


Fig. 9 Three EDS paths of length four in the 2FAC PRN. PRN edges are undirected. The arrowheads are used to show the direction the edges are traversed in the respective paths. The leftmost path is $\langle 75, 77, 80, 141, 139 \rangle$ which is a straight-forward path. The EDS path in the middle is $\langle 7, 12, 14, 10, 13 \rangle$ and it has a *short-cut edge* indicated in red. Without edge $(14, 10)$, EDS would have to backtrack to node 12 to get to node 10. A short-cut edge completes a *navigational cycle*, which in this instance is the triangle comprising nodes 14, 12, and 10. The rightmost EDS path is $\langle 72, 75, 72, 74, 76 \rangle$ and it has a *backtrack edge* indicated in blue. If edge $(75, 74)$ existed, it would be a short-cut edge and the back-track would be avoided. A non-existent short-cut edge marks a *navigational hole*, which in this instance is the two-edge path comprising nodes 75, 72 and 74. Short-cut and back-track edges are defined more formally in the text. The real numbers beside each node are the Euclidean distances to the respective target nodes, which need not decrease monotonically as an EDS progresses. For example, nodes 12 and 14 are much closer to the target node 13 than node 10. The construction of the rightmost path is described in detail in Table 1.

Unlike BFS which guarantees $\lambda(i, j) = \lambda(j, i)$ by definition (undirected graph), an average of 53.50% (std. dev. 6.28%) of EDS path-pairs are not length invariant, i.e. $\lambda(i, j) \neq \lambda(j, i)$. We do not consider this a disadvantage. In fact, if network topology plays a role in determining paths and their lengths, and the topology is not homogeneous everywhere, then $\lambda(i, j) \neq \lambda(j, i)$ is to be expected. For the results in this paper, BFS and EDS searches are run in both directions for each unique ordered node-pair. Average path

length of a network is then redefined as: $L = \frac{1}{N(N-1)} \sum_{i \neq j} \lambda(i, j)$ where $\lambda(i, j)$ is the length of a path (number

of edges in a path) from node i to node j . The total number of paths sampled by both BFS and EDS is $N(N-1)$. For BFS, sampling two possibly different paths per node-pair increases the data available to compute path related statistics such as node centrality and edge betweenness (section 3). EDS paths that are identical either way, and/or identical to BFS paths exists (Table 2). On average, the set of nodes along a BFS path from u to v is only 44% (std. dev. 6.03%) similar with the set of nodes along an EDS path from u to v . This similarity drops significantly to 41% (std. dev. 4.79%) for MGEO4 networks.

Table 1 EDS search for node 76 (target) starting at node 72 (source). At node 72, EDS inspects the 11 direct neighbors of node 72 in random order and computes their respective Euclidean distances to node 76. Since node 75 is the closest to node 76, EDS moves from node 72 to node 75. At this stage, EDS has visited nodes 72 and 75, and has memory of node 72 and its 11 direct neighbors. At node 75, EDS inspects its 11 direct neighbors and adds them to memory. From all the unvisited nodes in memory, EDS finds node 74 to be the closest to the target node. But EDS cannot move directly to node 74 since it is not a direct neighbor of node 75. To visit node 74, EDS must first move or back-track to node 72. At node 74, EDS inspects its 11 direct neighbors in random order, and finds node 76. The maximum cost of this EDS search is 23 (at most 23 unique nodes are visited or inspected in the course of this search). The EDS path is $\langle 72, 75, 72, 74, 76 \rangle$ which has length four. This path is an example of an EDS path with backtracking that is also hierarchical (section 3.6) since its degree path which is $\langle 11, 11, 11, 11, 4 \rangle$ decreases monotonically. The BFS path is $\langle 72, 74, 76 \rangle$. In the reverse direction, the EDS path is $\langle 76, 74, 72 \rangle$ which is also hierarchical since its degree path increases monotonically (section 3.6).

Visited node n	Distance to target node	Inspected nodes (direct neighbors of n)	Level of n	Distance to target node
72 Level = 0 Degree = 11	8.93095	75 74 49 70 2 69 68 67 6 3 65	1 1 1 1 1 1 1 1 1 1 1	3.81547 6.33784 8.08382 11.71590 12.84950 13.61700 13.97110 15.32500 15.50050 16.14170 18.82700
75 Level = 1 Degree = 11	3.81547	51 50 49 73 72 (x) 71 77 48 70 2 5	2 2 2 2 0 2 2 2 1 1 2	7.76938 7.80372 8.08382 8.90625 8.93095 9.10019 11.26160 11.65110 11.71590 12.84950 15.67090
74 Level = 1 Degree = 11	6.33784	76 51 50 49 72 (x) 71 52 70 53 69 57	2 2 2 2 0 2 2 1 2 1 2	0.00000 7.76938 7.80372 8.08382 8.93095 9.10019 11.11780 11.71590 13.05500 13.61700 18.29190
76 Level = 2 Degree = 4	0.00000			

Table 2 Comparing three pairs of EDS pathways through the 2FAC PRN with their BFS counterparts. Paths connecting two nodes need not be symmetrical. Unlike BFS paths, EDS paths connecting a node pair also need not be the same length. An EDS path can be identical to a BFS path.

Source				Target				EDS path	BFS path
Node	Ch	Id	AA	Node	Ch	Id	AA		
75	A	76	GLN	139	B	63	THR	75, 77, 80, 141, 139	75, 77, 80, 141, 139
139	B	63	THR	75	A	76	GLN	139, 144, 83, 78, 48, 75	139, 141, 80, 77, 75
72	A	73	ASN	76	A	77	ALA	72, 75, 72, 74, 76	72, 74, 76
76	A	77	ALA	72	A	73	ASN	76, 74, 72	76, 49, 72
7	A	8	LYS	13	A	14	GLN	7, 12, 14, 10, 13	7, 11, 13
13	A	14	GLN	7	A	8	LYS	13, 8, 6, 10, 7	13, 10, 7

Short-cuts (SC) and navigational cycles: Define $G_{s,d} = (V', E')$ as the sub-graph of a PRN induced by V' , the set of nodes on the EDS path from s to d in the PRN. E' is the subset of edges in the PRN that have both their endpoints in V' . While PRNs are not directed graphs, the edges in $G_{s,d}$ are oriented in the direction they are traversed by the EDS path from s to d . A bi-directional link denotes an edge that has been re-traced in a back-track. The search tree $T_{s,d}$ of an EDS path from s to d is induced by all oriented edges in $G_{s,d}$ and is rooted on s . $T_{s,d}$ spans the nodes of $G_{s,d}$. Let $L^T(x)$ be a non-negative integer denoting the level of node x in a search tree T , and $\mathcal{N}(x)$ be the set of nodes in the connected graph (PRN) adjacent to x . $L^T(s) = 0$. Every n in $\mathcal{N}(x)$ which has not been previously assigned a level is assigned $L^T(x) + 1$. The search tree in Fig. 10 has 6 levels.

Given the sub-graph G' and the search tree T for an EDS path from s to d : an edge (u, v) in T is a short-cut if $L^T(v) \leq L^T(u)$ and there exists an edge (w, v) in G' but not in T . Since $L^T(v) \leq L^T(u)$, there must be at least one other node in T besides u that is adjacent to v ; let w be one of these nodes and W be the set of all such w nodes. To identify the specific w node, EDS retraces its step from u until it finds the *first* (x, v) edge where $x \in W$. The path $\langle u, \dots, x, v \rangle$ together with the short-cut edge (u, v) forms a *navigational cycle*. Hence, short-cut edges complete navigational cycles, and are made possible by cycles in the underlying network. Since x is the first node that is adjacent to v when backtracking from u , navigational cycles are chordless.

The size of a navigational cycle is the number of edges it contains. The length of a short-cut is the size of the navigational cycle it closes less one. Since a short-cut edge may be part of one or more navigational cycles in different EDS searches, the length of a short-cut edge is context sensitive. As a consequence of reduced clustering and transitivity in MGEO networks, short-cut edges are significantly more abundant and significantly shorter in PRNs than in MGEO networks (Figs 12a & 12b).

The sub-graph in Fig. 10 contains one navigational cycle comprising nodes 51, 57, 55, 58, 46 which is completed by the short-cut edge (51, 46). The edge (46, 51) is back-tracked by this EDS search to get to node 56. Suppose, with everything else unchanged, that edge (55, 46) exists in the sub-graph but not in the search tree in Fig. 10. Then the EDS path is unchanged and (51, 46) still forms a short-cut. But

$L^T(46) = 4$, $W = \{55, 58\}$, and the navigational cycle associated with $(51, 46)$ in this EDS search is now circumnavigated by a shorter path: $\langle 51, 57, 55, 46, 51 \rangle$.

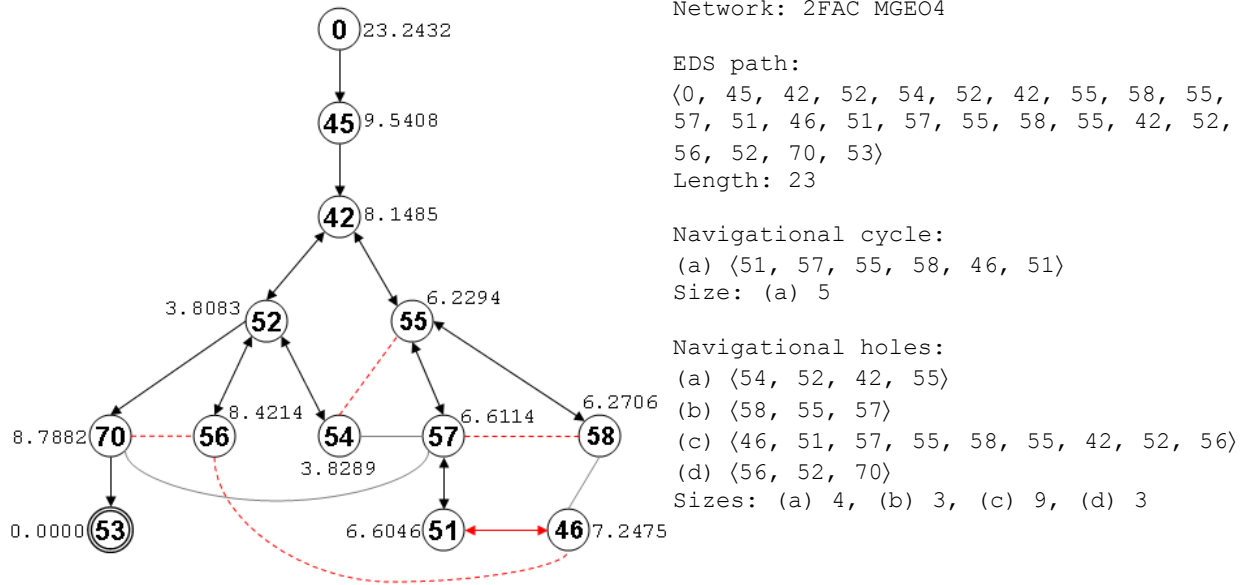


Fig. 10 The sub-graph $G_{0,53}$ for EDS path from 0 to 53 in the 2FAC MGEO4 network. All lines except the red dashed ones are edges of $G_{0,53}$. Edges are oriented in the direction they are traversed by this EDS path. Bi-directional edges are back-track edges. Un-oriented edges are not traversed but exist in the underlying MGEO4 network. The search tree for this EDS path is induced by all the oriented edges. The short-cut edge $(51, 46)$ is marked in red. The red dashed lines indicate the non-existent short-cuts (NESC), i.e. edges that would be short-cuts if they existed in the underlying network, with everything else unchanged. The length of a short-cut is the number of edges in the navigational cycle it closes less one. The length of a NESC is the number of edges in the navigational hole it would close less one. The real numbers beside each node are the Euclidean distances to the target node 53. For comparison, the EDS path from 0 to 53 in 2FAC PRN is a straight-forward path of length four $\langle 0, 2, 71, 51, 53 \rangle$.

Non-existent short-cuts (NESC) and navigational holes: If edge $(51, 46)$ is removed from the sub-graph in Fig. 10, all things being equal, EDS would need to retrace its steps to node 58 to reach node 46 from node 51, and the path $\langle 51, 57, 55, 58, 46 \rangle$ would form a *navigational hole*. Essentially, back-tracks travel along navigational holes until a direct neighbour of the node EDS needs to move to is met. The sub-graph in Fig. 10 has four navigational holes which could be closed by the red dashed edges if these edges exist in the underlying MGEO network. However, since these edges do not exist, they are called *non-existent short-cuts* (NESC). Two of these $(54, 55)$ and $(58, 57)$, cannot exist by our network definition (section 2.3) since their sequence distance is less than 2 (which violates the condition that covalent bonds are excluded from PRNs and their MGEO counterparts).

A NESC is found when EDS needs to move from u to v but (u, v) is not an edge in the network. However, if we assume that (u, v) exists, then (u, v) is a short-cut as defined previously, and a special w node x can be located as described previously. But since (u, v) does not actually exist, EDS adds (x, v) to the search tree instead of (u, v) , and the path $\langle u, \dots, x, v \rangle$ forms a navigational hole. Both navigational

cycles and holes can contain smaller cycles in them due to the back-tracking that was used to find them. E.g.: the largest navigational hole in Fig. 10 contains a cycle $\langle 55, 58, 55 \rangle$.

The size of a navigational hole is the number of edges in an EDS path that circumnavigates it plus one. The length of a non-existent short-cut is the size of the navigational hole it would close if it existed less one. The length of a *NESC* also gives the search depth for an EDS search. As with short-cut edges, the length of *NESCs* may be context dependent. As a consequence of reduced clustering in MGEO networks, *NESCs* are significantly more abundant and significantly longer in MGEO networks than in PRNs (Figs. 12c & 12d).

2.5 Molecular Dynamics simulation (MD) dataset

The dataset is obtained from the Dynameomics project [37, 38, 57]. *ilmm* (in lucem Molecular Mechanics) is used to simulate the native and unfolding dynamics of the mainly beta-sheet 2EZN protein which has 101 amino acids. There are nine MD runs in this dataset, each with a different number of snapshots (Table 3). Snapshots are taken at intervals of 1 ps, except for the first 2 ns of the unfolding runs where snapshots are taken at 0.2 ps. We ignore this detail at present, although this could be relevant for closer analysis of our findings from this MD dataset. A PRN is constructed for every snapshot following the method described in section 2.1. The results we report are produced by averaging over all snapshots in a run.

Table 3 Definition of labels and colors to identify the different 2EZN MD runs.

Run type	Run label	Color in plots	Number of snapshots
Native dynamics (298K)	6250	Black	51,000
Non-native dynamics (498K)	6251	Brown	51,000
	6252	Purple	68,845
	6253	Blue	2,000
	6254	Cyan	2,000
	6255	Green	2,000
	6256	Magenta	10,000
	6257	Orange	10,000
	6258	Yellow	10,000

3. Results

3.1 Path-length: clustering promotes navigability of PRNs

Both BFS and EDS search strategies found short paths in both PRNs and MGEO networks. The average length of both BFS and EDS paths increases logarithmically with increase in N (Fig. 11a), but BFS paths are significantly shorter than EDS paths. This is expected given that backtracking occurs in EDS paths and that BFS by definition should produce the shortest paths. The EDS paths are significantly more varied in length than the BFS paths (Fig. 11b). Large variation in path lengths is more congruent with the picture

of energy flow in globular proteins as “transport on a percolation cluster with channels through which energy flows easily and dead-end regions where energy flow stalls” [20].

MGEO networks have significantly shorter BFS paths than PRNs (Figs. 11c & 11d). In contrast, MGEO networks have significantly longer the EDS paths than PRNs (Figs. 11e & 11f). Thus, at the link density levels of the PRNs (Fig. 3a), the significantly weaker transitivity of the MGEO networks reduces global path length (L_G) but increases local path length (L_W). This result suggests a topological reason for the high levels of clustering in PRNs. Clustering is a barrier to short paths found through global search (BFS), but becomes a facilitator for short paths found with local search (EDS). Given the importance of short intra-protein communication pathways, striving towards (folding) and maintaining a configuration with high clustering makes sense, but only from a local search perspective. The benefit of high clustering in a protein’s native state, in terms of short intra-protein paths, may also act as a topological barrier preventing its unfolding. Thus we observe a significant gap in C and L values between native protein dynamics and protein unfolding (Fig. 1).

The effect clustering has on BFS path length follows from the relationship: $L_{ER} \sim \ln(N) / \ln(K)$. Random graphs have little to no clustering and are locally tree-like. The average degree K in ER graphs then approximates the branching factor of a search tree. By introducing cycles into the search tree, some of the branches now loop back to a previous tree level. In other words, clustering reduces the effective branching factor, or effective K . Consequently, L_G increases. But an increasing average path-length concomitant with an increasing clustering coefficient does not fit the picture in Fig. 2.

An explanation for the effect clustering has on EDS path length follows. Unlike the BFS strategy of branch first then prune (when the target node is found), EDS prunes first (or branches conservatively) then if necessary (with the help of backtracking) figures out how to branch further. Define the number of edges retraced to branch onto a more promising path as the *depth* of a search (search depth is also the length of a non-existence short-cut NESC, section 2.4). The search depth for PRNs is significantly shallower than the search depth for MGEO networks (Fig. 12d), which means that on average, EDS retraces fewer edges when searching PRNs than MGEO networks. EDS also does significantly less backtracking when searching PRNs than MGEO networks (Fig. 12f). Thus, PRNs have significantly shorter average EDS path length than MGEO networks.

The shallower search depths and fewer backtracking paths of PRNs are a consequence of their higher levels of clustering and stronger transitivity (Figs. 7b & 7d) which enrich PRNs with potential short-cut edges. The clustering coefficient C is a measure of the number of cycles of length three. Longer cycles are more possible when triangles are sticky than when they tend to exist in isolation (Fig. 8). In contrast, the lower levels of clustering and weaker transitivity of MGEO networks create significantly more navigational holes (Fig. 12c).

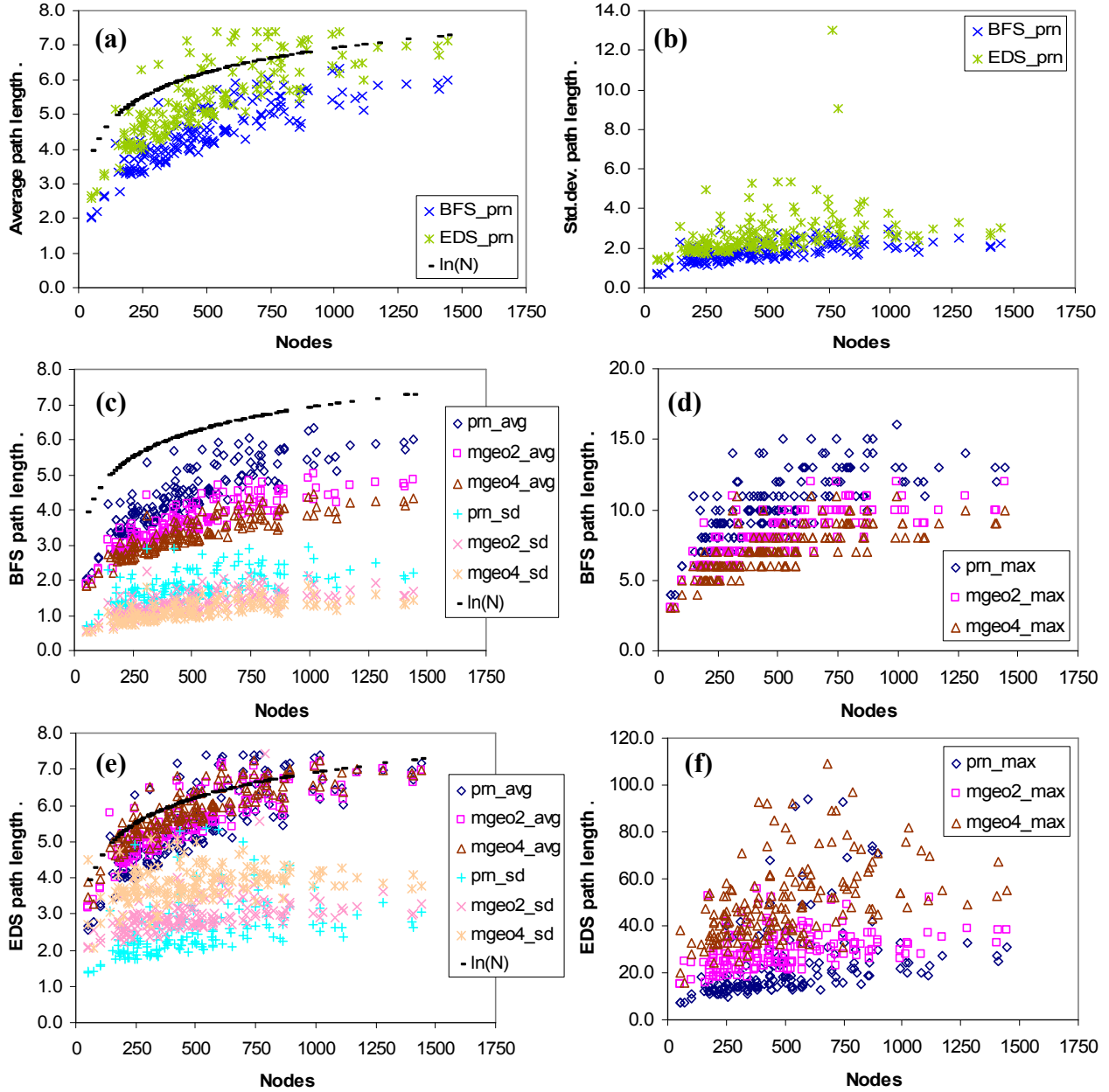


Fig. 11 Average path length. (a) Short paths are found by both BFS and EDS for both PRNs and MGE0 networks. The average length of both BFS and EDS paths increase logarithmically with N , but BFS paths are significantly shorter than EDS paths. This is expected given that backtracking occurs in EDS paths and that BFS by definition should produce the shortest path lengths. (b) The EDS paths are more varied in length than the BFS paths. The standard deviations for EDS path lengths of PRNs are significantly larger than the standard deviations for BFS path lengths of PRNs. (c & d) Both average and maximum BFS path length increase with clustering. PRNs have significantly longer average BFS path length than their less clustered MGE0 counterparts. (e & f) Both average and maximum EDS path length decrease with clustering. PRNs have significantly shorter average EDS path length than their less clustered MGE0 counterparts.

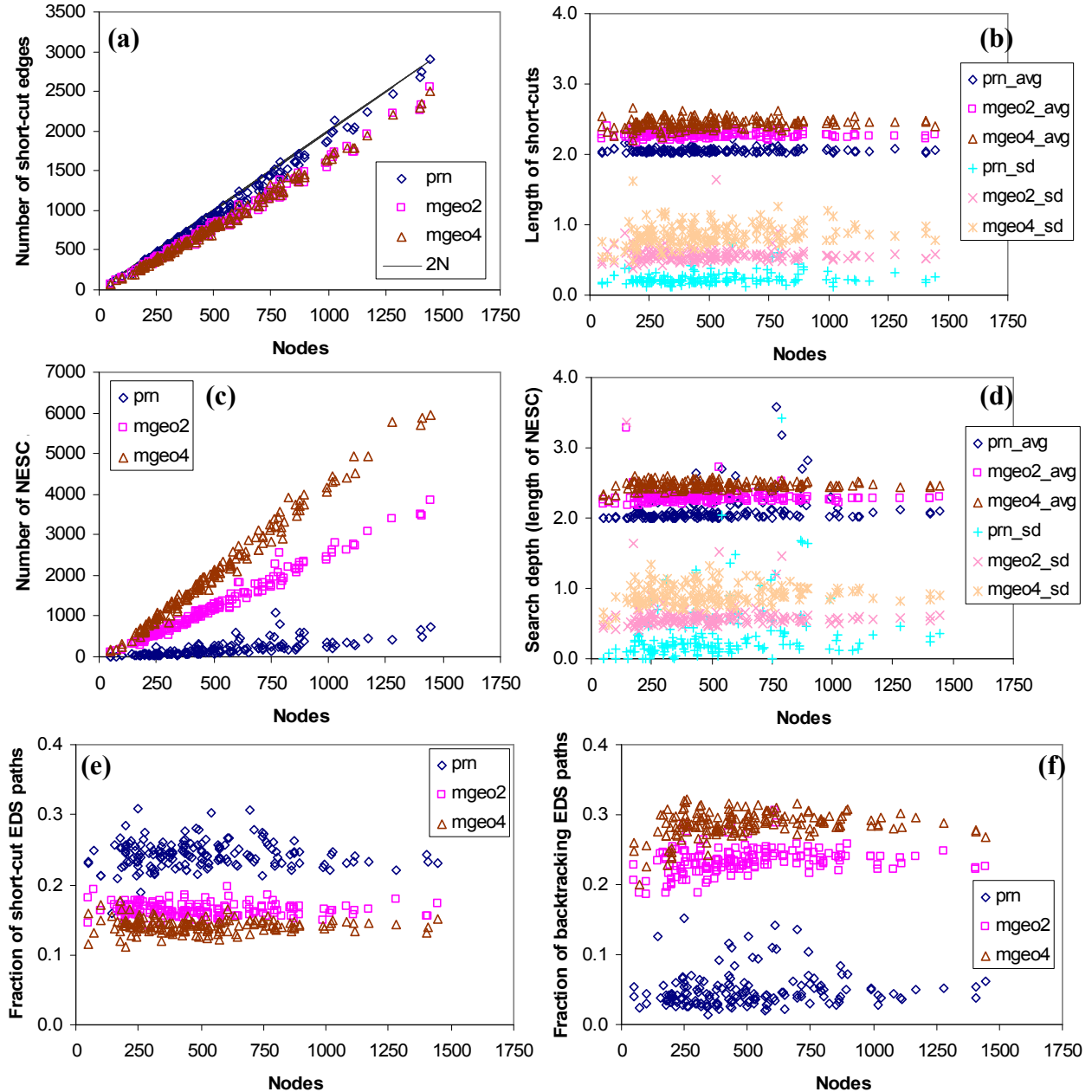


Fig.12 The more clustered PRNs have more short-cuts and fewer backtracking paths. (a) PRNs have significantly more short-cuts than MGEONetworks. The number of short-cuts in PRNs is about twice the number of nodes in a network, $|SC| \sim 2N$ (Fig. 24a). **(b)** The short-cuts in PRNs are significantly shorter than the short-cuts in MGEONetworks. The length of a short-cut is the size of the navigational cycle it closes less one (section 2.4). A short-cut may close more than one navigational cycle of different size. We recorded all lengths for each short-cut, and report the average length over all short-cuts found by EDS in a network. **(c)** MGEONetworks have significantly more non-existent short-cut edges (*NESC*) than PRNs. *NESCs* are missing bridges (section 2.4). Because they are missing, EDS needs to backtrack. **(d)** MGEONetworks have significantly longer *NESCs* than PRNs. The length of an *NESC* is the size of the navigational hole it would close if it existed less one (section 2.4). The length of an *NESC* is also the number of edges EDS needs to retrace when backtracking, i.e. search depth. Since an *NESC* can be part of more than one navigational hole of different size, we recorded all lengths for each *NESC*, and report the average length over all *NESCs* found by EDS in a network. **(e)** EDS paths in PRNs are more likely to contain short-cut edges than EDS paths in MGEONetworks. **(f)** EDS is more likely to backtrack in MGEONetworks than in PRNs.

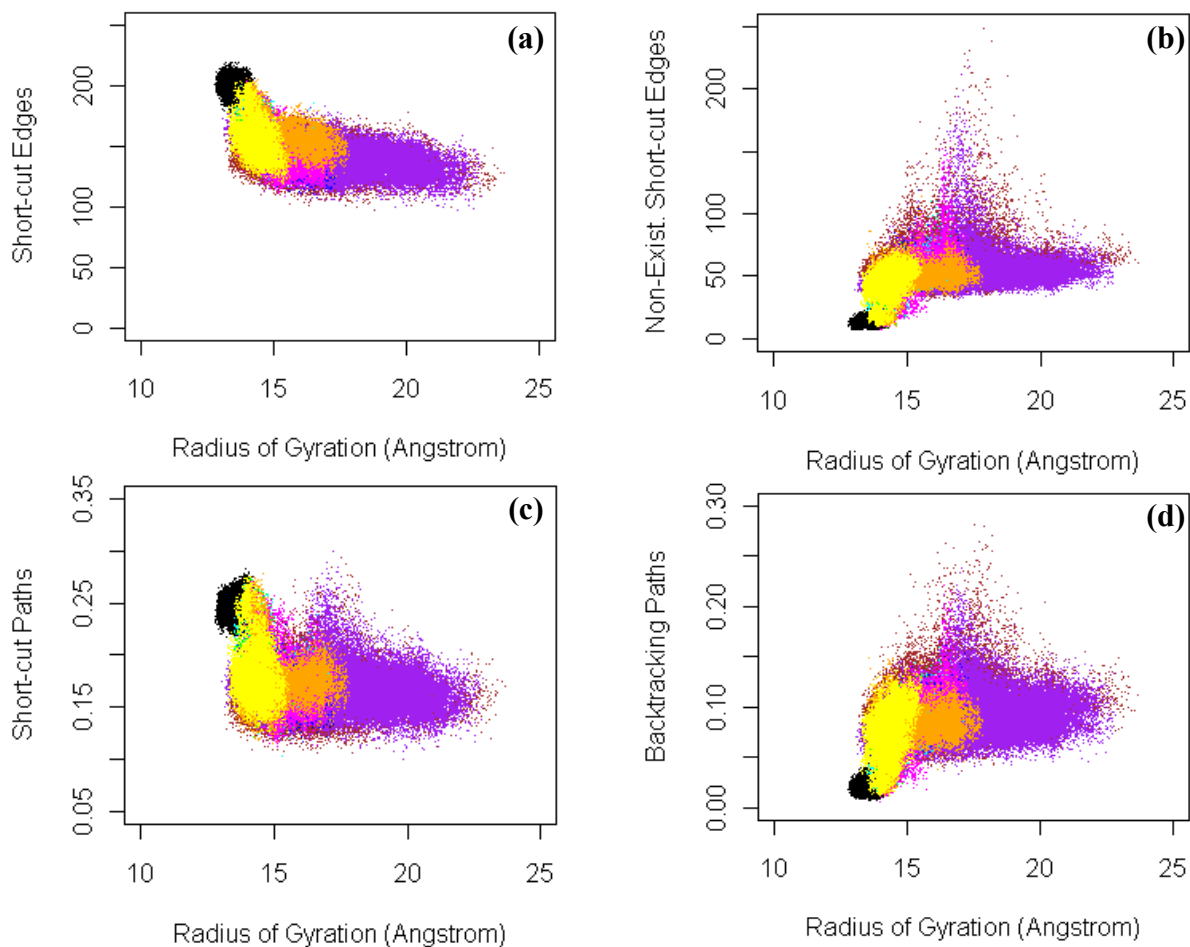


Fig. 13 Short-cuts and backtracks in the 2EZN MD simulation. As the protein becomes more compact (radius of gyration decreases), generally: **(a)** the number of short-cut edges increases, **(b)** the number of non-existent short-cuts decreases, **(c)** the fraction of EDS paths containing at least one short-cut increases, and **(d)** the fraction of EDS paths doing at least one backtrack decreases. In the four plots, the points in black denote data from the native dynamics run 6250, while the non-black points come from the rest of the eight runs simulating non-native dynamics (section 2.5).

The short-cut edges which are significantly more abundant in PRNs than in MGEO networks (Fig. 12a) reduce the need for and the extent of backtracking, which in turn keeps the length of EDS paths in check. So while cycles pose a problem for global search (BFS) and increase L_G , they help local search (EDS) to decrease L_W . In the MD simulations on 2EZN, as the protein becomes more compact (Fig. 13), generally: (a) the number of short-cut edges increases, (b) the number of non-existent short-cuts decreases, (c) the fraction of EDS containing at least one short-cut increases, and (d) the fraction of EDS paths doing at least one backtrack decreases. From Fig. 2, we know that clustering and edge multiplicity increases while average path length decreases as the protein becomes more compact in these runs. Taken together, the observations from the MD simulations on 2EZN are aligned with the results in Fig. 12 which

are made for PRNs – that clustering (and strong transitivity) facilitates navigation by increasing short-cuts and reducing backtracking.

When short-cut edges are removed from PRNs, there is significant increase in both BFS and EDS average path length (Figs. 14a & 14b). This is understandable since the reduced network ($PRN \setminus SC$) has fewer links. However, the increase in EDS average path length (L_{EDS}) is significantly larger than when a corresponding number of random edges are removed from PRNs (Fig. 14d). Hence, short-cut edges have a significant impact on L_{EDS} and are a non-random subset of PRN links. In contrast, the increase in BFS average path length is significantly smaller than when a corresponding number of random edges are removed from PRNs (Fig. 14c).

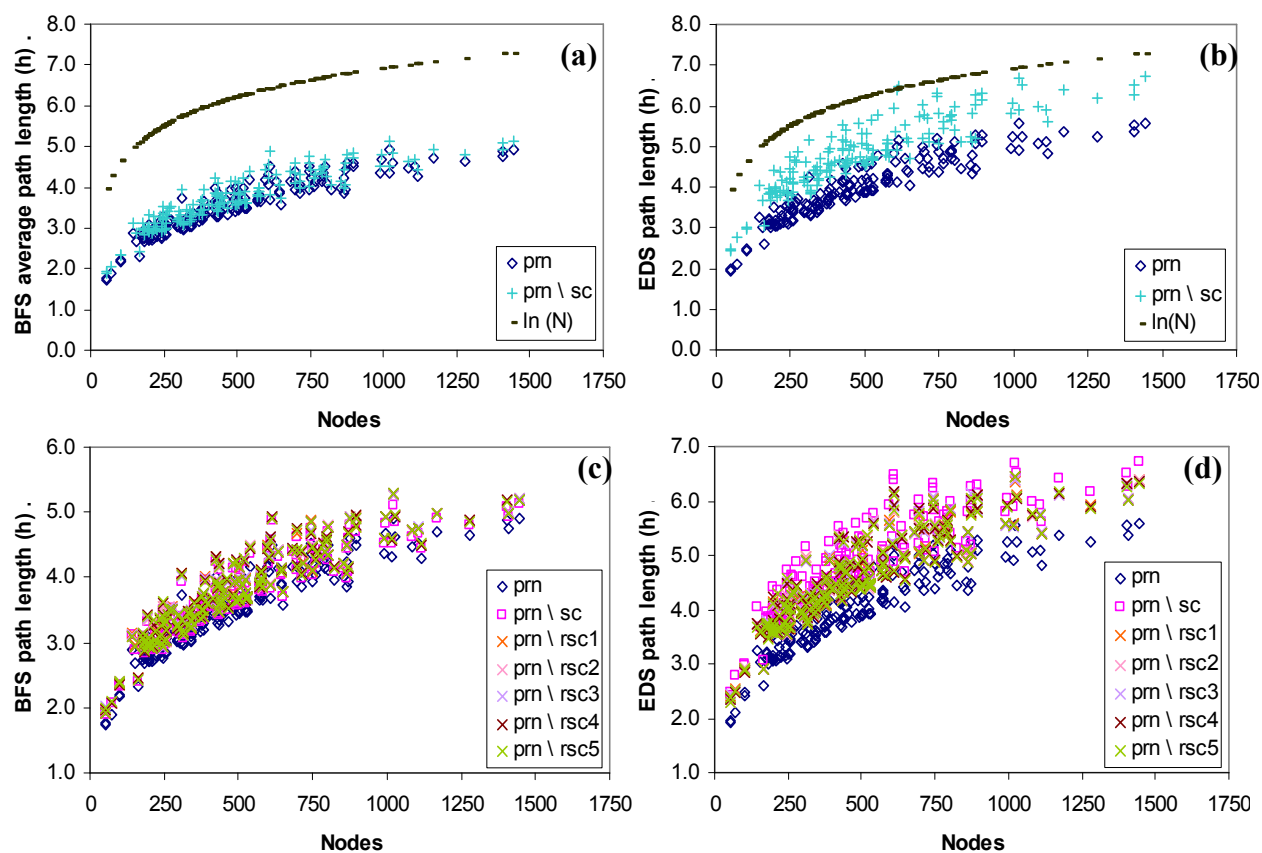


Fig. 14 Effect of short-cut edges on average path length. (a & b) Removal of short-cut edges from PRNs (denoted $prn \setminus sc$) significantly increases the lengths of both BFS and EDS paths, but the effect is greater for EDS paths. (c & d) rsc denotes a set of random edges identical in size to sc of each PRN. Five such sets were created with a different random seed number each time. Removal of rsc from PRNs also increased the lengths of BFS and EDS paths. However, on average, $prn \setminus sc$ produces significantly longer EDS paths than $prn \setminus rsc$. Hence the set of short-cuts for a PRN is a distinct set of edges. Since removing edges could potentially disconnect a PRN, the harmonic mean method of calculating average path length [6] (indicated by h) is used in these figures.

3.2 Search cost: EDS touches fewer nodes when path seeking

Define the cost of finding a path from node s to node d as the number of unique nodes in the network that is touched by an algorithm when searching for the path. The search cost of a BFS path is the number of unique nodes visited by the BFS algorithm. The search cost of an EDS path is the number of unique nodes stored in memory (visited and enquired) by the EDS algorithm (see Table 1 for an example). Due to the more diffusive nature of BFS, BFS paths rapidly become more expensive than EDS paths. BFS search cost increases linearly with network size, while EDS search cost scales logarithmically with N (Fig. 15).

Unlike BFS, EDS defers branching into other paths and only develops the path which appears most promising at the time. EDS touches only the direct neighbours of a node at each step of the way on a path. Thus, the cost of an EDS path p is at most the cardinality of the union of the direct neighbors of all nodes on p , and is unaffected by backtracking. Due to heavy clustering, average EDS cost of a path is much less than $\langle k \rangle \ln(N)$ and approximates $(1-C)\langle k \rangle \ln(N)$ (Fig. 15b). Both mean node degree $\langle k \rangle$ and the clustering coefficient C are almost constant for PRNs and MGEO networks (Fig. 7b). BFS search cost is unaffected by changes in network clustering introduced via the MGEO networks (Fig. 15a). However, reduced clustering has an inflationary effect on EDS search cost. EDS paths on PRNs are significantly less costly to find than EDS paths on MGEO networks (Fig. 15b). The lower search cost is another motivation for proteins to stay folded and maintain higher clustering.

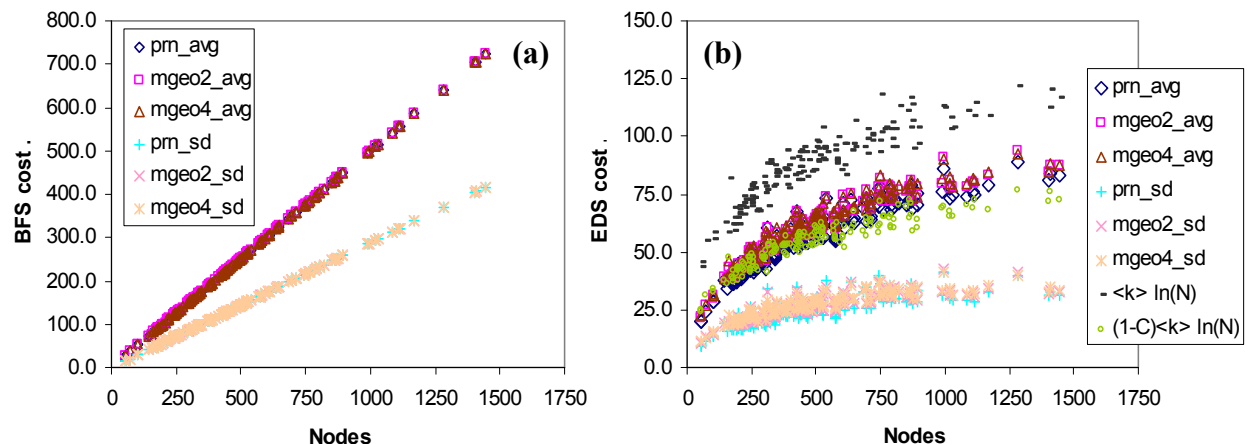


Fig. 15 Average cost of finding path. The cost of finding a path from node s to node d is the number unique nodes in the network that is touched by an algorithm when searching for the path. **(a)** BFS search cost increases linearly with the number of nodes in a network, N , and it is unaffected by changes in clustering. **(b)** EDS search cost scales logarithmically with N . The cost of an EDS path p is at most the cardinality of the union of the direct neighbors of all nodes on p , which due to heavy clustering is much less than $\langle k \rangle \ln(N)$ and approximates $(1-C)\langle k \rangle \ln(N)$. EDS search cost is affected by changes in clustering. Reduced clustering increases EDS search cost. EDS paths on PRNs are significantly less costly to find than EDS paths on MGEO networks.

3.3 Closeness centrality: EDS rank strongly correlates with BFS rank

A node is close to other nodes in the network if it is reachable via short paths. A node with high closeness centrality has a low average distance to other nodes in the network. Hence, closeness centrality of a node is inversely related to the length of the paths starting from node i to all the other $N-1$ nodes in the network: $CL_i = (N-1) / \sum_{j \neq i} \lambda(i, j)$. The average closeness centrality for a network with N nodes is:

$CL = \frac{1}{N} \sum_i CL_i$. Since closeness centrality is a topological measure based on path-length, it too is influenced by clustering.

The decreased levels of clustering in the MGEO networks decreases the length of BFS paths and thus average BFS closeness is significantly higher in MGEO networks than PRNs (Fig. 16a). In contrast, EDS closeness centrality decreases significantly when clustering decreases (Fig. 16b). EDS closeness centrality responds to changes in clustering in a way that is more in keeping with the notion that as a protein becomes more compact, clustering increases and nodes get closer to each other both in Euclidean distance and in graph distance.

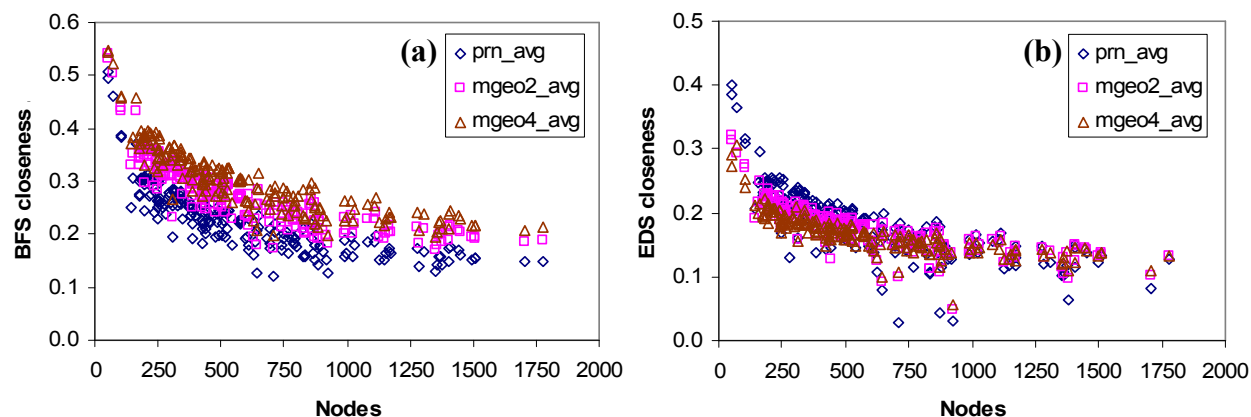


Fig. 16 Closeness centrality. (a) BFS closeness centrality decreases with increase in clustering. (b) EDS closeness centrality increases with clustering.

Closeness centrality has been applied to detect functional protein sites [39] and identify possible protein folding nucleation sites [41]. A strong and positive correlation between BFS and EDS closeness centrality rank is found, and this correlation is significantly stronger for PRNs than MGEO networks. The average Pearson correlation for PRN, MGEO2 and MGEO4 networks respectively are 0.9716 (std. dev. = 0.0470), 0.9541 (std. dev. = 0.0435) and 0.9329 (std. dev. = 0.0573). This means that nodes that are ranked highly by BFS closeness centrality are also likely to be ranked highly by EDS closeness centrality (Fig. 17).

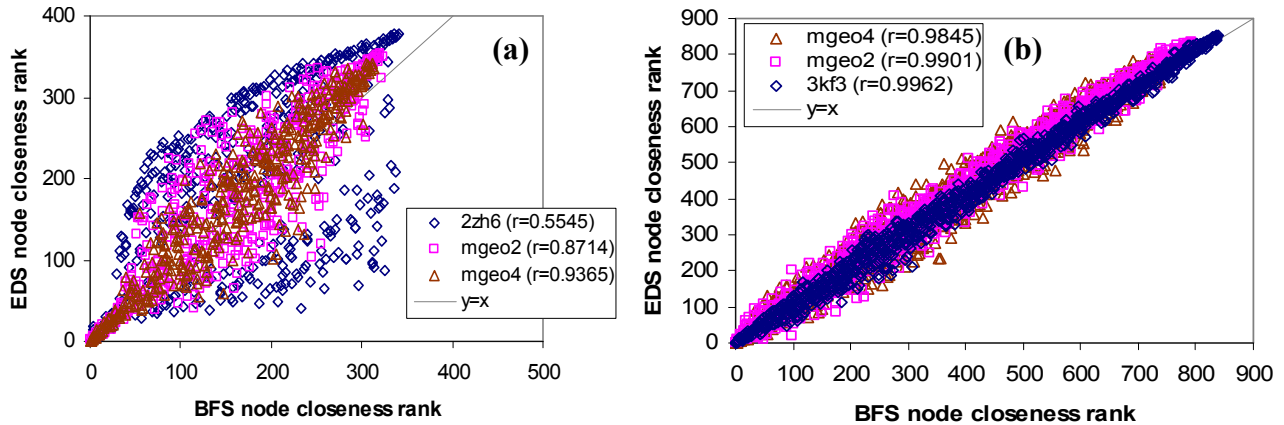


Fig. 17 BFS and EDS closeness centrality rank are strongly and positively correlated. Closeness CL_i is calculated for every node i in a network and the nodes are ranked by their CL_i values. E.g. if node 1 has the second largest BFS node closeness value and the largest EDS node closeness value, then its BFS node closeness rank is 2 and its EDS node closeness rank is 1. In the two scatter plots, each point compares the BFS closeness rank of a node with its EDS closeness rank. The protein in (a) is 2ZH6, chosen because its PRN has one of the smallest Pearson correlation coefficients (r), and because its correlation exhibits divergent behavior by gaining in strength as clustering decreases. The protein in (b) is 3KF3, chosen because its PRN has one of the largest Pearson correlation coefficients, which decreases as clustering decreases.

3.4 Node centrality: EDS rank strongly correlates with BFS rank

Node centrality is a measure of a node's involvement in the dynamics of a network. It has been quantified in a number of ways: by node degree, number of shortest paths passing through a node, and number of random walks passing through a node [56]. Ref. [2] observed that node centrality (using the shortest path method) changes as a protein folds towards its native state and that residues with high (large) node centrality during the transition state play a critical role in the folding process. We use the following definition of node centrality: Given a set of paths P , the centrality of a node v is the number of times paths in P passes through it, i.e. enter and exit, v .

There is a strong positive correlation between BFS node centrality and EDS node centrality, and the correlation is significantly stronger with PRNs than with the MGEO networks. The average Pearson correlation for PRN, MGEO2 and MGEO4 networks respectively are 0.9018 (std. dev. = 0.0341), 0.8425 (std. dev. = 0.0431) and 0.8117 (std. dev. = 0.0580). This means that nodes that are ranked highly by BFS node centrality are also likely to be ranked highly by EDS node centrality (Fig. 18).

The strong correlation between BFS and EDS node centrality rank, and between BFS and EDS closeness centrality rank, are encouraging from a practical perspective because it implies the transferability of existing research based on BFS, e.g. [39, 40, 41], and also the possibility of improving upon existing results with EDS.

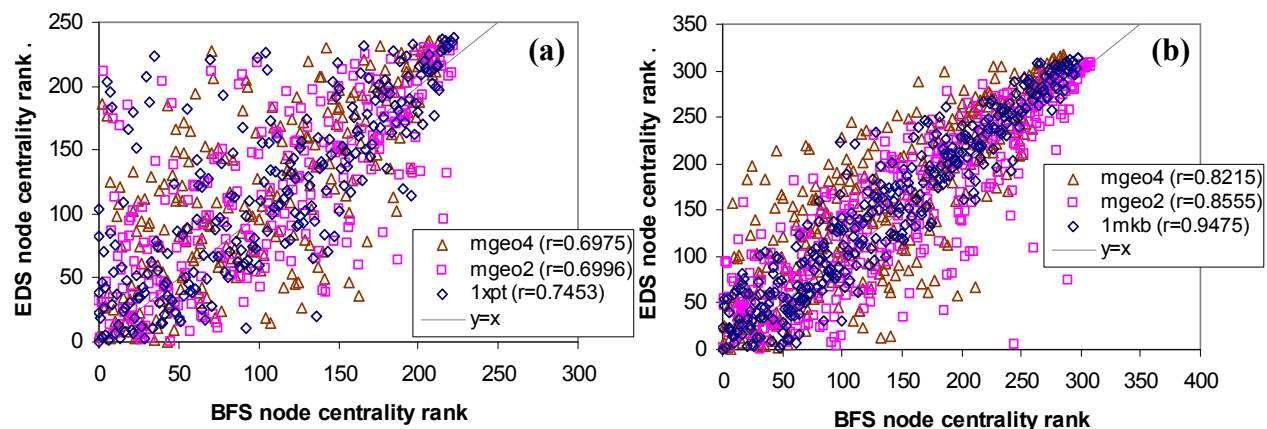


Fig. 18 BFS and EDS node centrality rank are strongly and positively correlated. Node centrality is calculated for every node in a network and the nodes are ranked by their centrality values. E.g. if node 1 has the largest BFS node centrality value and the second largest EDS node centrality value, then its BFS rank is 1 and its EDS rank is 2. In the two scatter plots, each point compares the BFS node centrality rank of a node with its EDS node centrality rank. The protein in **(a)** is 1XPT, chosen because its PRN has one of the smallest Pearson correlation coefficients (r), which decreases as clustering decreases. The protein in **(b)** is 1MKB, chosen because its PRN has one of the largest Pearson correlation coefficients, which also decreases as clustering decreases.

3.5 Link usage: EDS paths make more use of short-range links and 3did links than BFS paths

Short-range links are those with sequence distance $|u - v| \leq 10$ (section 2.1). Protein sequence distance is a familiar and meaningful metric in protein research. There is much discussion about the role of short- and long-range contacts in proteins [10]. There is a behavioral cost to the presence of long-range links in PRNs. Larger proteins with more long-range links tend to fold more slowly [42, 43, 44, 45]. There is also an entropic cost to the formation of long-range links early in protein folding as the conformational possibilities of a sequence segment book-ended by a long-range contact is greatly reduced [46]. And indeed, the ratio of long-range to short-range links (LE/SE) increases for PRN edges as the 2EZN protein folds under MD simulation, and so does the LE/SE ratio for short-cut edges (Fig. 19). The bias towards the appearance of short-range links before long-range links accords with the framework model of protein folding which envisions protein folding as ascending a hierarchy of more complex forms starting from the secondary structure elements and progressing to higher order folds that comprise the organization of lower order elements. This process need not however exclude the necessity for feedback between the levels of organization [63]. In spatial networks, where nodes are located in a metric space e.g.: transportation and neural networks, links cover actual physical distances and as such longer links have a higher wiring cost [47]. For these reasons, relying more heavily on shorter links is deemed preferable.

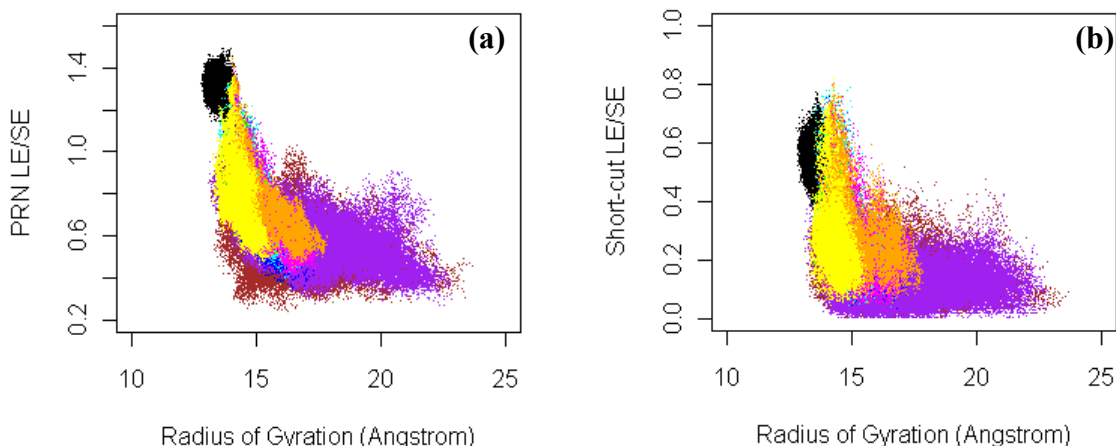


Fig. 19 The ratio of long-range to short-range links (LE/SE) for (a) PRN edges and (b) short-cut edges increases as the 2EZN protein folds under MD simulation. The LE/SE ratio for short-cut edges is less than 1.0.

Usage of an edge e is incremented by one with each traversal of e by a path. We observe that BFS paths are more biased towards long-range links than EDS paths (Fig. 20a). Since BFS paths are significantly shorter on average than EDS paths (Fig. 11a), link usage was normalized by average path length prior to statistical testing. We find after normalization that: (i) BFS paths make significantly less use of short-range links than EDS paths; (ii) BFS paths make significantly greater use of long-range links than EDS paths; and (iii) BFS paths make significantly less use of 3did links than EDS paths (Fig. 20b).

Short-cut edges identified by EDS paths are predominantly short-range (Fig. 21). In Fig. 19b, the LE/SE ratio for short-cut edges is less than 1.0. The cutoff of 10 residues was chosen so that links within secondary structure elements would be short-range (on average an α -helix is 11 residues in length and a β -strand, 6 residues) [27]. There is some experimental evidence that energy in proteins is transported via secondary structures [59, 60, 61]. Energy transfer is faster in helices (reaching the speed of sound if the helices are rigid) and slower in the hydrogen bond network of beta sheets. And indeed, EDS paths make heavier use of short-cut edges than non-short-cut edges (Fig. 22). This is so not only for PRNs of configurations at equilibrium, but also for PRNs of configurations not at equilibrium (Fig. 22c). EDS paths make significantly more use of short-cuts than non-short-cut links (Fig. 22a), and the length of EDS paths that traverse short-cuts are also longer (Fig. 22b), i.e. short-cuts are not only more central, they also carry heavier loads on average. A more detailed study of the EDS paths between protein binding sites is desirable. It may also be interesting to extend the idea of local search to inter-protein communication channels, e.g. in protein complexes.

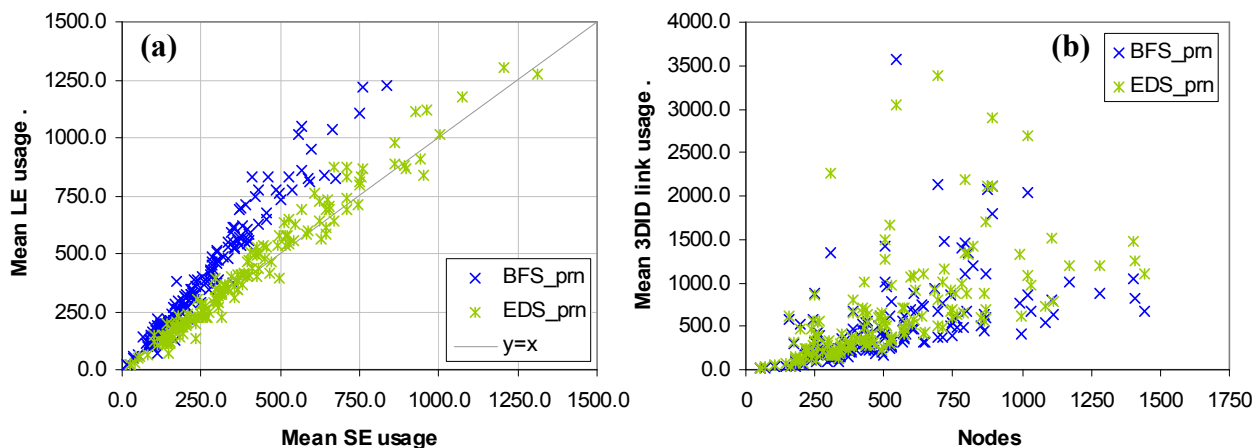


Fig. 20 EDS paths make significantly more use of short-range links than long-range links, and significantly more use of 3did links than BFS paths. Usage of an edge e is incremented by one with each traversal of e by a path. Each point in the plot reports the results for one of the 166 PRNs. **(a)** BFS paths are more biased towards long-range links than EDS paths. **(b)** BFS paths make significantly less use of 3did links than EDS paths.

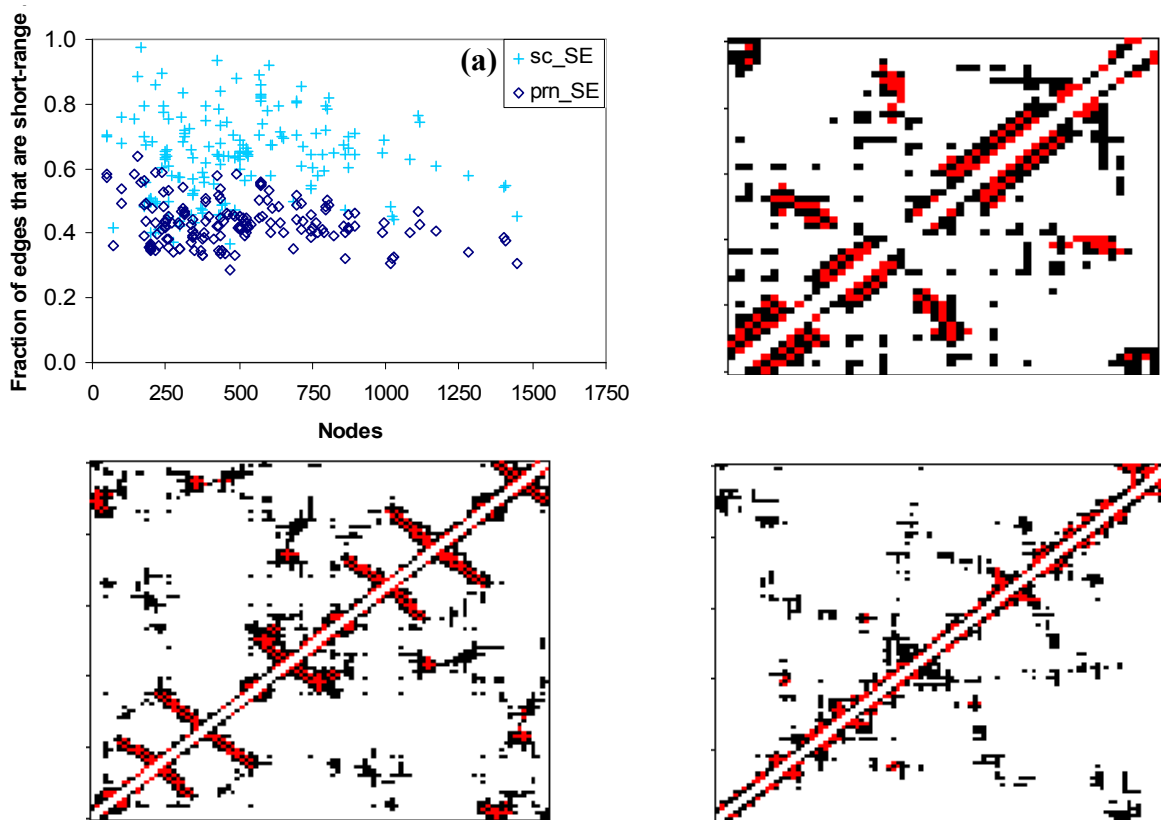


Fig. 21 Short-cut edges are significantly enriched with short-range links (SE). **Top left (a):** On average, 63.91% (std. dev. = 12.84%) of short-cut edge sets are comprised of short-range links, while 43.42% (std. dev.=6.95%) of PRN links are short-range. The cutoff of 10 residues was chosen so that links within secondary structure elements would be short-range (the average length of an α -helix is 11 residues and for a β -strand is 6 residues) [27]. **Top right:** The 1B19 PRN in contact map form as in Fig 5 but with cells representing short-cut edges in red. The majority of the red cells hug the main diagonal where the protein's three alpha helix structures are located. In contact maps, alpha helix contacts are located along the main diagonal, and beta sheet contacts are situated either parallel or perpendicular to the main diagonal [8]. **Bottom left:** Contact map for a 2EZN (beta sheet rich) native configuration with short-cuts indicated by red cells. **Bottom right:** Contact map for a 2EZN non-native configuration – the beta sheets are not discernable yet at this stage.

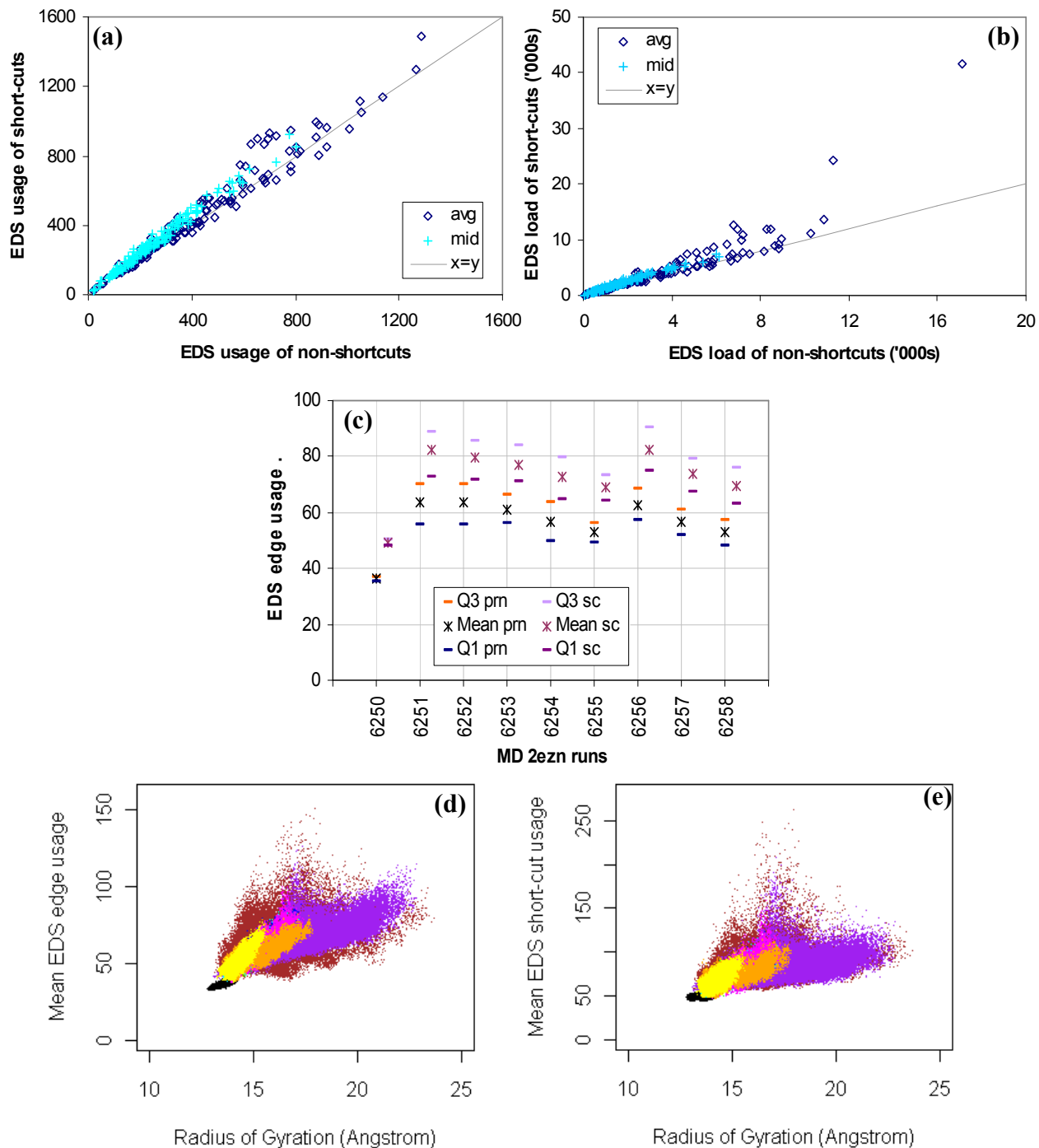


Fig. 22 EDS paths make heavier use of short-cuts than non-short-cut edges. (a) Short-cut edges see significantly more use than non-short-cut edges on average. (b) Significantly longer EDS paths traverse short-cuts than non-short-cut edges. (c) Short-cuts are also used more heavily than non-shortcut edges in non-equilibrium configurations. (d) EDS usage of PRN edges decreases on average as links increase and paths become more diverse during protein folding (Fig. 29a). (e) Average EDS usage of short-cut edges also decreases as short-cut links increase during protein folding (Fig. 13a).

3.6 Path analysis: EDS paths are hierarchical

Kleinberg describes his decentralized (local search) algorithm as homing in on a target node [4]. For PRNs however, even in EDS paths with no backtracking, Euclidean distance to target need not decrease monotonically. But for a fraction of EDS paths (and BFS paths), what does change monotonically is node degree (Fig. 23). Paths with either monotonically increasing (type 1), monotonically decreasing (type 2) or monotonically increasing then decreasing node degrees (type 3) are hierarchical paths [48]. The existence of both BFS and EDS hierarchical paths supports the notion that some hierarchical structure is present in PRNs. The fraction of hierarchical paths of a type is almost constant for $N > 250$ (larger multi-domain proteins). The majority of hierarchical paths are of type 3, which echoes the zoom-in zoom-out navigational pattern reported in other real-world networks [29]. Zoom-in correlates with increase in node degree and zoom-out with decrease in node degree.

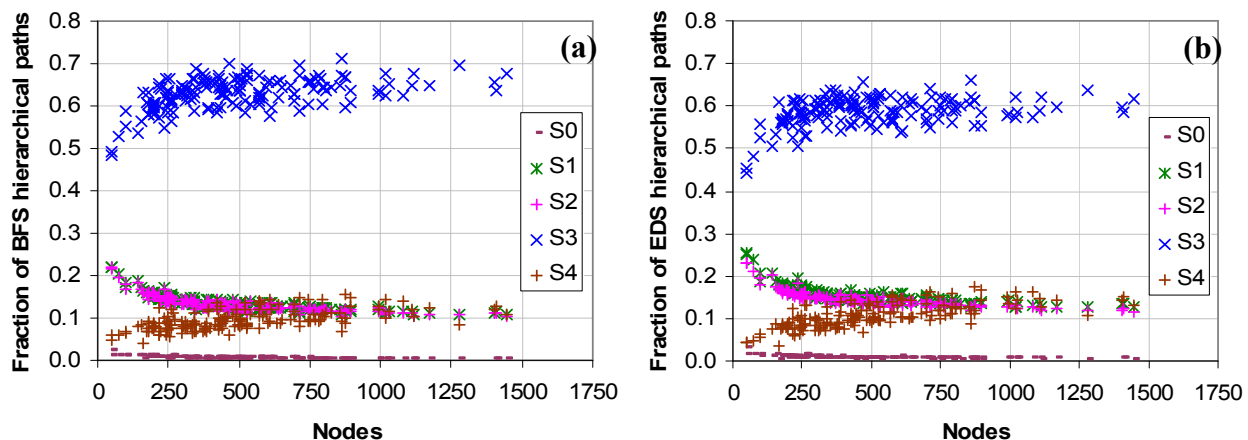


Fig. 23 BFS and EDS paths show similar hierarchical path composition. Most hierarchical paths are of type S3, which echoes the zoom-in zoom-out navigational pattern reported in other real-world networks [29]. Notably, the proportion of hierarchical paths by type is quite constant for larger proteins, $N > 250$. The hierarchical path types are: $S0$ which denotes paths with constant node degree, $S1$ which denotes paths with monotonically increasing node degree, $S2$ which denotes paths with monotonically decreasing node degree, $S3$ which denotes monotonically increasing then monotonically decreasing node degrees, and $S4$ which denotes paths with monotonically decreasing then monotonically increasing node degrees. $S4$ paths are not typical hierarchical paths; they may even be considered *anti-hierarchy*. But we include them since $S4$ paths also demonstrate structure.

4. PRN short-cut edges

In Fig. 14 (section 3.1), we reported that the removal of short-cut edges from PRNs increased EDS average path length more significantly than the removal of the same number of random edges. In this section, we purport to understand in more detail the role short-cut edges play in PRNs with a view to characterize their distinctness and to predict their formation during protein folding.

But first, we confirm that the linear relationship between the number of short-cuts and the number of nodes in a PRN as $\sim 2N$ reported in Fig. 12a is not an artifact of finding EDS paths both ways between all node-pairs. In Fig. 24a, prn is the same set of points as in Fig. 12a. It denotes the number of short-cuts

$|SC|$, when for every unique node-pair (u, v) , two EDS paths are made: one path from u to v and the other from v to u (section 2.4). prn_1 is the number of short-cuts when only one EDS path (chosen at random) is made between all pairs of unique nodes. prn_1 is significantly less than prn (paired t-test), but prn_1 still approximates $2N$. In the MD runs, the number of short-cuts in native state configurations also approximates $2N$ (run 6250 in Fig. 24b), while in non-native state configurations, the number of short-cuts is about $1.5N$ (runs 6251...6258 Fig. 24b) which implies an increase in the number of short-cuts as a protein folds (Fig. 13a).

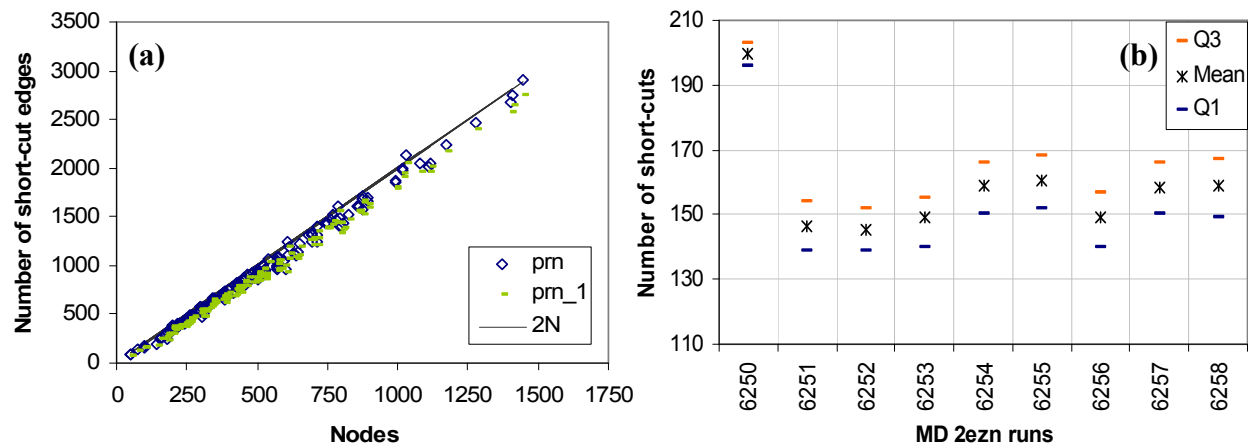


Fig. 24 Number of short-cuts, $|SC|$, in native vs. non-native state PRNs. For native state PRNs, i.e. PRNs from the 166 PDB files (a), and the PRNs from run 6250 (b), $|SC|$ is about twice the number of nodes, $\sim 2N$. This doubling is not due to finding a pair of EDS paths for each pair of unique nodes, as demonstrated in (a) where prn_1 is the number of short-cuts when only one EDS path is made between any pair of unique nodes. For non-native state PRNs, i.e. the non-6250 runs in (b), $|SC|$ is significantly smaller: $N \leq |SC| \leq 1.5N$. $N=101$ for 2EZN. In (b) Q1 and Q3 denote the first and third quartiles respectively. In all MD runs, the Mean values are situated approx. halfway between the Q1 and Q3 values.

The number of short-cuts found by EDS is sensitive to how the PRNs are constructed. In a less dense PRN, say one constructed as pure C_α - C_α with 7.5 Å cutoff, the number of short-cuts may be much fewer than $2N$ and this can be a limitation to the approach taken here which works from the hypothesis that the short-cut edges form a tree-like structure that spans almost all nodes in a PRN. Our reasons for adopting a spanning tree point of view of SCNs are revealed in section 4.2.

4.1 Short-cut network (SCN) structure

Define SC as the set of short-cut edges identified by EDS (section 2.4) for a PRN. The *short-cut network* (SCN) of a PRN is a graph whose edge set is SC , and whose vertex set is induced by its edge set. For comparison, we construct two types of pseudo short-cut networks: random short-cut (*rsc*) and random spanning tree (*rst*). A pseudo SCN has the same number of edges as its SCN counterpart, but depending on construction, can have significantly different number of nodes than its SCN counterpart. A *rsc* network is constructed from PRN edges chosen uniformly at random. A *rst* network is also constructed from PRN

edges but the selected edges come from the union of two or more trees spanning the PRN found via random walks. *rst* networks model splicers [49]. Multiple *rsc* and *rst* networks are generated per SCN with a different random seed each time. In the figures, *rsc* (*rst*) is used to denote either the network or the set of edges in the network, but it should be clear what is meant from context and the figure captions. Usually, we are interested in an SCN's largest connected component, denoted gSCN. Analogously, *grsc* (*grst*) denotes the largest connected component of a *rsc* (*rst*) network.

SCN node coverage quantified as $\frac{|V' \cap V|}{|V|}$ is the extent to which an SCN's vertex set V' intersects

with the vertex set of its PRN V . A larger intersection implies better SCN node coverage. For most PRNs, gSCN node coverage is almost maximum at 1.0 (*scn* data points in Figs. 25a & 25b), i.e. the largest connected component of an SCN spans almost all its PRN nodes. Node coverage for both *grsc* and *grst* networks are also close to 1.0, which is expected. With about $2N$ edges, the average degree of an *rsc* network approximates $2(2N)/N = 4$, which is larger than the threshold required for a random graph to have a giant component ([7], p.406). By definition of a spanning tree, a *rst* network should span all the nodes of a PRN. However, this may not be the case when edges need to be removed (which we do uniformly at random) in order to match a PRN's $|SC|$ (This trimming step could be avoided with a simple modification to the *rst* construction. Then $grst = rst$ and $grst$ node coverage = 1.0.). Nonetheless, the point is that even with our "less than optimal" *rst* construction, gSCN node coverage is still significantly worse (maximum p-value = 0.00022 over five trials) than *grst* node coverage. Over the five *rst* networks, at most 23.49% (39/166) of the 166 PRNs have gSCN node coverage greater than *grst* node coverage. At p-value < 0.10, gSCN node coverage is significantly better (maximum p-value = 0.08166 over five trials) than *grsc* node coverage. Over the five *rsc* networks, at least 92.77% (154/166) of the 166 PRNs have gSCN node coverage greater than *grsc* node coverage. That gSCN node coverage is significantly different from both *grsc* and *grst* node coverage argues for the distinctiveness of short-cut edges.

There is no significant difference between PRNs and MGEO4 networks in terms of gSCN node coverage (Fig. 25c). But we note that 150/166 PRNs have better gSCN node coverage than their MGEO4 networks. Good (about 95% or more on average) gSCN node coverage is also observed with PRNs from the MD runs. gSCN node coverage is significantly better for PRNs at equilibrium (6250 in Fig. 25d) than for PRNs of configurations not at equilibrium. This difference in gSCN node coverage suggests a process of SCN growth and formation as a protein folds, i.e. SCN node percolation on PRN.

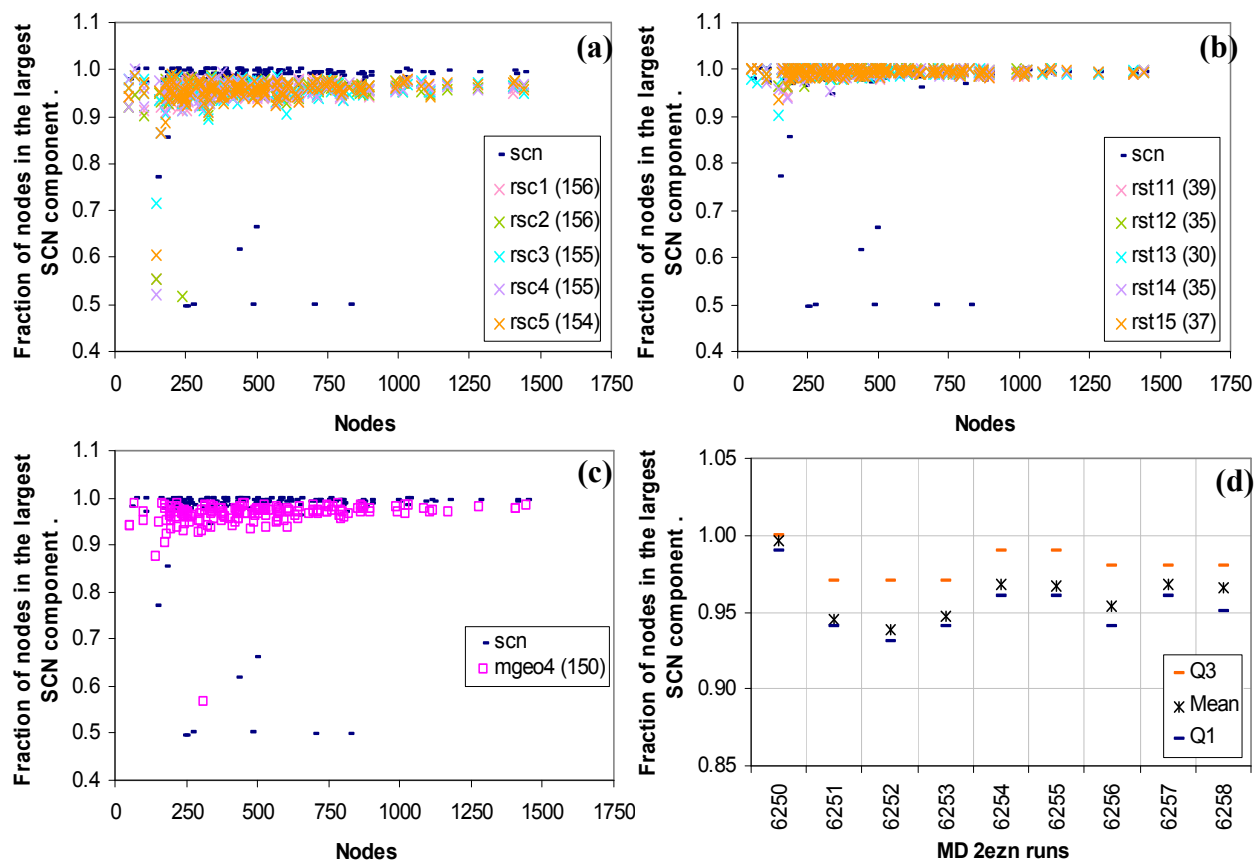


Fig. 25 SCN node coverage. For the 166 PRNs, node coverage of the largest SCN component (gSCN node coverage) is (a) significantly better (max p-value = 0.08166) than the coverage of the largest *rsc* component (*grsc* node coverage), and (b) significantly worse (max p-value = 0.00022) than the node coverage of the largest *rst* component (*grst* node coverage). See section 4.1 for details on *rsc* and *rst* construction. The numbers in parentheses in the legends of plots (a) and (b) give the number of PRNs where gSCN node coverage > *grsc* (*grst*) node coverage. That gSCN node coverage is significantly different from *rsc* and *rst* node coverage argues for the distinctiveness of short-cut edges. (c) gSCN node coverage in PRNs are not significantly different (p-value=0.3820) from gSCN node coverage in MGE04 networks. But 150/166 PRNs do have better gSCN node coverage than their MGE04 networks. (d) gSCN node coverage in PRNs of frames generated by the MD runs are about 95%. gSCN node coverage is significantly better in PRNs at equilibrium (6250) than in PRNs not at equilibrium. This suggests to us a process of SCN growth and formation as a protein folds. Q1 and Q3 denote the first and third quartiles.

SCN *edge coverage* is the fraction of short-cut edges needed to cover the edges of a PRN. A smaller fraction implies better edge coverage. An edge (u, v) covers all edges incident on nodes u and v . Edge coverage results in Fig. 26 are averaged over 20 permutations of each SCN, *rsc* or *rst* edge set. Ten *rsc* and ten *rst* edge sets were generated for this test.

For the set of 166 PRNs, SCN edge coverage is significantly worse than *rst* edge coverage, but significantly better than *rsc* edge coverage (Fig. 26a). That SCN edge coverage is significantly different from both *rsc* and *rst* edge coverage argues for the distinctiveness of the placement of short-cut edges within PRNs.

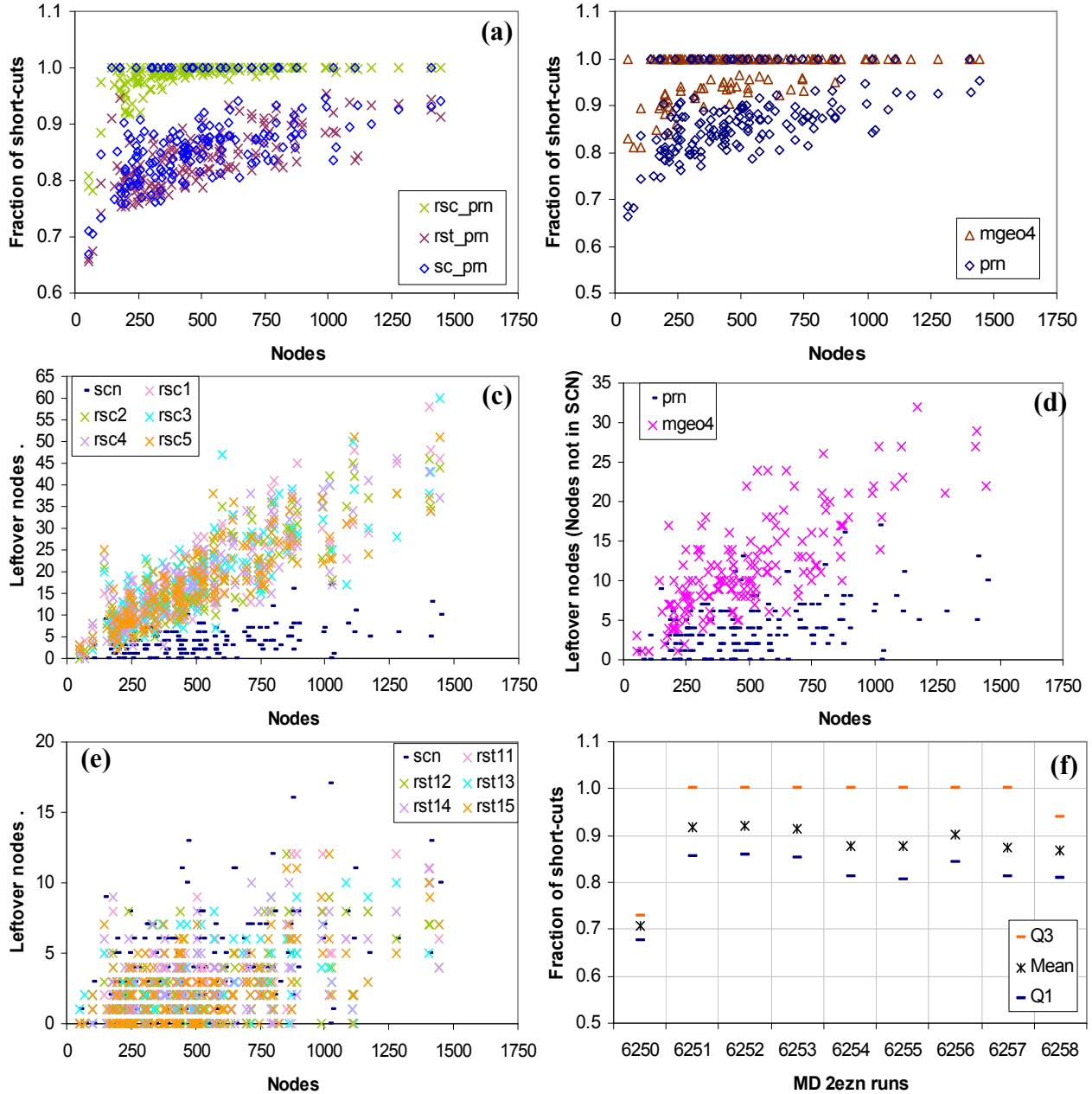


Fig. 26 SCN edge coverage is the fraction of short-cut edges needed to cover the edges of a PRN. A smaller fraction implies better edge coverage. An edge (u, v) covers all edges incident on nodes u and v . **(a)** Average SCN edge coverage for PRNs is 0.8729 ± 0.0735 (std.dev.). Edge coverage averaged over 20 permutations of the ten *rsc* edge sets is 0.9848 ± 0.0326 . Edge coverage averaged over 20 permutations of the ten *rst* edge sets is 0.8344 ± 0.0529 . **(b)** Average SCN edge coverage for MGEO4 networks is 0.9773 ± 0.0425 . **(c)** *rsc* networks have significantly more leftover nodes, i.e. non-SCN nodes, than PRNs. **(d)** MGEO4 networks have significantly more leftover nodes than PRNs. **(e)** *rst* networks have significantly fewer leftover nodes than PRNs. **(f)** SCN edge coverage is significantly better in native state configurations (6250, black) than in non-native state configurations. Q1 and Q3 denote the first and third quartiles.

MGEO4 networks have significantly worse SCN edge coverage than PRNs (Fig. 26b). A reason for this is MGEO4 networks have significantly fewer short-cuts than PRNs (Fig. 12a). Another reason is

MGEO4 networks have significantly more nodes that are not endpoints of at least one short-cut than PRNs (Fig. 26d). An SCN which excludes at least two nodes which are themselves connected to each other (which is about 40% likely given C for PRNs, and about 15% likely given C for MGEO4 networks in Fig. 7b) cannot have edge coverage < 1.0 . Like MGEO4 networks, *rsc* networks also have significantly more non-SCN nodes than PRNs (Fig. 26c) and significantly worse SCN edge coverage than PRNs (Fig. 26a). In short, the SCNs of MGEO networks are not as well percolated as the SCNs of PRN networks. *rst* networks, in contrast, have significantly fewer non-SCN nodes than PRNs (Fig. 26e) and significantly better SCN edge coverage than PRNs (Fig. 26a).

The number of short-cut edges tends to increase as the 2EZN protein becomes more compact (Fig. 13a), and native state PRNs have significantly larger short-cut sets than non-native state PRNs (Fig. 24b). Accordingly, SCN edge coverage improves as the 2EZN protein becomes more compact (smaller radius of gyration), and SCN edge coverage is significantly better in native state configurations than in non-native state configurations (Fig. 26f). For configurations undergoing native protein dynamics (run 6250), about 70% of short-cuts are sufficient on average to cover all PRN edges. This percentage increases to about 90% for configurations far from equilibrium but still on trajectories leading to/from the native state (runs 6251 to 6258).

From the observations in this section so far, it appears that SCNs face the problem of node percolation on PRNs, i.e. growing their largest connected component so that they span the nodes of their respective PRNs. Further, this node percolation problem has the additional condition that short-cut edges be suitably placed so that they provide efficient edge coverage. These two problems of node percolation and edge placement are not unrelated in the sense that they work together to support gSCN connectivity as it undergoes (node and) edge deletions and additions in its growth process.

Ref [31] found that, with degree distribution and clustering coefficient values being equal, networks with strong transitivity are more resilient to random edge removals than weakly transitive networks. The size reduction of the giant component as edges are removed uniformly at random actually slows down in strongly transitive networks as the probability of removing a random edge q increases. Conservatively, this effect is pronounced for $q > 0.2$. (Fig. 4 in [31]).

In the 2ezn MD dataset, on average between 20% – 30% of short-cut edges disappear (the short-cut edge either no longer exists in the PRN or it becomes a non-short-cut edge and so is no longer a part of a SCN) in a step in non-equilibrium runs (Fig. 27a). The fraction of short-cuts removed can be well above 35% in some steps, which calls for a SCN structure that is resilient to aggressive edge deletions. And indeed, gSCNs show more resilience to random edge removals than both *grsc* and *grst* networks. The

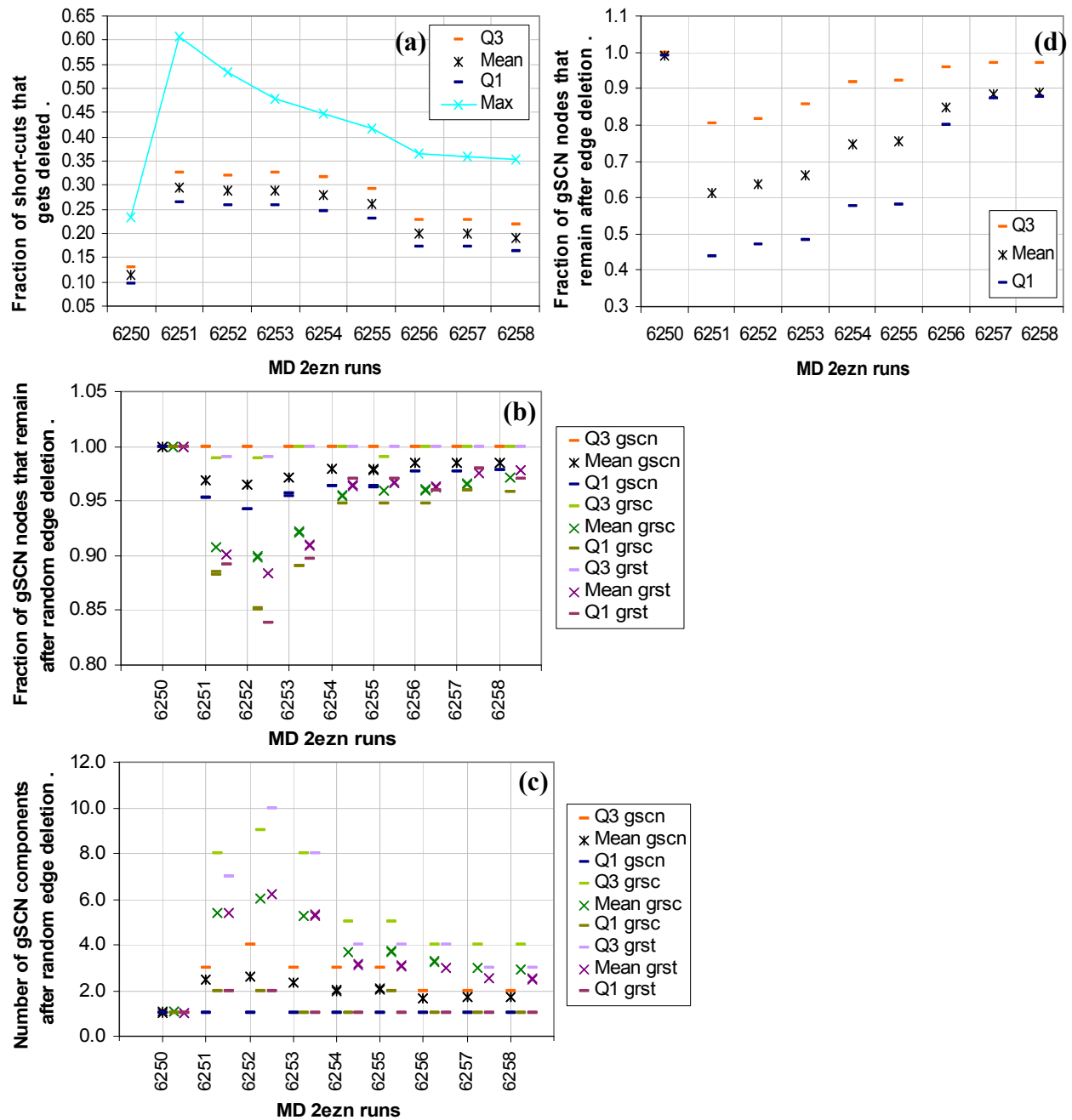


Fig. 27 Robustness of the largest SCN component (gSCN) to edge deletions. (a) In the non-equilibrium runs, an average between 20% – 30% of short-cut edges disappear, i.e. the short-cut edge either no longer exists in the PRN or it becomes a non-short-cut edge and so is no longer a part of a SCN in the next step. However, the fraction of short-cuts removed can be well above 35% in some steps, which calls for a SCN structure that is resilient to aggressive edge deletions its gSCN is to grow. (b) The fraction of nodes in the largest component that remain in the largest component after random edge deletion is significantly larger for gSCNs than for both *grsc* and *grst* networks. (c) Both *grsc* and *grst* networks split into significantly more pieces than gSCNs after random edge deletion. (d) The fraction of nodes in the largest component that remain in the largest component after non-random edge deletion (short-cuts that actually disappear are removed).

fraction of nodes in the largest component that remain in the largest component after random edge deletion is significantly larger for gSCNs than both *grsc* and *grst* networks (Fig. 27b). Both *grsc* and *grst* networks fracture into significantly more pieces than gSCNs after random edge deletion (Fig. 27c).

Let q_t be the fraction of edges deleted from gSCN_t (Fig. 27a gives the q value averaged over all steps in a run); and grsc_t and grst_t be respectively, the largest component of the *rsc* and *rst* networks associated with SCN_t . The *rsc* and *rst* networks are generated as described previously at the start of this section. For results reported in Figs. 27b & 27c, q_t of the edges in gSCN_t , grsc_t and grst_t were chosen uniformly at random for removal, and the results are averaged over all t per run. In Fig. 27d, q_t of the edges in gSCN_t is also removed but these edges are the actual short-cut edges that disappear at step $t+1$. The fraction of nodes in the largest component that remain in the largest component after this non-random edge deletion is significantly smaller than when the same number of random edges is removed from gSCN. Thus, the deleted SCN edges are not a random edge set.

Fittingly, SCNs of the 166 PRNs have significantly stronger transitivity than both *rsc* and *rst* networks (Figs. 28a & Fig. 28b). *SCN transitivity* is the average edge multiplicity (Fig. 8) of the edges of a SCN evaluated solely within the SCN. SCN transitivity is stronger when average edge multiplicity is larger. The weak transitivity of *rsc* networks is expected since they are essentially random graphs (edges in *rsc* are selected uniformly at random from PRN edges and so are not expected to be correlated). The weak transitivity of *rst* networks are also expected from their tree base construction.

SCNs of the 166 PRNs also have significantly stronger transitivity than SCNs of MGEO4 networks (Fig. 28c). This seems to follow from the earlier observation that MGEO4 networks have significantly weaker transitivity than PRNs (Fig. 7d). However, it is not necessarily true that the average edge multiplicity or transitivity strength of a sub-graph is limited by the transitivity strength of its parent graph. In particular, graphs where numerous edges have $\text{EM} = 0$, e.g. a kite graph with a long tail. On average, 86.49% of links in MGEO4 networks have $\text{EM} > 0$ (Fig. 7c).

SCN transitivity increases as the 2EZN protein folds in the MD simulation (Fig. 28d). The native configurations in the MD simulation have significantly stronger SCN transitivity than non-native configurations, and this strength is reflected in the results in Fig. 27 where the gSCN of native configurations are almost immune to both random and non-random edge deletions.

SCN transitivity is defined on SCNs and is independent of PRNs. Taken within the context of a PRN, short-cuts do not have significantly higher average edge multiplicity than non-short-cut edges. This follows from Fig. 21a which reports that short-cuts are dominated by short-range links, and from Fig 7f which reports that short-range edges have significantly smaller average EM. However, within the context of PRNs, the common first neighbors of short-cut edges exhibit significant local community structure. Clustering is significantly higher amongst the common first neighbors of short-cut edges than amongst

the common first neighbors of non-short-cut edges. In the terminology of [50], short-cut edges have significantly more local community links. A more in-depth study is required to assess whether this feature which is related to the CAR index [50] identifies short-cut edges in PRNs.

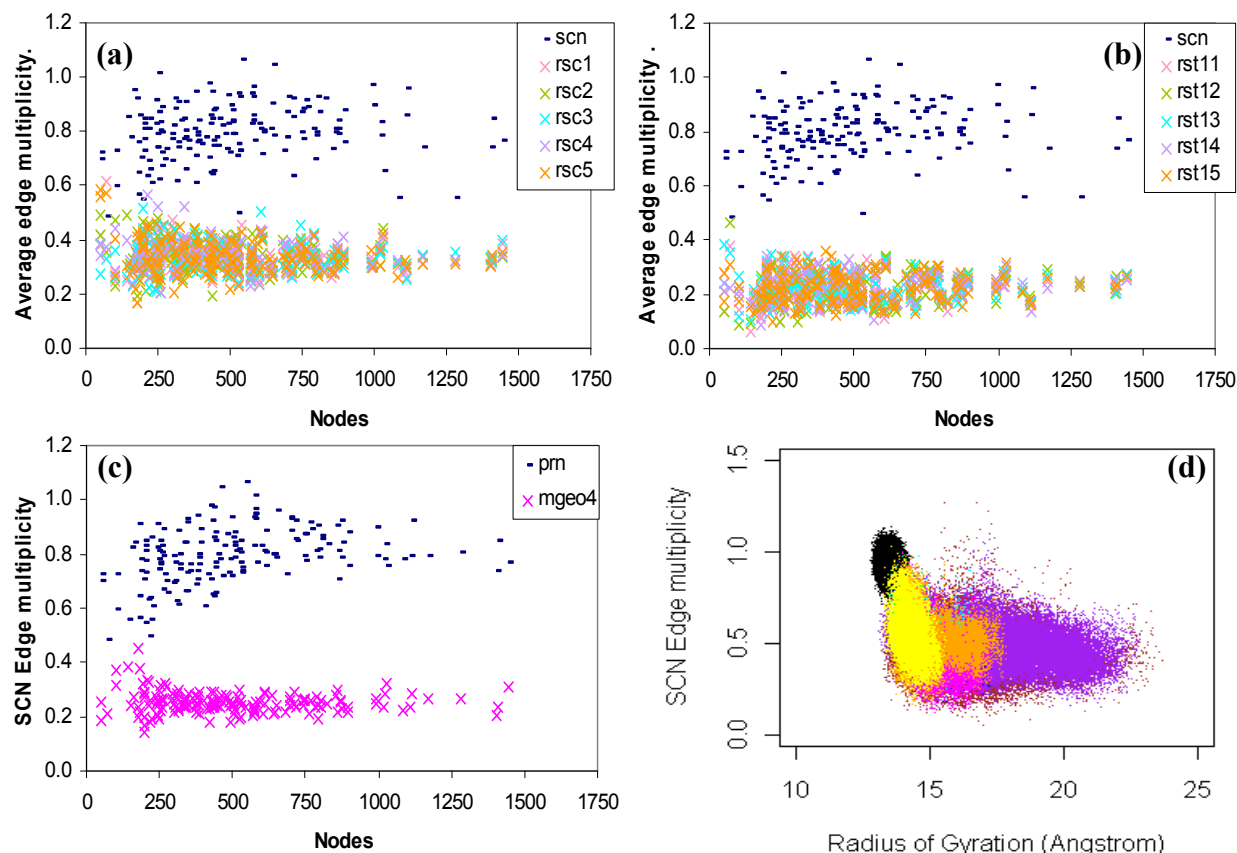


Fig. 28 SCN transitivity. (a & b) SCNs of the 166 PRNs have significantly stronger transitivity than both *rsc* and *rst* networks (c) SCNs of the 166 PRNs also have significantly stronger transitivity than SCNs of MGE04 networks. (d) SCN transitivity increases as the 2EZn protein folds in the MD simulation.

4.2 SCN function: short-cuts reduce stretch between EDS path-pairs

Our spanning tree point of view mentioned at the start of section 4 is motivated by several factors. Ref. [49] showed that the union of two random spanning trees can capture the expansion property of the underlying graph and is an efficient way to design scalable, fault-tolerant and path-diverse routing. Proteins are fairly robust to random attacks according to mutagenesis studies [39], and possess alternative pathways or redundant links between critical sites [12]. Further, path diversity helps to lower a network's congestion threshold [52, 53], and to increase ease of synchronization stability [54]. For proteins, the congestion threshold may be viewed as the maximum amount of stimulation (e.g. interaction with other proteins and molecules or the water substrate) a protein can process simultaneously without detriment to itself. Ref. [55] proposes to view protein folding as a process of synchronizing peptide planes. For these reasons, we consider the existence of alternate pathways (*edge independent* paths) with conservative

increase in average distance between alternate pathways (small *stretch* factor) to be an essential feature of PRNs.

Let p be a path from node u to node v , and q be a path from v to u . Paths p and q make a path-pair. p and q is an edge independent or edge disjoint path-pair if and only if p and q have no edges in common. A network that supports the existence of many edge independent path-pairs is *path diverse*. The stretch of a path-pair is the absolute difference between the lengths of its constituent paths. And indeed, the MD simulation of 2EZN shows that PRNs of native state configurations (run 6250 data points are denoted in black in Figs. 29a & 29c) have significantly more edge independent EDS path-pairs (Fig. 29b) and a significantly smaller stretch (Fig. 29d) than the PRNs of non-native state configurations. Further, edge independence generally increases while stretch generally decreases as the 2EZN protein becomes more compact (radius of gyration decreases).

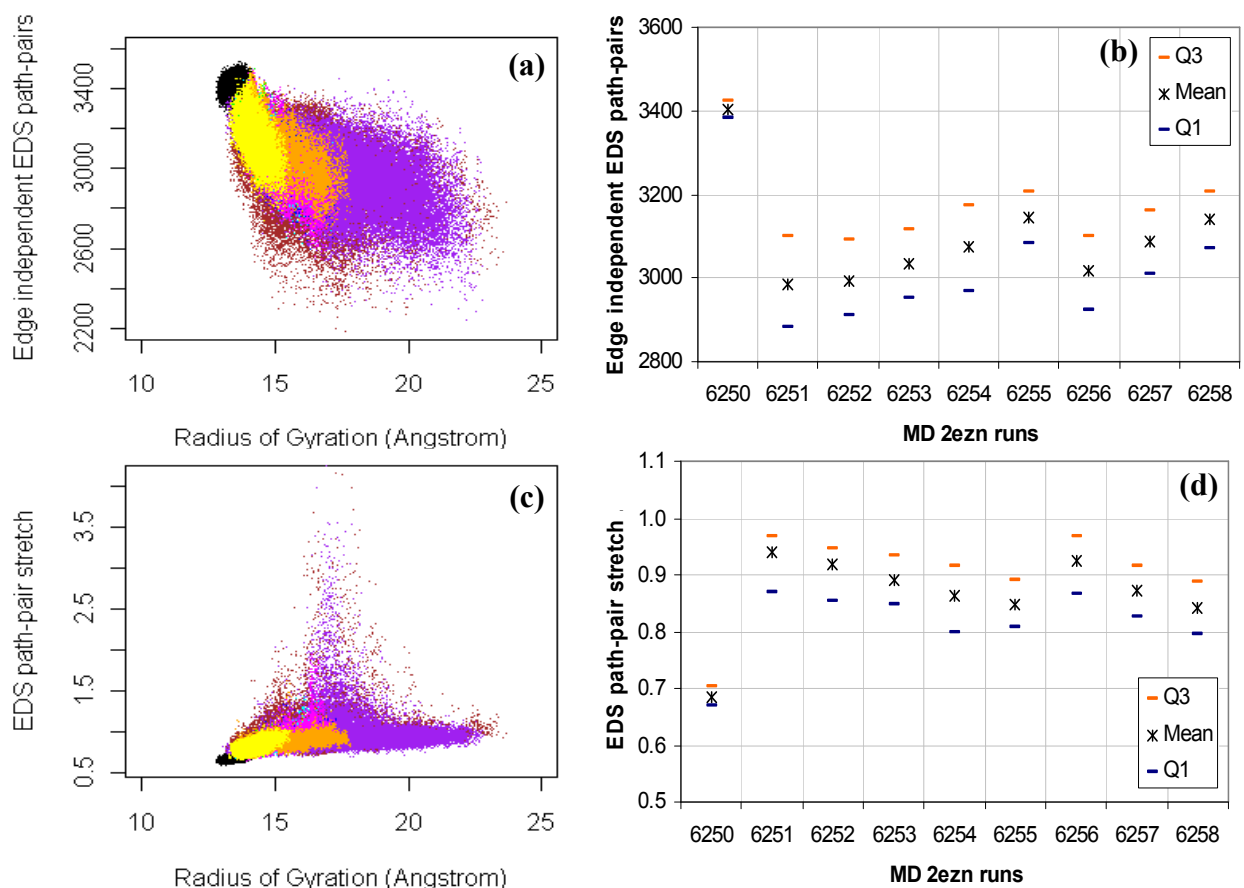


Fig. 29 Edge-independence and stretch of EDS path-pairs in 2EZN MD runs. (a) The number of edge independent EDS path-pairs generally increases as the 2EZN protein becomes more compact (radius of gyration decreases). Data points for the native dynamics MD run (6250) is in black (section 2.5). (b) PRNs of native state configurations (6250) have significantly more edge independent EDS path-pairs. (c) EDS path-pair stretch generally decreases as the 2EZN protein loses its gyration freedom. (d) PRNs of native state configurations (6250) have significantly smaller stretch than the PRNs of non-native state configurations. In (b) and (d), Q1 and Q3 denote the first and third quartiles respectively.

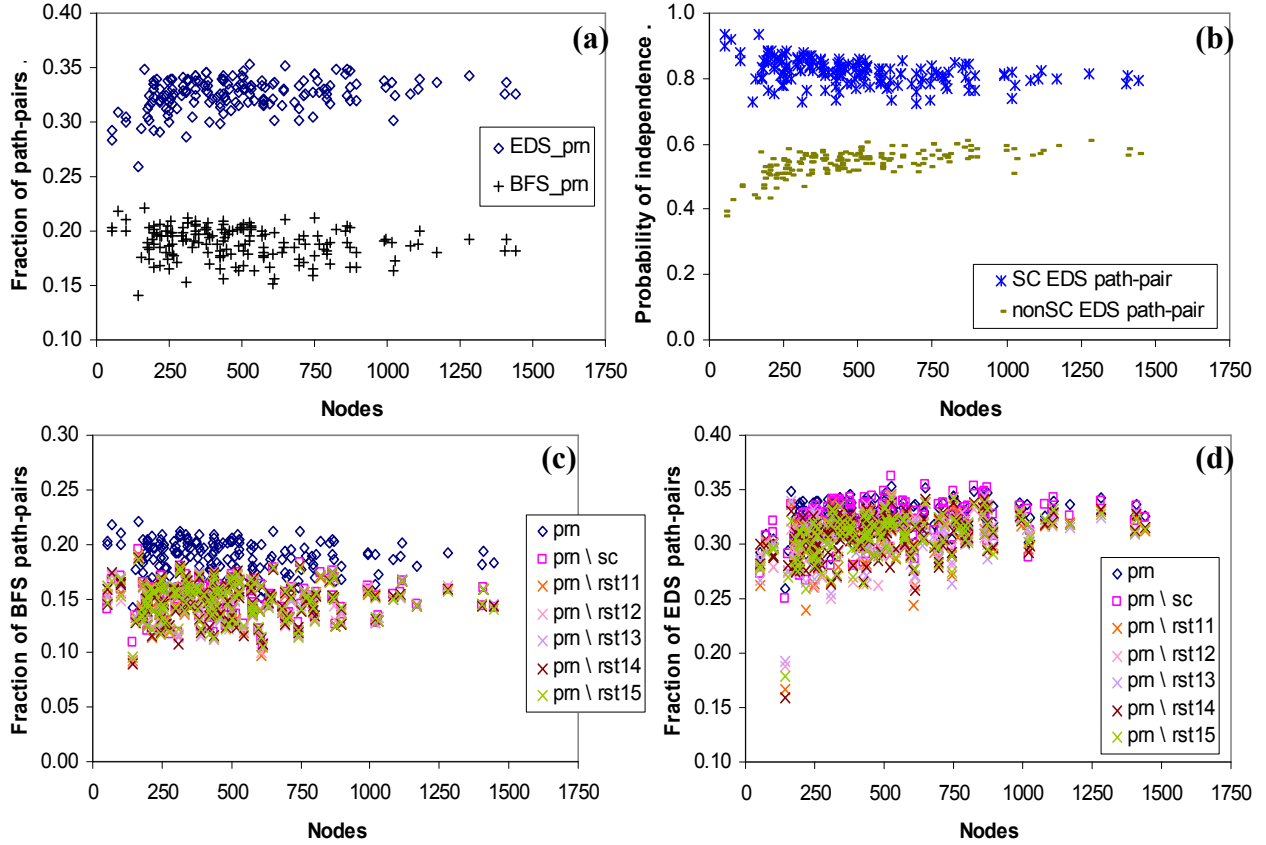


Fig. 30 Effect of short-cut edges on edge independence of path-pairs. (a) For the set of 166 native state PRNs, the proportion of EDS path-pairs which are edge independent is significantly larger than the proportion of BFS path-pairs which are edge independent. About 30% to 35% of EDS path-pairs are edge independent while only 15% to 20% of BFS path-pairs are edge independent. (b) An EDS path-pair where either one or both paths traverse at least one short-cut edge (SC EDS path-pair) is more likely to be edge-independent than an EDS path-pair where neither paths traverse at least one short-cut edge (nonSC EDS path-pair). If an EDS path-pair traverses at least one short-cut edge then it has about 80% chance of being edge independent. The chance for edge independence drops to at least 60% for an EDS path-pair that does not traverse any short-cut. (c) BFS path diversity is significantly compromised by the removal of short-cuts ($pm \setminus sc$) and also by the removal of rst edges ($pm \setminus rst$). (d) EDS path diversity is robust to the removal of short-cuts ($pm \setminus sc$) and also to the removal of rst edges ($pm \setminus rst$). See section 4.1 for details on rst construction. Roughly, it comprises $|SC|$ PRN edges from two or more random spanning trees.

For the set of 166 native state PRNs, the proportion of EDS path-pairs which are edge independent is significantly larger than the proportion of BFS path-pairs which are edge independent (Fig. 30a). An average of 32.55% (std. dev. 1.48%) of EDS path-pairs are edge independent while only 18.89% (std. dev. 1.45%) of BFS path-pairs are edge independent. An EDS path-pair where either one or both paths traverse at least one short-cut edge is more likely to be edge-independent than an EDS path-pair where neither paths traverse at least one short-cut edge (Fig. 30b). It appears then that short-cut edges play a role in keeping path-pairs edge-wise separate from each other. Investigation by elimination reveals that this conclusion applies to BFS path-pairs more so than to EDS path-pairs (Figs. 30c). Compared with BFS, EDS path diversity is more robust to the removal of short-cut edges and also to the removal of rst edges from PRNs (Fig. 30d). Hence, EDS is more able than BFS to exploit the alternative connections already

present between nodes in PRNs. Nonetheless the removal of short-cut edges from PRNs does reduce path diversity significantly, but this reduction is significantly smaller in magnitude than the reduction caused by the removal of *rst* or *rsc* edges. The fraction of independent EDS path-pairs in 111 of the 166 PRNs decrease when short-cuts are removed. In contrast, the removal of *rst* (*rsc*) edges negatively affected path diversity in at least 156 (138) PRNs.

This last observation, coupled with the structural differences between SCNs and *rst* networks identified earlier in section 4.1, weakens the hypothesis that the set of short-cut edges of a PRN is the union of two or more *random* trees spanning a PRN. Path stretch is actually not an explicit design consideration in the proposal of splicers [49]. Other graph sparsification strategies designed to preserve different characteristics of the original graph up to a factor exist. It could be insightful to investigate SCNs in terms of these other graph sparsification techniques.

The removal of short-cut edges from PRNs ($prn \setminus sc$) increases EDS path stretch significantly (Fig. 31), and this increase is significantly larger compared to the removal of *rst* edges ($prn \setminus rst$ in Fig. 31a), and to the removal of *rsc* edges ($prn \setminus rsc$ in Fig. 31b). EDS path-pairs of the 166 PRNs (prn in Fig. 31) experience an average stretch of 1.1650 with a standard deviation of 0.3502. The average stretch for PRNs without short-cuts is 2.9890 with a standard deviation of 0.6182. Greater average stretch contributes to longer average path lengths, and indeed PRNs sans short-cuts have significantly longer EDS average path lengths than PRNs (Figs. 14b & 14d).

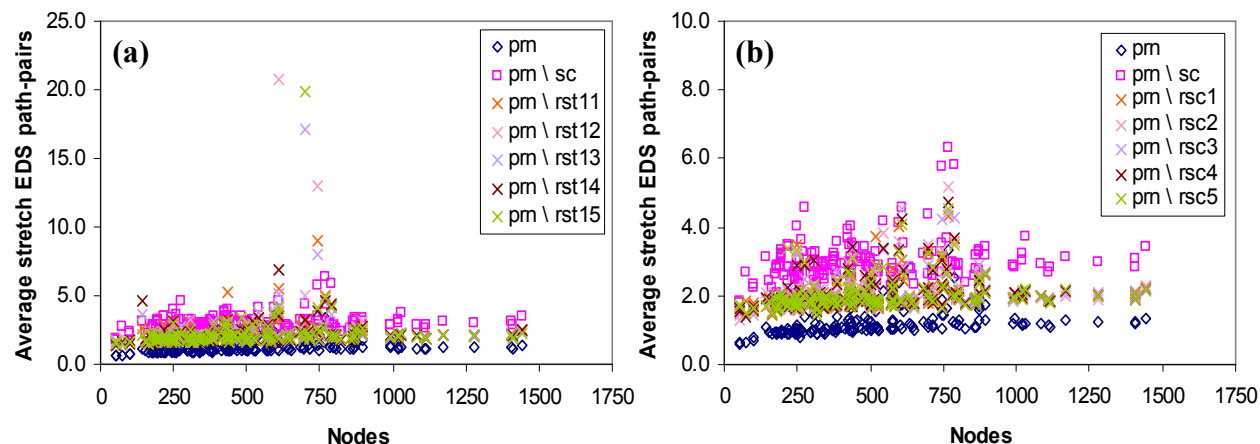


Fig. 31 Removal of short-cut edges from PRNs increases EDS path stretch significantly. Let p be an EDS path from u to v , and q be an EDS path from v to u . p and q make an EDS path-pair and its stretch is the absolute difference in its path lengths. **(a)** $prn \setminus rst$ denotes PRNs with a number of edges from the union of two random spanning trees removed (see section 4.1 for details). Five such *rst* edge sets were created using the random walk method [49] with a different random seed each time. **(b)** $prn \setminus rsc$ denotes PRNs with a number of random edges removed (see section 4.1 for details). Five such *rsc* edge sets were created with a different random seed each time. EDS path-pairs in $prn \setminus sc$ networks exhibit significantly longer stretch on average than EDS path-pairs in all three prn , $prn \setminus rst$ and $prn \setminus rsc$ networks.

A consequence of a SCN's role in path diversity and stretch is the volatility of its short-cut edges. The atoms of a protein are in flux, more so when the protein is far from equilibrium. This means changes in EDS paths. To preserve or increase path diversity and to maintain or reduce path stretch, the formation and destruction of short-cut edges need to be responsive to the changes in paths and their lengths. PRNs of native state configurations are more path diverse and do have smaller stretch than the PRNs of non-native state configurations (Fig. 29). Compared to the set of edges that are not short-cuts, the set of short-cut edges is significantly more volatile (Fig. 32). Except for the equilibrium state configurations (6250), a short-cut edge is significantly more likely to transition out of its current state, i.e. become a non-short-cut edge or a non-edge in the next step, than a non-short-cut edge. Non-edges are most likely to remain in their current state as non-edges in the next step. On the right of Fig. 32 is a state transition diagram for the three different states a contact map entry can be in: 0 is the non-edge state, 1 is the non-short-cut edge state and 2 is the short-cut state.

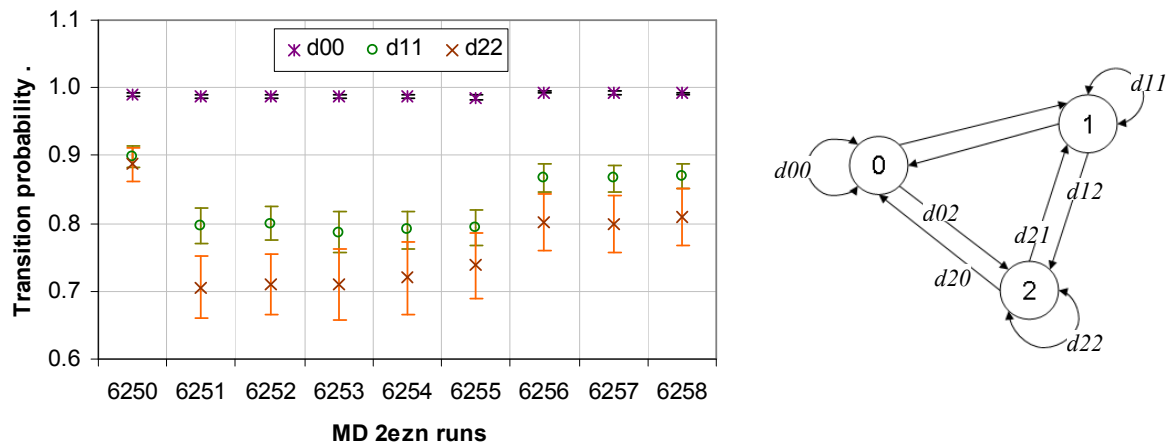


Fig. 32 Short-cut edges are significantly more volatile than non-short-cut edges as a result of having to adapt to changes in movement of nodes and changes in edges to support route diversity and to restrain stretch in path-pairs. $d00$ denotes non-links that persist from one step to another. Since PRNs are sparse, it is unsurprising that almost all zero entries in the contact map (adjacency matrix of a PRN) at step t remain zero at step $t+1$. $d11$ denotes non-short-cut links at step t that remain a non-short-cut link at step $t+1$. Except for run 6250, about 80% of non-short-cut links remain as such in the next step time. $d22$ denotes short-cut links at step t that remain a short-cut link at step $t+1$. Except for run 6250, about 70% of short-cut links remain as such in the next step time. This means that about 30% of short-cut links undergo a change in state, i.e. either become non-links or become non-short-cut links in the next step. This significantly higher percentage of state change is why short-cut edges are considered more volatile than non-short-cut edges. Run 6250 is a native dynamics simulation. Expectedly, its $d11$ and $d22$ values are both significantly larger than the other runs. The state transition diagram on the right summarizes the possible transitions between the three different states a contact map entry can be in: 0 is the non-edge state, 1 is the non-short-cut edge state and 2 is the short-cut state. In an MD run, zero or more of these transitions can happen from one step to the next. Error-bars denote standard deviation about the mean.

4.3 SCN formation

Ideally, we would like to have a function of the form $SC_{t+1} = f(SC_t)$ that derives the set of short-cuts at time $t+1$ from the set of short-cuts at time t . Then the formation of a SCN is fully characterized by changes in the initial SCN. Towards this end, we work from the premise that SCN connectivity is

important, i.e. when short-cut edges disappear at time t , they are replaced with other short-cut edges that appear at time t which help to preserve most of the largest SCN component (gSCN) and help it to grow as suggested in section 4.1. For this to happen, each deleted short-cut needs to be replaced with at least an edge from its cut-set that is also a short-cut (we assume for now that any edge can substitute for another edge). The idea of replacing a deleted edge with another edge from its cut-set to maintain connectivity is borrowed from dynamic graph theory [e.g.: 51], and we implement it as follows:

1. Identify delSC_{t+1} , the set of deleted short-cuts at step $t+1$. An edge in delSC_{t+1} is a short-cut edge at step t and either a non-short-cut edge or a non-edge at step $t+1$. Per the state transition diagram in Fig. 32, deleted short-cuts are those that make either a $d21$ or $d20$ transition.
2. Create a spanning tree ST_t from gSCN_t (the largest SCN component at step t), taking care to pack into ST_t as many of the edges in delSC_{t+1} as possible.
3. Generate the cut-set for each edge e in $ST_t \cap \text{delSC}_{t+1}$. The removal of e from ST splits ST into two sub-trees. All edges with one endpoint in one sub-tree and another endpoint in the other sub-tree completes the cut-set for e . CUTS_t is the union of cut-sets for edges in $ST_t \cap \text{delSC}_{t+1}$.
4. Identify addSC_{t+1} , the set of added short-cuts at step $t+1$. An edge in addSC_{t+1} is a non-short-cut edge at step t and a short-cut edge at step $t+1$. Per the state transition diagram in Fig. 32, added short-cuts are edges that make a $d12$ transition. It is also possible for a non-edge at step t to become a short-cut at step $t+1$ (via a $d02$ transition) but such an added short-cut edge will not be in any cut-set generated in step 3. Non-edges that become short-cuts in the next step ($d02$ edges) are much fewer than $d12$ edges (Figs. 33b). Nonetheless, $d02$ edges may be pivotal for correct SCN formation and this is a limitation of our current approach.
5. Define gSCN'_t as gSCN_t augmented by all edges in PRN_t that have both endpoints in gSCN_t . For each edge in $\text{gSCN}'_t \cap \text{addSC}_{t+1}$, find a cut-set from step 3 that includes it. If a cut-set is found, then we say that the short-cut edge is *matched* and the cut-set that matches it is *used*.

The implementation here assumes that most of the short-cut changes take place within the largest SCN component, and it does. For the 2ezn MD dataset, almost all of the deleted short-cuts (edges in delSC_{t+1}) are in gSCN_t (Fig. 33c). About 85% of the added short-cuts (edges in addSC_{t+1}) can be found in gSCN'_t (Fig. 33d). The average number of short-cuts removed in a step is almost balanced by the average number of short-cuts added (Figs. 33a & 33b).

A good outcome is one where most cut-sets are used, and most added short-cuts are matched. About 21% of the edge cut-sets (which is generated only for the deleted short-cuts in ST) are unused (Fig. 34a), and about 12% of added short-cuts (in gSCN'_t) are unmatched (Fig. 34b). This means that replacement edges for about a fifth of the deleted short-cuts is not found in the augmented gSCN. But because of

strong transitivity (section 4.1), this may not weaken gSCN connectivity too much. The unmatched added short-cuts are unmatched with respect to the cut-sets of the deleted short-cuts in the spanning-tree, but since the added short-cuts are all *d12* edges, they must exist in a cut-set of an edge of ST_t . The quality of $CUTS_t$ depends on the edges that make ST_t . For this reason, we repeated the procedure on five spanning trees generated with a different random seed but still taking care to pack into each ST_t as many of the edges in delSC_{t+1} as possible. The results from these different spanning trees are not significantly different from each other (the results from these multiple trials are superimposed in Fig. 34). Nonetheless, some optimization in this area, or a different approach, could prove beneficial.

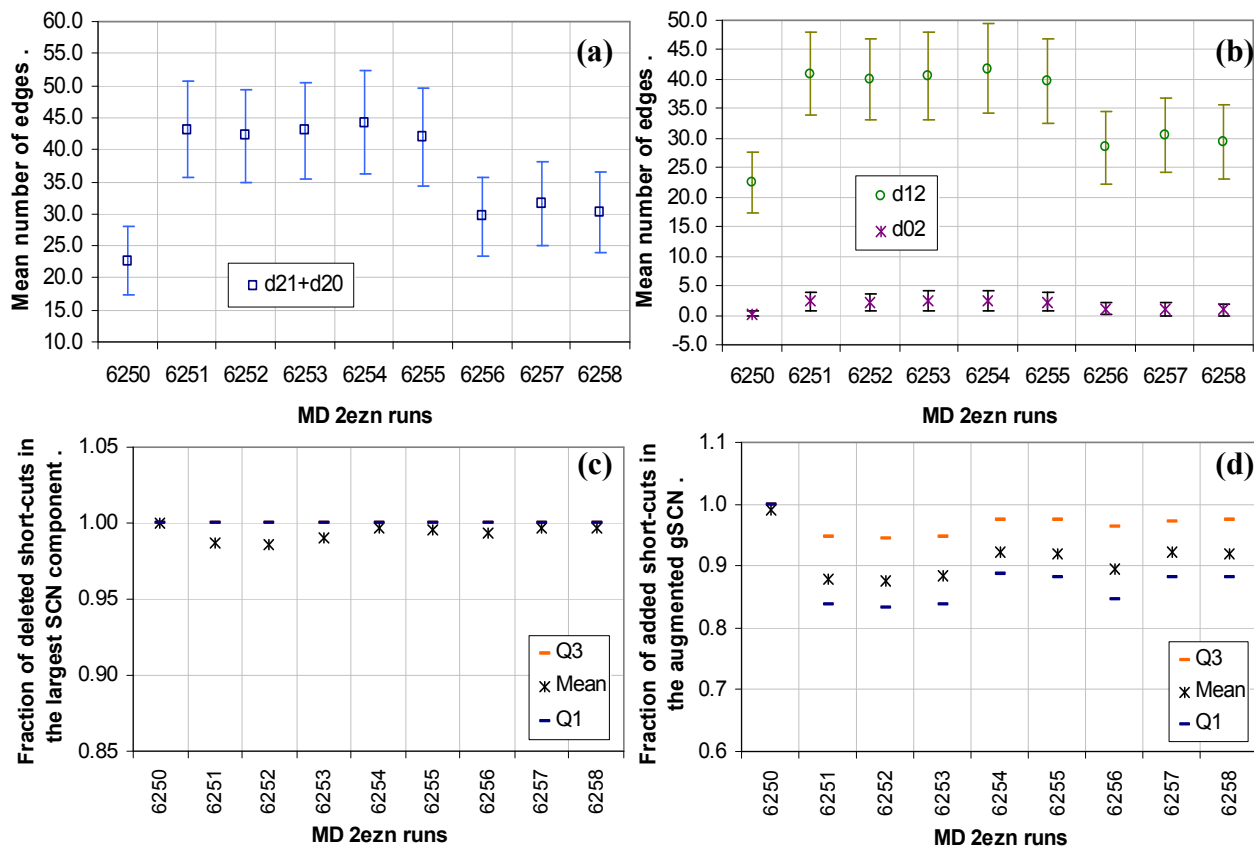
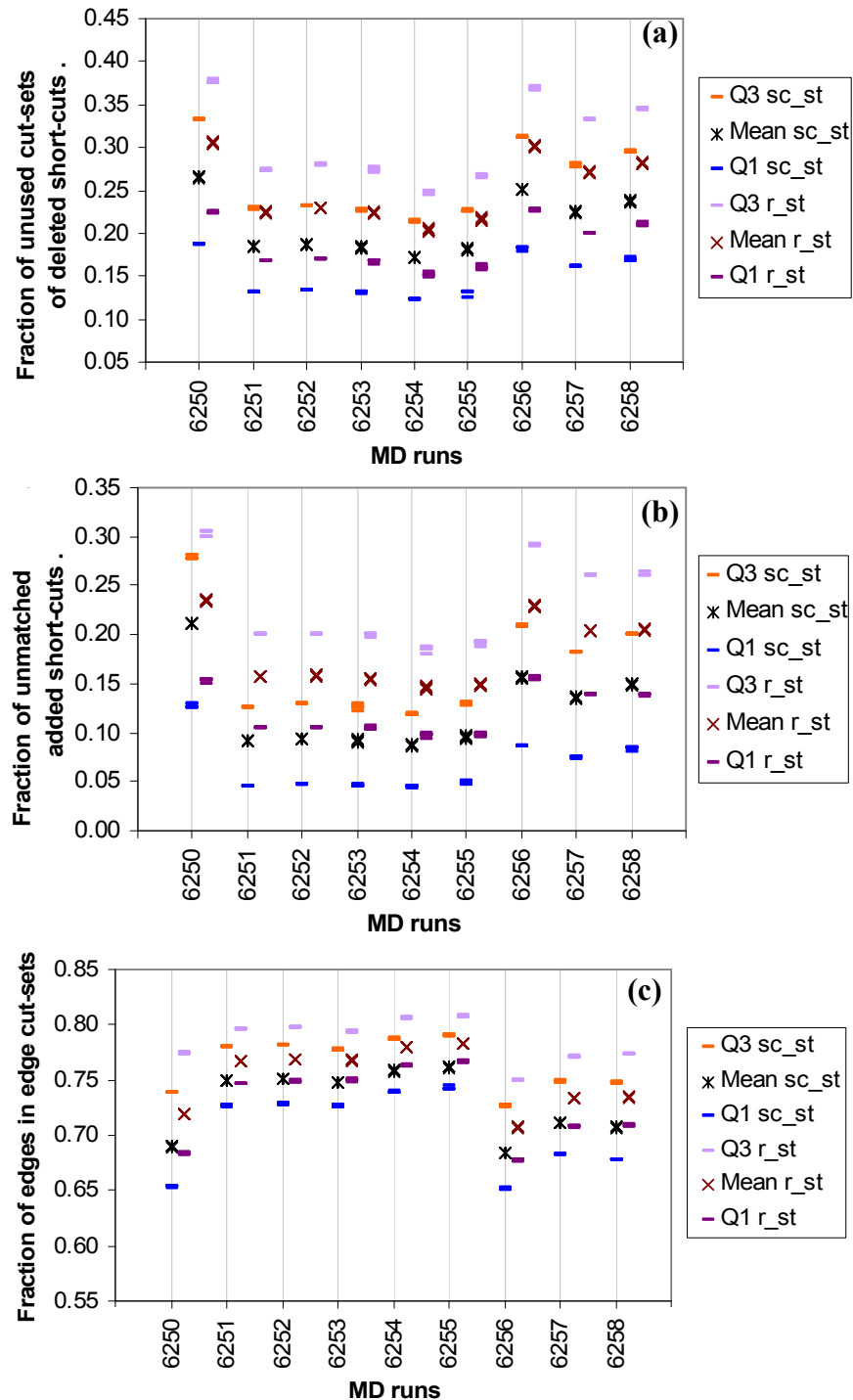


Fig. 33 (a) The average number of short-cuts removed (edges making either a d21 or a d20 transition) in a step. (b) The average number of short-cuts added in a step. d12 denotes non-short-cut edges that become short-cuts in the next MD step. d02 denotes non-edges that become short-cut edges in the next MD step. (c) Almost all of the deleted short-cuts (d21 and d20 edges) are found in the largest SCN component. (d) An average of at least 85% of the added short-cuts (d12 edges) can be found in the augmented largest SCN component. In (a) & (b), error bars denote standard deviation about the mean. In (c) & (d), Q1 and Q3 denote the first and third quartiles respectively.

The unused and unmatched percentages increase significantly when ST is supplemented with random edges (r_{st}) instead of short-cut edges (sc_{st}) in step 2. The poorer performance of r_{st} cut-sets is not because as a whole, they cover fewer edges than cut-sets generated with sc_{st} . On the contrary, the union of r_{st} cut-sets covers on average, a significantly larger fraction of edges in the augmented gSCN than the union of sc_{st} cut-sets (Fig. 34c). This furthers the case for the distinctiveness of short-cuts as a set of

well-placed edges within PRNs. It also establishes that the deleted short-cuts and the added short-cuts are not random, and that a relationship exists between the two sets. One of the tasks ahead is to decipher the conditions under which short-cuts get deleted and how their replacements are selected, or conversely the conditions for promoting non-short-cut edges and demoting short-cut edges.



(a) A deleted short-cut with an unused cut-set implies that a replacement edge is not found from the set of added short-cuts. Averaged over all (*sc_st*) runs, about 20.97% (std. dev. 3.33%) of deleted short-cuts have unused cut-sets. This percentage increased significantly to 25.07% (std. dev. 3.70%) when *ST* is supplemented with random edges (*r_st*) in step 2.

(b) An unmatched added short-cut is one whose existence is not explained by it being a replacement for one or more deleted short-cuts. Averaged over all (*sc_st*) runs, about 12.35% (std. dev. 4.07%) of added short-cuts are unmatched. This percentage increased significantly to 18.21% (std. dev. 3.42%) when *ST* is supplemented with random edges (*r_st*) in step 2.

(c) The fraction of edges in $gSCN'_t$ that are in $CUTS_t$ is significantly larger when *r_st* is used to produce the edge cut-sets than when *sc_st* is used. $CUTS_t$ is the union of cut-sets for edges in $ST_t \cap delSC_{t+1}$. Despite this, *r_st* produced poorer outcomes in (a) & (b). That *sc_st* produces significantly better (or at least different) $CUTS$ than *r_st*, supports our argument for the distinctiveness of short-cuts as a set of well-placed edges within PRNs.

Fig. 34 Results for 2EZN.

There is an intimate relationship between cycles and cut-sets of a graph G with respect to a spanning-tree T . Essentially, knowing the set of (fundamental) cycles associated with T gives one the set of cut-sets associated with T for free, and vice versa. This relationship brings this research full circle to our initial motivation for understanding clustering, i.e. cycles, within the context of the small-world network structure of proteins. The presence of cycles in PRNs may not only facilitate their navigability but also their formation.

4.4 Discussion

Hitherto, we have identified several characteristics of short-cuts and described properties of well-formed SCNs. In this section, we apply what we have discovered on other datasets. The intention is to verify our findings in an integrated way and to build robustness for our findings.

First, we complete the study of the artificially constructed MGEO4 networks. In section 4.1, we concluded that SCNs in MGEO4 networks are less well-formed than SCNs in PRNs since MGEO4 SCNs have worse SCN edge coverage and weaker SCN transitivity than PRN SCNs (Figs. 26 & 28). Accordingly, we find that MGEO4 SCNs do not fulfill their function as well as PRN SCNs. Compared with PRN EDS path-pairs, a significantly smaller fraction of MGEO4 EDS path-pairs are edge independent (Fig. 35a), and MGEO4 EDS path-pairs suffer significantly larger stretches than PRN EDS path-pairs (Fig. 35b). This provides a connection between the structure and function of SCNs.

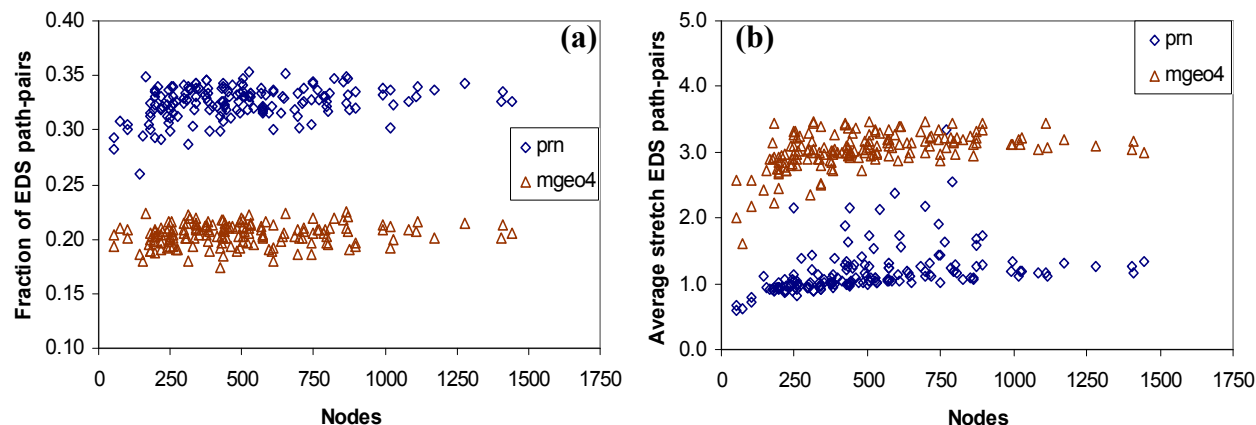


Fig. 35 MGEO4 path diversity and stretch. (a) EDS path-pairs in MGEO4 networks are significantly less edge independent than EDS paths-pairs in PRNs. (b) EDS path-pairs in MGEO4 networks have significantly larger stretch on average than those in PRNs.

The connection between structure and function of SCNs is also observable when decoy structures are compared with their respective native folds. We retrieved the publicly available decoy dataset from http://babylone.ulb.ac.be/decoys/Links_download_decoys/decoy_st_set.tar.gz. For each of the 36 native folds in the dataset, PRNs were created for 50 decoy folds, chosen at random from all decoys available per native fold, subject to the conditions in section 2.1. Network analysis was performed on the PRNs of

native and decoy folds. Statistics for a native fold are compared with statistics averaged over the decoys associated with the native fold.

There is no significant difference between the link densities of native and decoy PRNs (Fig. 36a). The decoys have significantly higher levels of clustering and significantly stronger transitivity than native folds (Fig. 36b & 36d), but significantly longer average EDS path length than native folds (Fig. 36c). At first glance, this last observation contradicts our results in section 3. However, it also indicates that differences in EDS path length could be correlated with a deeper property, and we propose that SCN well-formness is one such property. The decoy PRNs tested here are on the smaller side ($N \leq 200$ nodes) compared to the MGEO networks in section 3, and the results in section 3 were obtained under a highly controlled environment. In contrast, the decoys come from an external independent dataset. Nonetheless, the longer average EDS path length of decoy PRNs can still be explained by them having significantly more NESCs than native PRNs, which means more backtracking for EDS on decoy PRNs (Fig. 36f). The native and decoy PRNs both have short-cut edges whose sizes approximate $2N$ (Fig. 36e).

While there is no significant difference between native and decoy PRNs in terms of the number of short-cut edges, their SCNs differ significantly in a number of structural ways. SCN node coverage is significantly better in native than in decoy folds (Fig. 37a). SCNs of native folds comprise significantly fewer connected components than decoy SCNs (Fig. 37b). SCN edge coverage is significantly better in native than decoy folds (Fig. 37c). Native SCNs have significantly stronger transitivity than decoy SCNs (Fig. 37d). This despite decoy PRNs having stronger transitivity than native fold PRNs (Fig. 36d). In short, short-cut edges are more strategically placed in native folds than in decoys.

The SCNs of native folds have better span, are less fragmented and are more transitive. As such, native SCNs are better formed than decoy SCNs. And as expected, native SCNs perform their function better than decoy SCNs. Native folds are more path diverse than decoys (Fig. 37e) and EDS path-pairs experience significantly less stretch traversing native fold PRNs than decoy PRNs (Fig. 37f).

That a connection should exist between SCN structure and function was already hinted at by several observations made with the 2EZN MD dataset. As the 2EZN protein folds under MD simulation conditions, SCN edge multiplicity increases (Fig. 28d), EDS path-pair edge independence increases (Fig. 29a) and EDS path-pair stretch decreases (Fig. 29c). Similar correlations are observable in another MD simulation dataset. With this second dataset, we find a strong positive correlation ($r=0.8865$) between SCN transitivity and EDS path-pair edge independence (Fig. 38a), and a strong negative correlation ($r = -0.8751$) between SCN transitivity and EDS path-pair stretch (Fig. 38b).

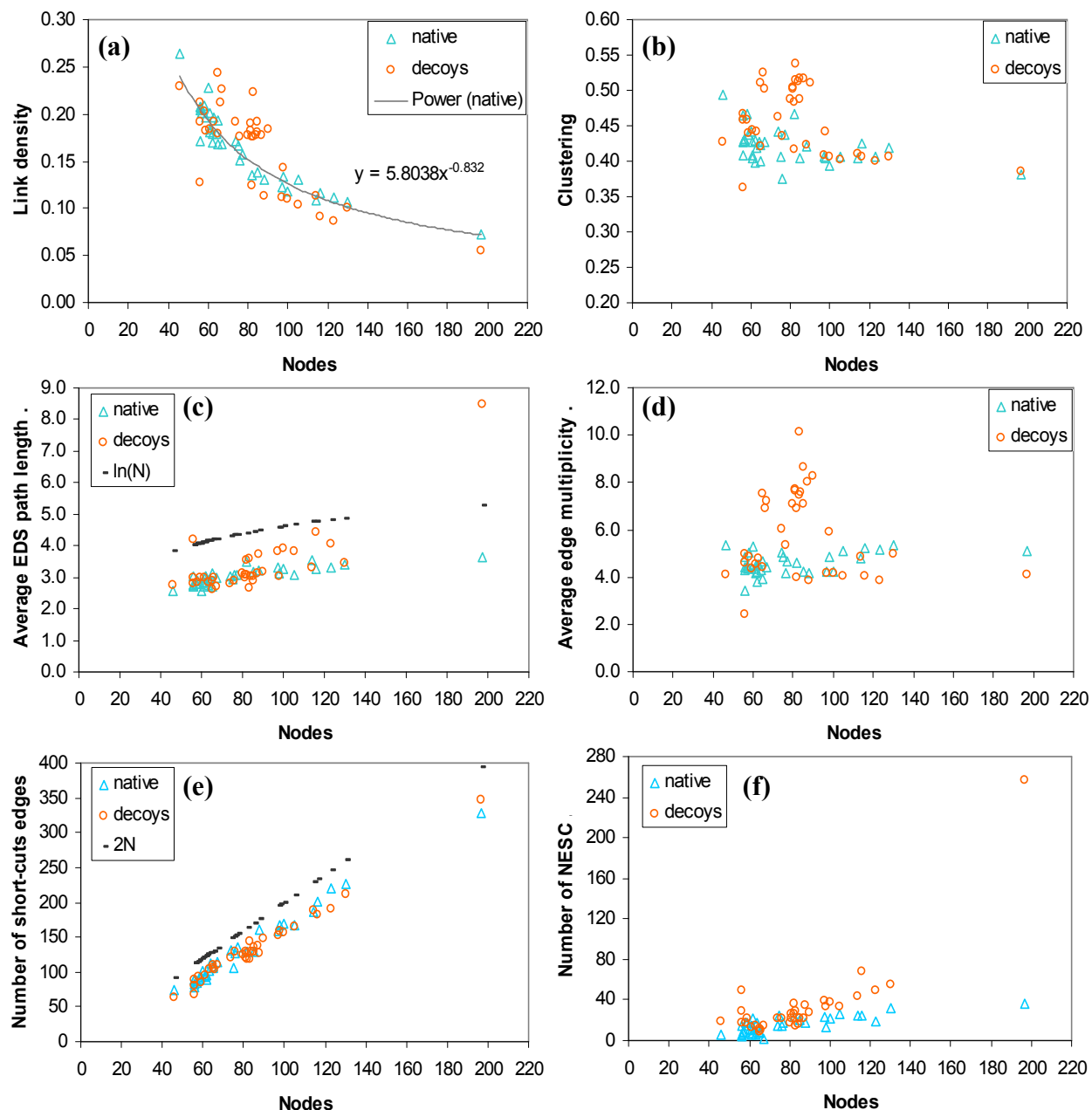


Fig. 36 Structural properties of native and decoy PRNs. (a) There is no significant difference between the link densities of native and decoy PRNs. Link density is the fraction of links that are actually present from the set of all possible links amongst the nodes present in a network (section 2.3). (b & d) The decoy PRNs have significantly (p -value=0.000141) higher levels of clustering and significantly (p -value=0.000651) stronger transitivity than native folds. (c) The decoys have significantly (p -value=0.015213) longer average EDS path length than native folds. Since the average EDS path length of decoys increase as $\ln(N)$, they are navigable small-worlds too. Hence having small-world network structure, even if navigable, does not characterize proteins sufficiently. (e) The number of short-cuts in decoy PRNs are not significantly different from the number of short-cuts in native PRNs. The number of short-cuts in decoys and native folds both approximate $2N$. (f) The decoys have significantly (p -value=0.002383) more non-existence short-cuts than the native folds.

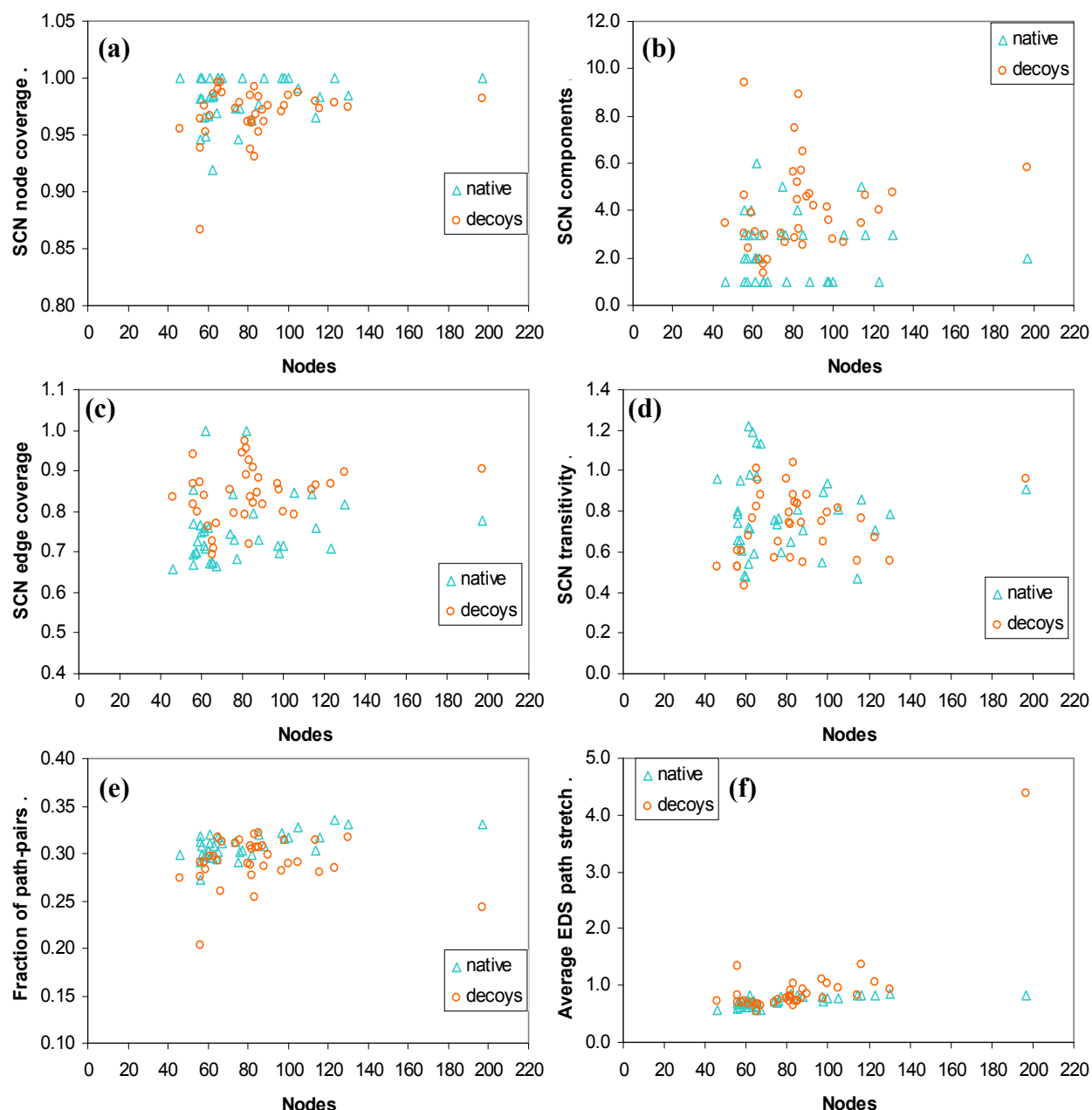


Fig. 37 Structure and function of native and decoy SCNs. (a) Native folds have significantly (p -value=0.00718) better SCN node coverage than decoys. (b) SCNs of native folds are composed of significantly (p -value=0.000038) fewer components than SCNs of decoys. Thus, not only do the SCNs of native folds span more of their underlying PRN nodes, they are also less fragmented. (c) Native folds have significantly (p -value=0.00000482) better SCN edge coverage than decoys. (d) Native fold SCNs are significantly (p -value=0.05154) more transitive than decoy SCNs. (e) Native fold PRNs are significantly (p -value=0.001228) more path diverse than decoy PRNs. (f) Average EDS path-pair stretch is significantly (p -value=0.022458) smaller in native folds than in decoys.

This second MD dataset is publically available from <https://simtk.org/home/foldvillin> and it was generated with GROMACS simulating the folding of a subdomain of the mainly alpha-helix 2F4K protein. The subdomain (HP-35 Nle Nle) has 35 amino acids and is modified for fast folding. Folding starts with a different denatured configuration in each run. The nine MD runs in this dataset is partitioned

into two sets for reasons stated in [62], and we follow this delineation. In the “successful” set are runs 4, 7, and 8. The starting structures of these runs either folded much faster or folded to a significant extent [62]. In the “unsuccessful” set are runs 0, 1, 2, 3, 5, and 6. The starting structures of these runs generated trajectories that either only briefly visited a folded configuration or did not fold at all [62]. We chose at least two trajectories (clones) at random from each run, with preference for clones with more frames (a frame comprises many snapshots). A PRN is constructed for every snapshot following the method described in section 2.1. Duplicate snapshots used to splice frames are removed. The results we report are produced by averaging over all snapshots in a clone (trajectory).

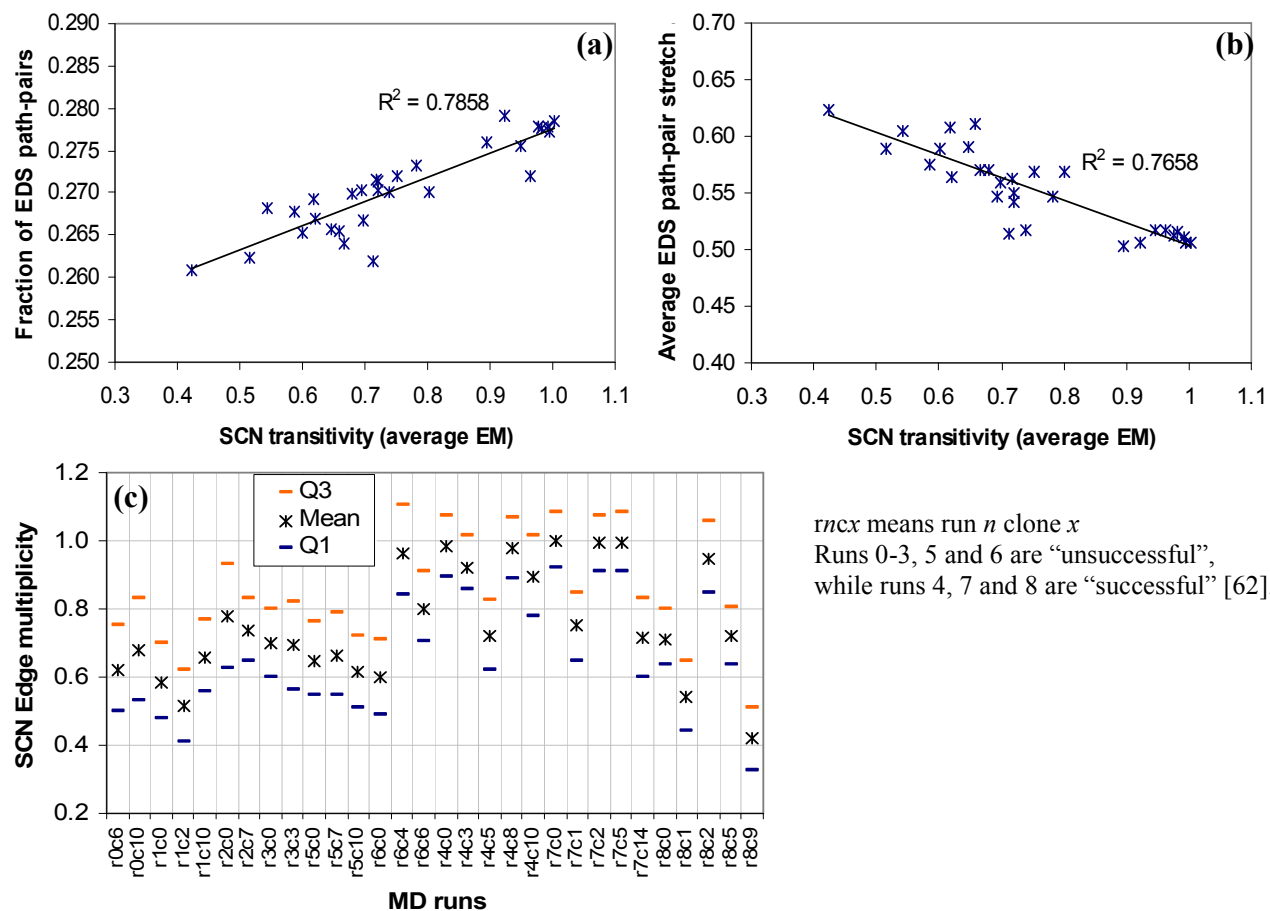


Fig. 38 Structure and function of SCNs from the HP-35 NLE NLE MD simulation dataset. (a) SCN transitivity correlates positively with path diversity. (b) SCN transitivity correlates negatively with EDS path-pair stretch. (c) SCNs from “successful” runs have significantly stronger transitivity than SCNs from “unsuccessful runs.

We also find that the configurations in the “successful” HP-35 NLE NLE MD runs have SCNs that are significantly (t test p-value=0.0101) more strongly transitive on average than the configurations in the “unsuccessful” MD runs (Fig. 38c). Accordingly, EDS path-pairs in the “successful” MD runs are significantly (t test p-value=0.0070) more edge independent and suffer significantly (t test p-value=0.0073) smaller average stretch than EDS path-pairs in the “unsuccessful” MD runs. This last

observation suggests that SCN growth and structure may be a factor in determining success or failure of protein folding MD trajectories, and more fundamentally characterize protein folding pathways.

We have exposed SCNs as exhibiting a number of qualitative similarities with PRNs from a network perspective (e.g.: Figs. 19 & 22). Since a SCN is sparser than its PRN (mathematically its size is about twice its order), it may be easier to study PRNs in terms of their SCNs. SCNs could prove to be an useful abstraction in the study of proteins just as the backbones of proteins have.

Acknowledgements

This work was made possible by the facilities of the Shared Hierarchical Academic Research Computing Network (SHARCNET:www.sharcnet.ca) and Compute/Calcul Canada.

References

- 1 Watts DJ and Strogatz SH (1998) Collective dynamics of ‘small-world’ networks. *Nature* 393, 440-442.
- 2 Vendruscolo M, Dokholyan NV, Paci E and Karplus M (2002) Small-world view of the amino acids that play a key role in protein folding. *Physical Review E* 65 061910-1.
- 3 Kleinberg J (2000) Navigation in a small world. *Nature* 406, 845
- 4 Kleinberg J (2000) The small-world phenomenon: an algorithmic perspective. Proc. of the 32nd Annual ACM Symposium on Theory of Computing, pp. 163-170.
- 5 Kasturirangan R (1999) Multiple scales in small-world graphs. cond-mat/9904055.
- 6 Newman MEJ (2003) The structure and function of complex networks. *SIAM Review* 45:167-256.
- 7 Newman MEJ (2010) *Networks: An introduction*. Oxford University Press.
- 8 Gaci O and Balev S (2009) Node degree distribution in amino acid interaction networks. Computational Structural Bioinformatics Workshop, Washington DC, USA.
- 9 Cohen R and Havlin S (2003) Scale-free networks are ultrasmall. *Phys. Rev. Lett* 90, 058701.
- 10 Whitley MJ and Lee AL (2009) Frameworks for understanding long-range intra-protein communication. *Curr Protein Pept Sci*. April, 10(2):116-127.
- 11 Dokholyan NV, Li L, Ding F and Shakhnovich EI (2002) Topological determinants of protein folding. *PNAS* (13): 8637-8641.
- 12 Atilgan AR, Akan P and Baysal C (2004) Small-world communication of residues and significance for protein dynamics. *Biophysical Journal* 86:85-91.
- 13 Del Sol A, Fujihashi H, Amoros D and Nussinov R (2006). Residues crucial for maintaining short paths in network communication mediate signaling in proteins. *Mol. Sys. Biol.* Doi:10.1038/msb4100063
- 14 Atilgan AR, Turgut D and Atilgan C (2007) Screened non-bonded interactions in native proteins manipulate optimal paths for robust residue communication. *Biophys. J.* 92(9):3052-3062.
- 15 Park K and Kim D (2011) Modeling allosteric signal propagation using protein structure networks. *BMC Bioinformatics* 12. From The 9th Asia Pacific Bioinformatics Conference (APBC 2011) Incheon, Korea.
- 16 Bagler G and Sinha S (2005). Network properties of protein structures. *Physica A: Statistics Mechanics and its Apps.* 346(1-2) pp. 27—33.
- 17 Chatterjee S, Ghosh S and Vishveshwara S (2013). Network properties of decoys and CASP predicted models: a comparison with native protein structures. *Mol. BioSyst.* 9:1774-1788.

- 18 Bhattacharyya M, Bhat, CR and Vishveshwara S (2013). An automated approach to network features of protein structure ensembles. *Protein Science* 22:1399-1416.
- 19 Emerson IA and Gothandam KM (2012). Network analysis of transmembrane protein structures. *Physica A* 391:905-916.
- 20 Leitner DM (2008). Energy flow in proteins. *Annu. Rev. Phys. Chem.* 59:233-259.
- 21 Jackson MB (2006). *Molecular and cellular biophysics*. Cambridge University Press.
- 22 Suel GM, Lockless SW, Wall MA and Ranganathan R (2003). Evolutionarily conserved networks of residues mediate allosteric communication in proteins. *Nature Structural Biology* 10(1):59-69.
- 23 Estrada E. (2010) Universality in protein residue networks. *Biophysical Journal* 98:890-900.
- 24 Berman HM, Westbrook J, Feng Z, Gilliland G, Bhat TN, Weissig H, Shindyalov IN and Bourne PE (2000). The Protein Data Bank. *Nucleic Acids Research* 28: 235-242. <http://www.rcsb.org/pdb>
- 25 Kannan N and Vishveshwara S (1999). Identification of side-chain clusters in protein structures by a graph spectral method. *J. Mol. Biol.* 292:441-464.
- 26 Mosca R, Ceol A, Stein A, Olivella R and Aloy P (2013). 3did: a catalog of domain-based interactions of known three-dimensional structure. *Nucleic Acids Research* 1-6.
- 27 Greene LH and Higman VA (2003). Uncovering network systems within protein structures. *Journal of Molecular Biology* 334:781-791.
- 28 Milenkovic T, Filippis I, Lappe M and Przulj N (2009) Optimized null model for protein structure networks. *PLoS ONE* 4(6): e5967.
- 29 Boguna M, Krioukov D and Claffy KC (2008). Navigability of complex networks. *Nature Physics* 5:74-80.
- 30 Serrano MA and Boguna M (2006) Clustering in complex networks. I. General formalism. *Phys. Rev. E* 74, 056114
- 31 Serrano MA and Boguna M (2006) Clustering in complex networks. II. Percolation properties. *Phys. Rev. E* 74, 056115.
- 32 Colomer-de-Simon P, Serrano MA, Beiro MG, Alvarez-Hamelin I and Boguna M. (2013) Deciphering the global organization of clustering in real complex networks. *Scientific Reports* 3:2517.
- 33 Atilgan AR and Atilgan C (2012) Local motifs in proteins combine to generate global functional moves. *Briefings in Functional Genomics* 2(6):479-488.
- 34 Bagler G and Sinha S (2007). Assortative mixing in Protein Contact Networks and protein folding kinetics. *Structural Bioinformatics* 23(14) pp. 1760—1767.
- 35 Turgut D, Atilgan AR and Atilgan C (2010) Assortative mixing in close-packed spatial networks. *PLoS ONE* 5(12):e15551
- 36 Bartoli L, Fariselli P and Casadio, R (2007) The effect of backbone on the small-world properties of Protein Contact Maps. *Physical Biology* 4:L1-L5.
- 37 Van der Kamp MW, Schaeffer RD, Jonsson AL, Scouras AD, Simms AM, Toofanny RD, Benson NC, Anderson PC, Merkley ED, Rysavy S, Bromley D, Beck DAC and Daggett V (2010) *Dynameomics: A comprehensive database of protein dynamics*. *Structure*, 18: 423-435.
- 38 Beck DAC, Jonsson AL, Schaeffer RD, Scott KA, Day R, Toofanny RD, Alonso DOV and Daggett V (2008) *Dynameomics: Mass Annotation of Protein Dynamics by All-Atom Molecular Dynamics Simulations*. *Protein Engineering Design & Selection* 21: 353-368.
- 39 Amitai G, Shemesh A, Sitbon E, Shklar M, Netanel D, Venger I and Pietrokovski S. (2004) Network analysis of protein structures identifies functional residues. *Journal of Molecular Biology* 344 1135-1146.
- 40 Del Sol A, Fujihashi H, Amoros D and Nussinov R (2006) Residue centrality, functionally important residues and active site shape: Analysis of enzyme and non-enzyme families. *Protein Science* 15:2120-2128. Cold Spring Harbor Laboratory Press.
- 41 Li J, Wang J and Wang W. (2008) Identifying folding nucleus based on residue contact networks of proteins. *Proteins* 71: 1899 – 1907.

- 42 Plaxco KW, Simons KT and Baker D (1998) Contact order, transition state placement and the refolding rates of single domain proteins. *J. Mol. Biol.* 277:985-994.
- 43 Gromiha MM and Selvaraj S (2001) Comparison between long-range interactions and contact order in determining the folding rate of two-state proteins: Application of long-range order to folding rate prediction. *J. Mol. Biol.* 310:27-32.
- 44 Ivankov DN, Garbuzynskiy SO, Alm E, Plaxco KW, Baker D and Finkelstein AV (2003) Contact order revisited: Influence of protein size on the folding rate
- 45 Faisca PFN, Travasso RDM, Parisi A and Rey A (2012). Why do protein folding rates correlate with metrics of native topology? *PLoS ONE* 7(4):e35599.
- 46 Baker D (2000) A surprising simplicity to protein folding. *Nature* 405, 39-42.
- 47 Barthelemy M (2010) Spatial networks. arXiv:1010.0302 [cond-mat.stat-mech].
- 48 Gao L (2001). On inferring autonomous system relationships in the Internet. *IEEE/ACM Trans. On Networking* 9: 733-745.
- 49 Goyal N, Rademacher L and Vempala S (2009) Expanders via random spanning trees. *Proceedings of the 20th Annual ACM-SIAM Symposium on Discrete Algorithms (SODA)*, pp. 576-585.
- 50 Cannistraci CV, Alanis-Lobato G and Ravasi T (2013) From link-prediction in brain connectomes and protein interactomes to the local-community-paradigm in complex networks. *Scientific Reports* 3:1613. doi: 10.1038/srep01613.
- 51 Kapron BM, King V and Mountjoy B. (2013) Dynamic graph connectivity in polylogarithmic worst case time. *Proceedings of the 24th Annual ACM-SIAM Symposium on Discrete Algorithms (SODA)*, pp. 1131-1142.
- 52 Sreenivasan S, Cohen R and Lopez E. (2006) Communication bottlenecks in scale-free networks. arXiv:cs/0604023.
- 53 Danila B, Yu Y, Marsh JA and Bassler KE. (2006) Optimal transport on complex networks. *Physical Review E* 74 046106.
- 54 Belykh I, Hasler M, Lauret M and Nijmeijer H. (2005) Synchronization and graph topology. *Int. Journal of Bifurcation and Chaos* 15(100):3423-3433.
- 55 Nadaletti LP, de Lima BSL and Guimaraes S (2013) Synchronization as a unifying mechanism for protein folding. arXiv:1310.5091
- 56 Newman MEJ (2003) A measure of betweenness centrality based on random walks. arXiv:cond-mat/0309045 [cond-mat.stat-mech].
- 57 Jonsson AL, Scott KA and Daggett V (2009) Dynameomics: A consensus view of the protein unfolding/folding transition state ensemble across a diverse set of protein folds. *Biophysical Journal* 97:2958-2966.
- 58 Maiya AS and Berger-Wolf TY (2010) Expansion and search in networks. *ACM Int. Conf. on Info. and Knowledge Mgmt. (CIKM)*. Toronto, Canada.
- 59 Young HT, Edwards SA and Grater F (2013) How fast does a signal propagate through proteins? *PLoS ONE* 8(6):e64746.
- 60 Botan V, et. al. (2007) Energy transport in peptide helices. *PNAS* 104(31):12749-12754.
- 61 Li G, Magana D and Dyer RB (2014) Anisotropic energy flow and allosteric ligand binding in albumin. *Nature Communications* 5:3100.
- 62 Ensign DL, Kasson PM and Pande VS. (2007) Heterogeneity even at the speed limit of folding: large-scale molecular dynamics study of a fast-folding variant of the Villin Headpiece. *J. Mol. Biol.* 374:806-816.
- 63 Go N. (1983) Theoretical Studies of Protein Folding. *Ann. Rev. Biophys. Bioeng.* 12:183-210.

Appendix A

Normalization values for the 20 residue types from [25], expanded with alternatives (marked with *) for the MD simulation datasets.

Residue Type	Norm	Residue Type	Norm
ALA	55.7551	LEU	72.2517
ARG	93.7891	NLEU	72.2517 *
ASN	73.4097	NLE	72.2517 *
ASP	75.1507	LYS	69.6096
CYS	54.9528	LYP	69.6096 *
CYH	54.9528 *	MET	69.2569
GLN	78.1301	PHE	93.3082
GLU	78.8288	CPHE	93.3082 *
GLY	47.3129	CPH	93.3082 *
HIS	83.7357	PRO	51.3310
HIE	83.7357 *	SER	61.3946
ILE	67.9452	THR	63.7075
		TRP	106.7030
		TYR	100.719
		VAL	62.3673

Appendix B

Although [28] reported that random geometric graphs (RGG) have many network statistics that are quantitatively similar to residue interaction networks, we note that, apart from the connectivity issue which we address by introducing a “backbone” in MGEO networks (section 2.2), the $|LE|/|SE|$ ratio of RGGs depart radically from Fig. 3b and clearly increases linearly with N (Fig. B1). The number of short-cuts found by EDS in RGGs is $< N$, much fewer than the $\sim 2N$ for PRNs and MGEO networks in Fig. 24a.

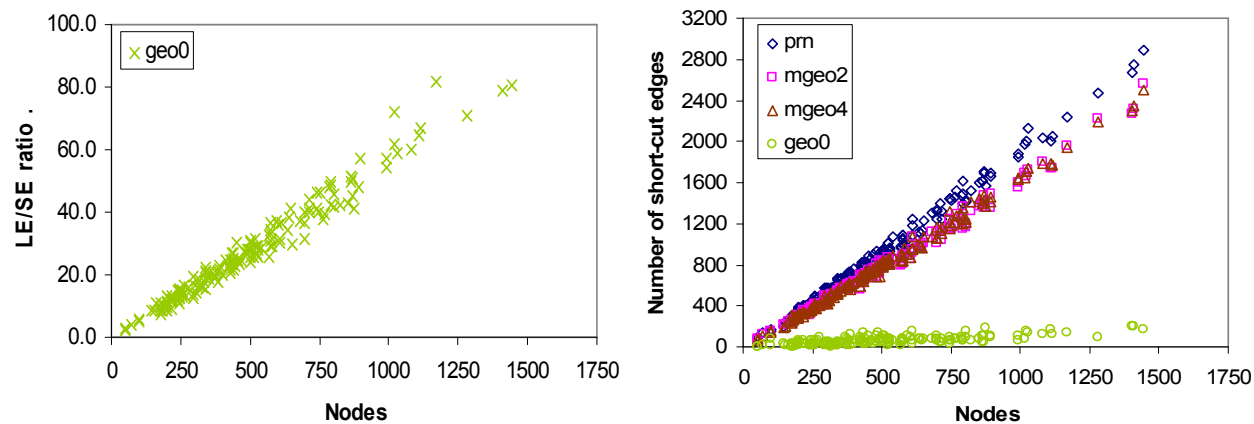


Fig. B1 (Left) The LE/SE ratio of geo0 networks (contrast with Fig. 3b). **(Right)** geo0 networks have significantly fewer short-cut edges. geo0 networks (skip=0) are constructed the same way as MGEO networks except with random x, y, z coordinates.